NPS69-86-007

NAVAL POSTGRADUATE SCHOOL
Monterey, California

THESIS

STRAIN DEPENDENT DAMPING CHARACTERISTICS
OF A HIGH DAMPING
MANGANESE-COPPER ALLOY

Dwight D. Dew

September 1986

Thesis Advisor: Y. S. Shin

Approved for public release; distribution unlimited.

Prepared for:
David W. Taylor Naval Ship R & D Center
Annapolis, MD 21402

NAVAL POSTGRADUATE SCHOOL
Monterey, CA 93943-5000

This thesis prepared in conjunction with research sponsored in part by David W. Taylor Naval Ship R & D Center under N0001486WR4B103/AA.

Unclassified

SECURITY CLASSIFICATION OF THIS PAGE

REPORT DOCUMENTATION PAGE

1a REPORT SECURITY CLASSIFICATION Unclassified	1b. RESTRICTIVE MARKINGS
2a SECURITY CLASSIFICATION AUTHORITY	3 DISTRIBUTION / AVAILABILITY OF REPORT Distribution unlimited.
2b DECLASSIFICATION / DOWNGRADING SCHEDULE	
4 PERFORMING ORGANIZATION REPORT NUMBER(S) NPS 69-86-007	5 MONITORING ORGANIZATION REPORT NUMBER(S) N0001486WR4B103/AA
6a. NAME OF PERFORMING ORGANIZATION Naval Postgraduate School Monterey, CA 93943-5000 — 6b OFFICE SYMBOL (If applicable) 69	7a. NAME OF MONITORING ORGANIZATION Naval Postgraduate School Monterey, CA 93943-5000
6c. ADDRESS (City, State, and ZIP Code) Monterey, CA 93943-5000	7b. ADDRESS (City, State, and ZIP Code) Monterey, CA 93943-5000
8a NAME OF FUNDING / SPONSORING ORGANIZATION David W. Taylor Naval Ship Research & Development Center — 8b. OFFICE SYMBOL (If applicable)	9. PROCUREMENT INSTRUMENT IDENTIFICATION NUMBER
8c. ADDRESS (City, State, and ZIP Code) Annapolis, Maryland 21402	10 SOURCE OF FUNDING NUMBERS PROGRAM ELEMENT NO 62761N; PROJECT NO; TASK NO RS561541Soo; WORK UNIT ACCESSION NO See 5

11 TITLE (Include Security Classification)

STRAIN DEPENDENT DAMPING CHARACTERISTICS OF A HIGH DAMPING MANGANESE-COPPER ALLOY

12 PERSONAL AUTHOR(S)
LCDR DWIGHT D. DEW, USN

13a TYPE OF REPORT	13b TIME COVERED	14 DATE OF REPORT (Year, Month, Day)	15 PAGE COUNT
Masters Thesis/Technical	FROM 8 Feb86 TO 30 Sep86	1986 September	145

16 SUPPLEMENTARY NOTATION

—

17 COSATI CODES			18 SUBJECT TERMS (Continue on reverse if necessary and identify by block number)
FIELD	GROUP	SUB-GROUP	Strain Dependent Material Damping, Manganese-Copper Alloy, Sonoston, Damping Measurement Technique, Random Excitation, Swept Sine Excitation

19 ABSTRACT (Continue on reverse if necessary and identify by block number)

The Naval Postgraduate School is investigating measurement techniques for the determination of strain-dependent damping characteristics of materials in an air environment. The material is a high damping manganese-copper alloy called sonoston. The measurement techniques employ cantilevered flat beam specimens in bending and cylindrical specimens in torsion. The specimens were subjected to three different heat and aging treatments. Pure random and sinusoidal sweep excitations are used as an excitation source in the frequency range of 20 to 500 HZ. Miniature accelerometers and strain gages were mounted on the specimens to obtain both input excitation and output responses. The results of the investigation are presented graphically as damping factor vs. resonant frequency, damping factor vs. strain, damping factor vs. input acceleration, strain vs. resonant frequency, strain vs. input acceleration, and input acceleration vs. resonant frequency.

20 DISTRIBUTION / AVAILABILITY OF ABSTRACT ☒ UNCLASSIFIED/UNLIMITED ☐ SAME AS RPT ☐ DTIC USERS	21 ABSTRACT SECURITY CLASSIFICATION Unclassified
22a NAME OF RESPONSIBLE INDIVIDUAL Young S. Shin	22b TELEPHONE (Include Area Code) (408) 646-2568 — 22c OFFICE SYMBOL Code 69Sg

DD FORM 1473, 84 MAR — 83 APR edition may be used until exhausted. All other editions are obsolete

SECURITY CLASSIFICATION OF THIS PAGE
Unclassified

Strain Dependent Damping Characteristics of a High Damping Manganese-Copper Alloy

by

Dwight D. Dew
Lieutenant Commander, United States Navy
B.A., University of South Florida, 1975

Submitted in partial fulfillment of the
requirements for the degrees of

M.S. IN MECHANICAL ENGINEERING
and
MECHANICAL ENGINEER

from the

NAVAL POSTGRADUATE SCHOOL
September 1986

ABSTRACT

This paper presents the studies on measurement techniques developed for the determination of strain-dependent damping characteristics of materials in an air environment. The material is a high damping manganese-copper alloy called Sonoston. The measurement techniques employ cantilevered flat beam specimens in bending and cylindrical specimens in torsion. The specimens were subjected to three different heat and aging treatments. Pure random and sinusoidal sweep excitations are used as an excitation source in the frequency range of 20 to 500 Hz. Miniature accelerometers and strain gages were mounted on the specimens to obtain both input excitation and output responses. The results of the investigation are presented graphically as damping factor vs. resonant frequency, damping factor vs. strain, damping factor vs. input acceleration, strain vs. resonant frequency, strain vs. input acceleration, and input acceleration vs. resonant frequency.

TABLE OF CONTENTS

I. INTRODUCTION 12
A. GENERAL AND OBJECTIVE 12
B. BACKGROUND 12
C. MN-CU ALLOYS 14
D. METALLURGY OF MN-CU ALLOYS 16

II. CANTILEVER BEAM EXPERIMENTAL METHOD 20
A. GENERAL 20
B. METHOD 20
C. CALIBRATION 33

III. CANTILEVER BEAM RESULTS AND DISCUSSION 38
A. GENERAL 38
B. INPUT ACCELERATION -VS- STRAIN 38
C. LOSS FACTOR -VS- STRAIN 45
D. STRAIN -VS- FREQUENCY 52
E. INPUT ACCELERATION -VS- FREQUENCY 59
F. INPUT ACCELERATION -VS- LOSS FACTOR 66
G. LOSS FACTOR -VS- FREQUENCY 73
H. DISCUSSION 80

IV. TORSION SAMPLE EXPERIMENTAL METHOD 81

V. TORSION SAMPLE RESULTS AND DISCUSSION 88
A. GENERAL 88
B. INPUT ACCELERATION -VS- SHEAR STRAIN 88
C. LOSS FACTOR -VS- SHEAR STRAIN 91
D. SHEAR STRAIN -VS- FREQUENCY 91
E. INPUT ACCELERATION -VS- FREQUENCY 91
F. INPUT ACCELERATION -VS- LOSS FACTOR 98

G. LOSS FACTOR -VS- FREQUENCY 98
H. DISCUSSION 98

VI. DISCUSSION AND RECOMMENDATIONS 103

APPENDIX A: HALF-POWER POINT METHOD 104

APPENDIX B: DETERMINATION OF NATURAL FREQUENCIES 105
1. CANTILEVER BEAM 105
2. TORSION 108

APPENDIX C: TORSION DAMPING APPARATUS DESIGN 109

APPENDIX D: CANTILEVER BEAM AND TORSION SAMPLE TRANSFER FUNCTION GRAPHS 116
1. CANTILEVER BEAM REPRESENTATIVE GRAPHS 116
2. TORSION SAMPLE REPRESENTATIVE GRAPHS 120

APPENDIX E: CANTILEVER BEAM AND TORSION SAMPLE DATA 124
1. CANTILEVER BEAM DATA 124
2. TORSION SAMPLE DATA 138

LIST OF REFERENCES 141

BIBLIOGRAPHY 142

INITIAL DISTRIBUTION LIST 143

LIST OF TABLES

1. VALUES OF A FOR DIFFERENT BEAM CONFIGURATIONS 106
2. CALCULATED RESONANT FREQUENCIES OF CANTILEVER BEAMS 107
3. CALCULATED RESONANT FREQUENCIES OF TORSION SAMPLES 108
4. MODE 1 - AS QUENCHED SAMPLE 124
5. MODE 1 - 1 HOUR AGED SAMPLES 125
6. MODE 1 - 2 HOUR AGED SAMPLES 126
7. MODE 2 - AS QUENCHED SAMPLE 127
8. MODE 2 - 1 HOUR AGED SAMPLES 128
9. MODE 2 - 2 HOUR AGED SAMPLES 129
10. MODE 3 - AS QUENCHED SAMPLE 130
11. MODE 3 - 1 HOUR AGED SAMPLES 131
12. MODE 3 - 2 HOUR AGED SAMPLES 132
13. MODE 1 - UNAGED SAMPLE (SWEPT SINE) 133
14. MODE 1 - 1 HOUR AGED SAMPLES (SWEPT SINE) 133
15. MODE 1 - 2 HOUR AGED SAMPLES (SWEPT SINE) 134
16. MODE 2 - UNAGED SAMPLE (SWEPT SINE) 134
17. MODE 2 - 1 HOUR SAMPLES (SWEPT SINE) 135
18. MODE 2 - 2 HOUR SAMPLES (SWEPT SINE) 135
19. MODE 3 - UNAGED SAMPLE (SWEPT SINE) 136
20. MODE 3 - 1 HOUR AGED SAMPLES (SWEPT SINE) 136
21. MODE 3 - 2 HOUR SAMPLES (SWEPT SINE) 137
22. TORSION - SOLUTION ANNEALED SAMPLE (RANDOM INPUT) 138
23. TORSION - SOLUTION ANNEALED SAMPLE (SWEPT SINE) 138
24. TORSION - 1 HOUR AGED SAMPLE (RANDOM INPUT) 139
25. TORSION - 1 HOUR AGED SAMPLE (SWEPT SINE) 139

26. TORSION - 2 HOUR AGED SAMPLE (RANDOM INPUT) 140
27. TORSION - 2 HOUR AGED SAMPLE (SWEPT SINE) 140

LIST OF FIGURES

1.1	Material Damping Index	13
1.2	Potential Applications	15
1.3	Cu-Mn Binary Phase Diagram	17
1.4	Summary of Heat Treatment	18
2.1	Stress/Strain Curves for Sonoston	21
2.2	Fortran Program for Location of Maximum Strain	22
2.3	Cantilever Beam Sample Photograph	24
2.4	Cantilever Beam Test Fixture	25
2.5	Accelerometer Location	26
2.6	Equipment Line Diagram	27
2.7	Baseband Measurement of the Solution Annealed Sample	28
2.8	Baseband Measurement of the 1-Hour Aged Sample	29
2.9	Baseband Measurement of the 2-Hour Aged Sample	30
2.10	Time Sample of the Input Accelerometer	31
2.11	Time Sample of the Root Strain Gage	32
2.12	Accelerometer/Accelerometer Transfer Function	34
2.13	Accelerometer/Strain Gage Transfer Function	35
2.14	Calibration Curve	36
2.15	Free-fall Section	37
3.1	Mode 1 - Input Acceleration -vs- Strain (Random Input)	39
3.2	Mode 1 - Input Acceleration -vs- Strain (Swept Sine)	40
3.3	Mode 2 - Input Acceleration -vs- Strain (Random Input)	41
3.4	Mode 2 - Input Acceleration -vs- Strain (Swept Sine)	42
3.5	Mode 3 - Input Acceleration -vs- Strain (Random Input)	43
3.6	Mode 3 - Input Acceleration -vs- Strain (Swept Sine)	44
3.7	Mode 1 - Loss Factor -vs- Strain (Random Input)	46
3.8	Mode 1 - Loss Factor -vs- Strain (Swept Sine)	47
3.9	Mode 2 - Loss Factor -vs- Strain (Random Input)	48

3.10 Mode 2 - Loss Factor -vs- Strain (Swept Sine) 49
3.11 Mode 3 - Loss Factor -vs- Strain (Random Input) 50
3.12 Mode 3 - Loss Factor -vs- Strain (Swept Sine) 51
3.13 Mode 1 - Strain -vs- Frequency (Random Input) 53
3.14 Mode 1 - Strain -vs- Frequency (Swept Sine) 54
3.15 Mode 2 - Strain -vs- Frequency (Random Input) 55
3.16 Mode 2 - Strain -vs- Frequency (Swept Sine) 56
3.17 Mode 3 - Strain -vs- Frequency (Random Input) 57
3.18 Mode 3 - Strain -vs- Frequency (Swept Sine) 58
3.19 Mode 1 - Input Acceleration -vs- Frequency (Random Input) 60
3.20 Mode 1 - Input Acceleration -vs- Frequency (Swept Sine) 61
3.21 Mode 2 - Input Acceleration -vs- Frequency (Random Input) 62
3.22 Mode 2 - Input Acceleration -vs- Frequency (Swept Sine) 63
3.23 Mode 3 - Input Acceleration -vs- Frequency (Random Input) 64
3.24 Mode 3 - Input Acceleration -vs- Frequency (Swept Sine) 65
3.25 Mode 1 - Input Acceleration -vs- Loss Factor (Random Input) 67
3.26 Mode 1 - Input Acceleration -vs- Loss Factor (Swept Sine) 68
3.27 Mode 2 - Input Acceleration -vs- Loss Factor (Random Input) 69
3.28 Mode 2 - Input Acceleration -vs- Loss Factor (Swept Sine) 70
3.29 Mode 3 - Input Acceleration -vs- Loss Factor (Random Input) 71
3.30 Mode 3 - Input Acceleration -vs- Loss Factor (Swept Sine) 72
3.31 Mode 1 - Loss Factor -vs- Frequency (Random Input) 74
3.32 Mode 1 - Loss Factor -vs -Frequency (Swept Sine) 75
3.33 Mode 2 - Loss Factor -vs- Frequency (Random Input) 76
3.34 Mode 2 - Loss Factor -vs- Frequency (Swept Sine) 77
3.35 Mode 3 - Loss Factor -vs- Frequency (Random Input) 78
3.36 Mode 3 - Loss Factor -vs- Frequency (Swept Sine) 79
4.1 Torsion Sample Test Fixture 83
4.2 Torsion Sample Photograph 84
4.3 Time Sample of Shear Strain Gage 85
4.4 Time Sample of Torsion Input Accelerometer 86
4.5 Baseband Response for Solution Annealed Sample 87
5.1 Torsion - Input Acceleration -vs Shear Strain (Random Input) 89

5.2 Torsion - Input Acceleration -vs- Shear Strain (Swept Sine) 90
5.3 Torsion - Loss Factor -vs- Shear Strain (Random Input) 92
5.4 Torsion - Loss Factor -vs- Shear Strain (Swept Sine) 93
5.5 Torsion - Shear Strain -vs- Frequency (Random Input) 94
5.6 Torsion - Shear Strain -vs- Frequency (Swept Sine) 95
5.7 Torsion - Input Acceleration -vs- Frequency (Random Input) 96
5.8 Torsion - Input Acceleration -vs- Frequency (Swept Sine) 97
5.9 Torsion - Input Acceleration -vs- Loss Factor (Random Input) 99
5.10 Torsion - Input Acceleration -vs- Loss Factor (Swept Sine) 100
5.11 Torsion - Loss Factor -vs- Frequency (Random Input) 101
5.12 Torsion - Loss Factor -vs- Frequency (Swept Sine) 102
A.1 Half-Power Point Method 104
B.1 Sonoston Beam Configuration 106
C.1 Torsion Specimen 110
C.2 Turning Disc - Top View 111
C.3 Turning Disc - Side View 111
C.4 Torsion Sample Upper Test Stand 112
C.5 Torsion Sample Lower Test Stand 113
C.6 Assembled Torsion Test Apparatus 114
C.7 Electromagnetic Shaker Stand for Torsion Test 115
D.1 Mode 1 - Solution Annealed Sample Transfer Function (Cantilever Beam - Random Input) 116
D.2 Solution Annealed Transfer Function - Linear Scale (Cantilever Beam - Random Input) 117
D.3 Mode 1 - Solution Annealed Sample Coherence Function (Cantilever Beam - Random Input) 118
D.4 Mode 1 - Phase Shift for the Solution Annealed Sample (Cantilever Beam - Random Input) 119
D.5 Solution Annealed Transfer Function (Torsion Sample - Random Input) 120
D.6 Solution Annealed Transfer Function - Linear Scale (TorsionSample - Random Input) 121
D.7 Solution Annealed Sample Coherence Function (Torsion Sample - Random Input) 122
D.8 Torsion - Phase Shift for Solution Annealed Sample (Torsion Sample - Random Input) 123

ACKNOWLEDGEMENTS

I would like to express my appreciation to Professor Young S. Shin and Dr. Kil Soo Kim for their support and patience in making this project a productive task.

My appreciation is also expressed to Professor Jeff Perkins who took the time to conscientiously review this work and to Mrs. Kathy Wong and Mr. Bob Hardy of the David W. Taylor Naval Ship R&D Center for their continued support of the work being done at the Naval Postgraduate School.

Additionally, I commend the conscientious efforts and the high quality of the support from the mechanical engineering shop facility at the Naval Postgraduate School, specifically, Mr. Charles Crow.

I. INTRODUCTION

A. GENERAL AND OBJECTIVE

Minimizing vibrations has long been an important part of engineering design. Suppressing noise and vibrations, especially in the lower frequency ranges, is very important for the Navy since submarines and surface ships become quieter and detection becomes more difficult. Noise suppression usually is accomplished by using high-damping non-metallic materials to isolate the machinery from the hull; or by dissipating the energy within the structure. The Navy's primary efforts have been on isolating the machinery. The methods of isolation include:

1. Use of a viscoelastic mount.
2. Blanketing the structure.
3. Increasing the stiffness of the structure creating the noise.
4. Tuning.
5. Reducing manufacturing tolerances.

Among these methods extensive use of resilient mounts is the primary approach used. This stems partly from the fact that hardly any structural metal or alloy possesses any significant damping capacity. If a metal or alloy with a high damping capacity could be found, ship silencing could be better accomplished by using these energy absorbing materials as component parts.

Damping is a property of a structure describing how rapidly vibration decays once it is excited. It is a function of many variables such as geometry, exciting frequency, temperature, and stress/strain level. Cast iron has been considered to be the only acceptable structural material with significant damping capacity currently available. However, it can be seen (Figure 1.1) that other materials are also available, especially the manganese-copper alloys.

The objective of this thesis is to recommend a standardized measurement technique to provide consistent and reliable damping characteristics of high damping alloys.

B. BACKGROUND

Initial Naval Postgraduate School material damping research implemented a testing procedure for measuring viscous damping in large metal plate specimens at low

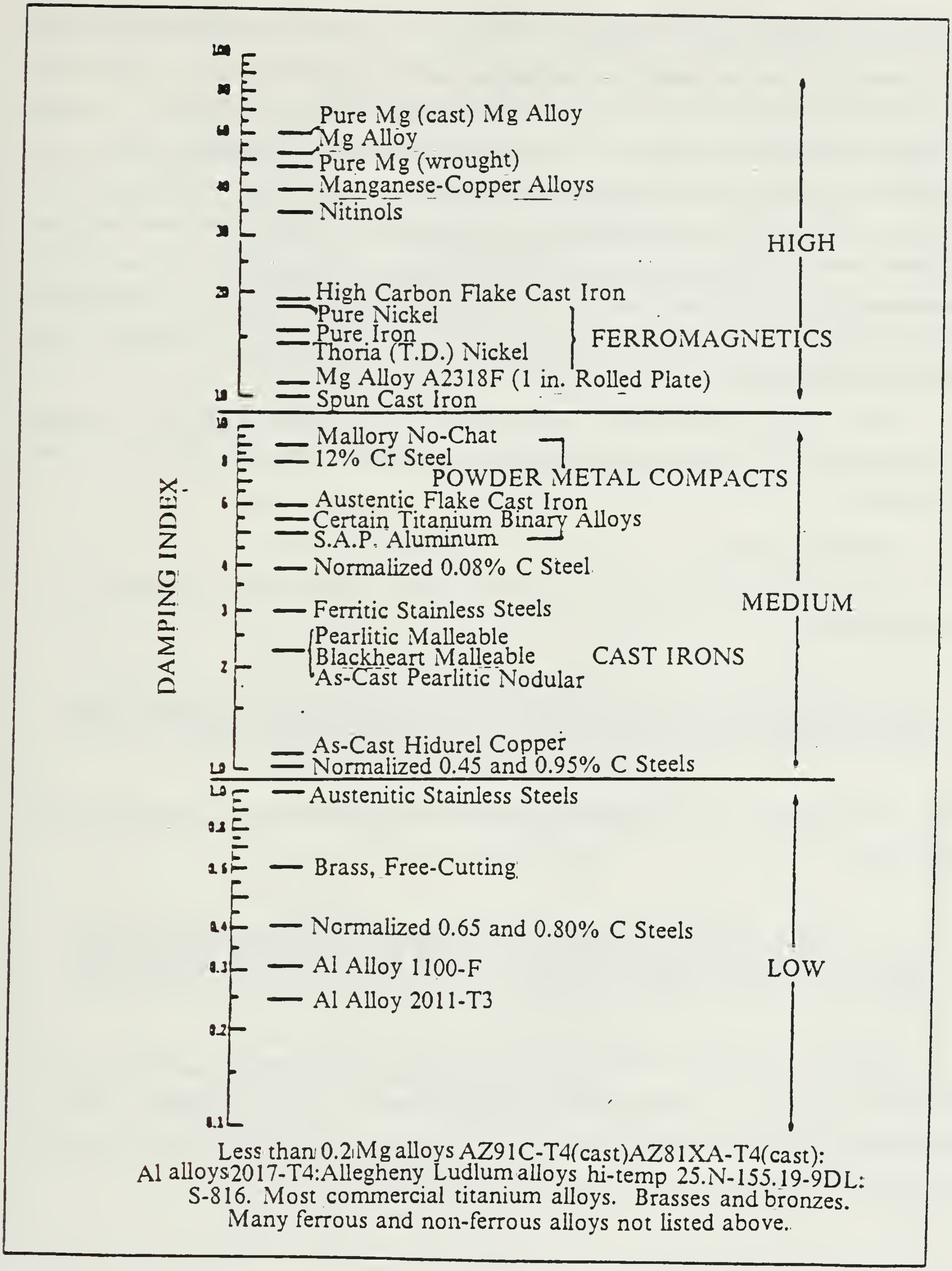

Figure 1.1 Material Damping Index (Ref. 1)

stress levels using an impulse hammer technique. The specimen could be placed in an environmental chamber for testing in either an air or water environment. Temperature control allowed testing to be conducted in the range of 30°F. to 90°F [Ref. 2]. Further testing introduced and validated a random force excitation technique adapted for underwater use and examined the effects of four specimen boundary conditions on system damping measurements [Ref. 3]. Following this work the environmental chamber was utilized to investigate how the damping characteristics of a cast nickel aluminum bronze plate specimen varied in both an air and a saltwater environment. Work to determine the damping characteristics of composite and constrained layer plates was also performed [Ref. 4].

This paper presents an investigation to determine how the damping characteristics of a high damping manganese-copper alloy vary with strain in an air environment.

C. MN-CU ALLOYS

The high damping capacity of Mn-Cu alloys gives it great potential as a structural metal.

> Previously the alloys were found physically unsatisfactory because of poor quality castings. More advanced alloys tested later were found physically sound but susceptible to general corrosion and stress cracking. [Ref. 1:p. 15]

Their susceptibility to corrosion and stress cracking made them unsatisfactory for marine use.

> In general, alloys that possess high damping capacity are not usually the best adapted to construction purposes since the gain in damping is often at the expense of stiffness, strength, durability, corrosion resistance, cost, machinability, or long-term stability. [Ref. 5:p. 64]

Situations (especially in the Navy) where these high damping materials can be utilized do occur. A commercially produced Mn-Cu alloy (Sonoston), with a composition of 54.25 wt% Mn, 37.0 wt% Cu, 4.25 wt% Al, 3.0 wt% Fe, and 1.5 wt% Ni, could be used in gear trains , brake discs, etc. (Figure 1.2).

Potential applications of quiet metals

General:

- Plug inserts to noisy machine parts
- Cladding for virtually any noisy part
- Reduction of resonant amplification factors
- Attenuation of ringing
- Machinery diagnostic techniques

Specific:

- Gears and gear webs
- Pump castings
- Diesel engine parts
- Brake discs
- Wheel rims
- Submarine/torpedo/ship propellers
- Helicopter gears
- Machinery frames and bases
- Aircraft/missile structural members
- Phonograph pickups/playing arms
- Transducers
- Office/textile/printing machinery components
- Hi-fi audio microphone components
- Bimetallic strips-control devices
- Plates for tuning capacitors
- Resistors
- Hearing aid components
- Movie camera gears, etc. etc.

Figure 1.2 Potential Applications {Ref. 6}

D. METALLURGY OF MN-CU ALLOYS

The fact that Mn-Cu Alloys can have a high damping capacity has been known for years. High damping is associated with alloys greater than 20% Mn with practical alloys ranging from 70%Cu-30%Mn to 30%Cu-70%Mn. To properly condition these alloys to obtain high damping capacity, four heat-treatment steps are required: (Figure 1.3)

1. Solution treatment in (γMn) single phase region (a face centered cubic structure).
2. Water quenching to retain the single phase metastable supersaturated solid structure.
3. Aging treatment in the two phase (γMn + αMn) region.
4. Water quenching to room temperature (a martensitic type transformation of the matrix occurs during this time). (Figure 1.4)

> The structure of the quenched solution treated sample is face centered cubic (FCC), but becomes tetragonal if aged between 400°C-600°C. Aging produces areas of manganese enrichment prior to the precipitation of α-Manganese where the tetragonal structure can exist at room temperature. On cooling from the aging temperature, the transformation, nucleated at dislocations and α-precipitate, occurs by a diffusionless shear process (martensitic). The tetragonal phase has the same volume as the cubic structure from which it is formed; and to minimize internal strains, the matrix becomes self-accomodating by splitting up into domains of common orientation analogous to martensitic platelets or mechanical twins. [Ref. 7:p. 4]

When the material is stressed, deformation occurs by movement of the domain boundaries, resulting in a macromechanical hysteresis effect. This is a reversible process causing no damage. This strain induced reorientation of the tetragonal domains causes the high damping capacity. Damping capacity increases with aging time up to 8 hours as the number of microtwins increases. After aging for 9 hours the density of microtwins gradually decreases until after 20 hours they can only occasionally be seen. Therefore, the optimal aging time is 8 hours in order to get the highest damping capacity.

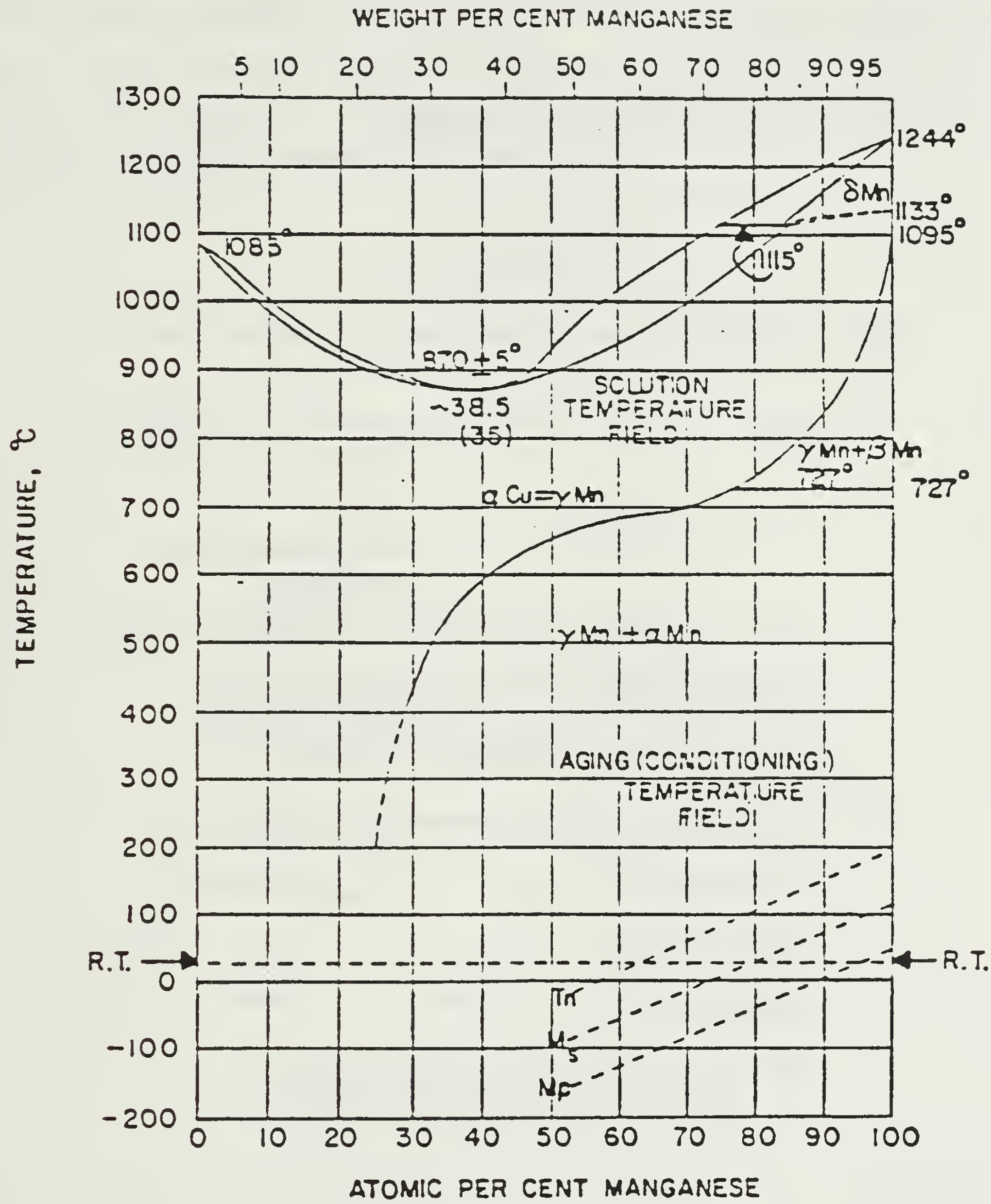

Figure 1.3 Cu-Mn Binary Phase Diagram {Ref. 1}

Summary of Heat Treatment Effects in Cu-Mn Alloys

Step 1: Solution treatment:

γ_{Mn} ($\approx \alpha_{Cu}$) (A1:FCC)

Step 2: Quench from solution treatment temperature:

If < 80 w/o Mn: γ_{Mn} retained @ room temperature

If > 80 w/o Mn: γ_{Mn} ↓

antiferromagnetic ordering, @ T_N

↓

martensitic transformation @ M_s ($T_N > M_s$)

Step 3: Aging treatment (assuming alloy < 80 w/o Mn) (in two-phase region:

γ_{Mn}(A1:FCC) + α_{Mn} (A12: complex BCC))

Stage I: $\gamma_{Mn} \xrightarrow{\text{(initial)}} \gamma_{Mn}$ (Mn-enriched) (matrix) + "α" (metastable Cu-rich precipitates, 100Å)

Stage II: $\xrightarrow{\text{(more time)}} \gamma_{Mn}$ (Mn-enriched (matrix) + "α" + α_{Mn} (Widmanstatten precipitate) (small amount)

Stage III: $\xrightarrow{\text{(more time)}} \gamma_{Mn}$ (Mn-depleted) + $\cancel{\text{"}\alpha\text{"}}$ dissolves + α_{Mn} (equilibrium amount)

NOTE: The condition of Stage II is typically that leading to optimum damping; Stage III is overaged, i.e. no martensitic transformation of the γ_{Mn} matrix will occur on subsequent quenching - such will occur only if the matrix is conditioned to the necessary Mn-rich state by metastable "α" precipitation.

Step 4: Quench from the aging treatment (assuming Stage II condition from Step 3 above):

γ_{Mn} (Mn-enriched) +	"α" +	α_{Mn} (small amount)
↓ antiferromagnetic ordering @ T_N ↓ martensitic transformation @ M_s	↓ retained ?	↓ retained

NOTE: The martensitic transformation is triggered by the strain associated with the tetragonal distortion (FCC → FCT) of the antiferromagnetic ordering reaction; $T_N > M_s$.

Figure 1.4 Summary of Heat Treatment (Ref. 1)

Mn-Cu alloys have several unique problems because of their metallurgy. Their strength and hardness increases during the aging process while their damping capacity decreases with increasing temperature. The damping capacity is reduced drastically at the transformation temperature (100°C to 200°C) where the material returns to a cubic structure. Since the cubic-tetragonal transformation is well below room temperature, storage at room temperature is equivalent to a low temperature aging leading to a decrease in damping capacity over a few years.

II. CANTILEVER BEAM EXPERIMENTAL METHOD

A. GENERAL

Two measurement techniques were developed for the determination of strain-dependent damping characteristics of Sonoston in an air environment. The measurement techniques employ cantilevered flat beam specimens in bending and cylindrical specimens in torsion. The specimens were subjected to three different heat and aging treatments. Pure random and sinusoidal sweep excitations are used as an excitation source in the frequency range of 20 to 500 Hz. Both methods use transfer function techniques. Miniature accelerometers and strain gages were mounted on the specimens to obtain both input excitation and output responses.

B. METHOD

Sonoston is a non-linear metal with a nominal Modulus of Elasticity (E) of 12 x 10^6 psi and a yield strength of 45 Kpsi. Since aging increases the Modulus of Elasticity, it was decided that 3 tensile specimens would be tested. All three specimens were solution annealed at 800°C for 45 minutes. One was aged for 1 hour at 425°C, one was aged at 425°C for 2 hours, and the third was left unaged. Engineering Stress/Strain curves were constructed from the test results (Figure 2.1). The Young's Modulus used in further calculations was obtained from these results. For the unaged sample E was calculated as 17.5 x 10^6 psi; for the 1 hour aged sample E was 19.7 x 10^6 psi; and for the 2 hour aged sample E was 25.5 x 10^6 psi. These values were then used to calculate the resonant frequencies of the cantilever beam specimens as well as that of the torsion samples (Appendix B).

Five cantilever beam specimens were then manufactured and solution annealed. Two specimens were aged for 1 hour, two were aged for 2 hours, while the fifth was left unaged. Three strain gages were mounted on each specimen at locations where the maximum strain due to bending moment occurs. With L the total length of the cantilever beam from the root to the tip and X being the distance along the beam measured from the root, Reference 8 lists the locations where maximum bending occurs for the first three modes in X/L increments of 0.04. A Fortran program was written to calculate the moment for any point along the beam in X/L increments of 0.01 (Figure 2.2).

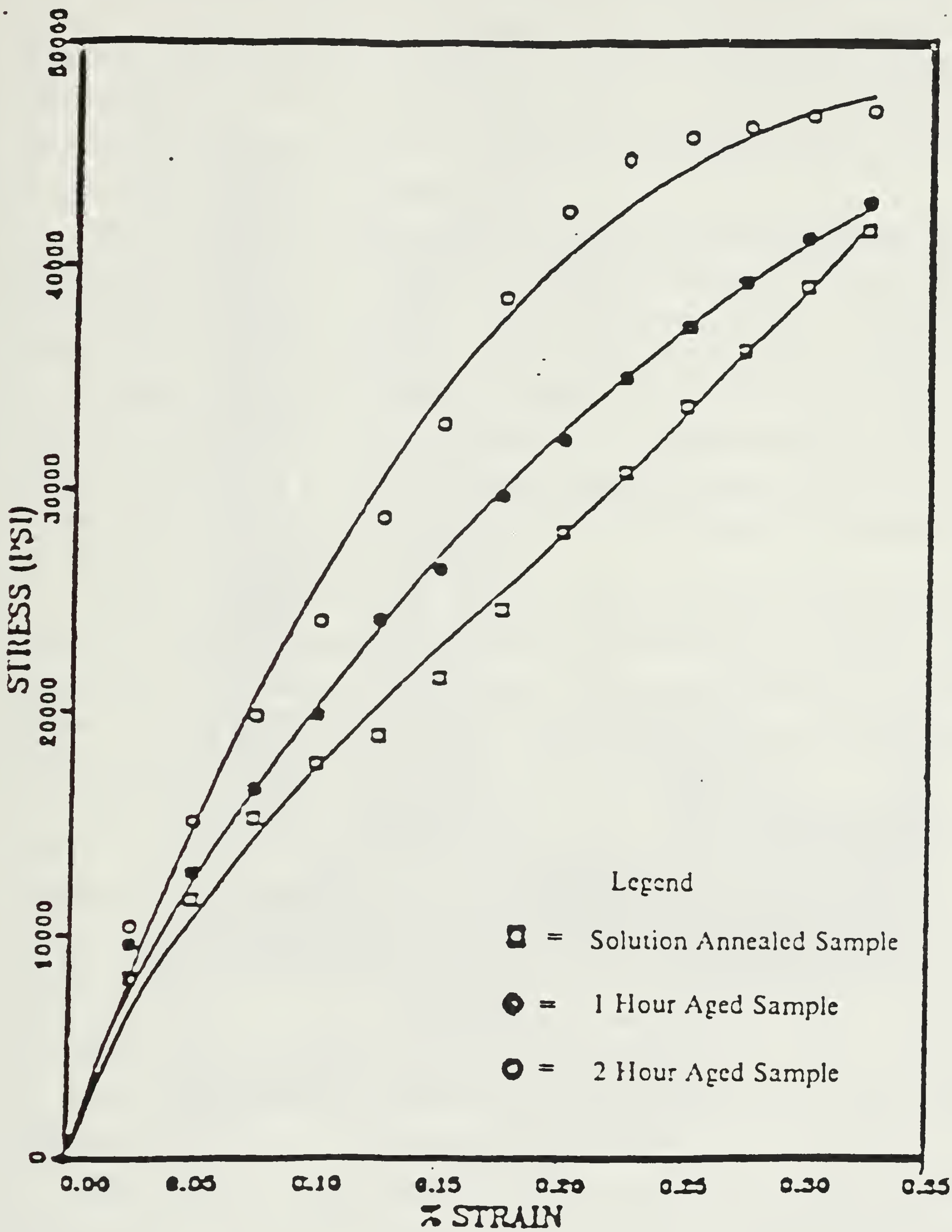

Figure 2.1 Stress/Strain Curves for Sonoston

```
      IMPLICIT REAL (M)
      DIMENSION B(4),A(4)
      READ(5,20)B
      READ(5,20)A
      DO 200 J=1,4
      WRITE(6,229)
      WRITE(6,230)J
      WRITE(6,228)
      S=B(J)
      AR=A(J)
      DO 300 I=1,101
      X=FLOAT(I-1)/100.0
      C=SIN(S)
      D=SIN(S*X)
      E=SINH(S)
      F=SINH(S*X)
      G=COS(S)
      H=COS(S*X)
      P=COSH(S)
      Q=COSH(S*X)
C   SLOPE=AR*S*((C-E)*(H-Q)-(G+P)*(D+F))
      MOMENT=-AR*S*S*((C-E)*(D+F)+(G+P)*(H+G))
C   BENDING STRAIN=(MC)/(EI)
C   IN THIS CASE C=0.0625 IN.; E=12*10**6; I=81.3802*10**-6
      STRAIN=(MOMENT*0.0625)/976.5624
      WRITE(6,225)X,MOMENT,STRAIN
      WRITE(6,227)
300   CONTINUE
200   CONTINUE
230   FORMAT('*****MODE #', I1,'*****')
225   FORMAT(' X/L=',F4.2,5X,'MOMENT=',F22.8,5X,'STRAIN=',F18.8,/)
227   FORMAT('****************************************************')
229   FORMAT(/////,'**********************************************')
228   FORMAT('**********************************************',/////)
20    FORMT(F16.4)
      STOP
      END
```

Figure 2.2 Fortran Program for Location of Maximum Strain

For mode 1 the maximum moment occurs at the root; for mode 2 it occurs at the root and at X/L=0.53; for mode 3 it occurs at the root, X/L=0.31, and at X/L=0.71. In all three modes the maximum moment occurs at the root of the beam and for mode 3 the moment at X/L=0.71 was greater than at X/L=0.31. Based on this information the three strain gages were mounted on all the cantilever beams at a) the root, b) at X/L=0.53, and c) at X/L=0.71 (Figure 2.3).

The beam samples were then placed in the test fixture for testing (Figure 2.4). By monitoring the acceleration of both the supporting system and the beam tip, the response frequency can be determined. Two 4-mg Endevco 2250A-10 accelerometers were mounted, one on the supporting structure above the root of the cantilever beam and the other on the tip of the beam (Figure 2.5). A random input signal was generated by the HP 3582 spectrum analyzer and was then passed through the Crown solid state amplifier to the electromechanical vibration generator (Figure 2.6). The accelerometer output was passed through a Endevco 4416A Signal Conditioner to the HP 5451-C Fourier Analyzer for processing.

To get an initial idea where the specimen's natural resonant frequencies lie in the frequency spectrum, a baseband measurement was made from 0 to 1KHz. These measurements for the solution treated sample, 1 hour aged sample, and 2 hour aged sample are shown in Figures 2.7 to 2.9. Use of Band Selectable Fourier Analysis (BSFA or zoom) was then used on the first three resonant frequencies.

The RMS input acceleration level (root accelerometer) was determined as follows: A signal in the time domain was captured for a 5mSec period (Figure 2.10), squared and then integrated for the period. The square root was then calculated and multiplied by the conversion factor to obtain mv. Ten time samples were taken for an average value. This value was then converted to g by dividing by a calibration factor (10.31 mv/g) which was determined as described in section C of this chapter. This gives the RMS g level. The RMS strain level was determined in the same way. In this case the strain signal was sent through an Ectron (model 563F) .strain gage amplifier calibrated so that 2.5V dc = 10,000µstrain. (Figure 2.11)

Swept sine tests were performed using the HP-3562A Signal Analyzer. Measurements of input acceleration and strain were made in the same way except that, since the strain and input force varies with frequency, the time domain data was obtained at the peak of the transfer function.

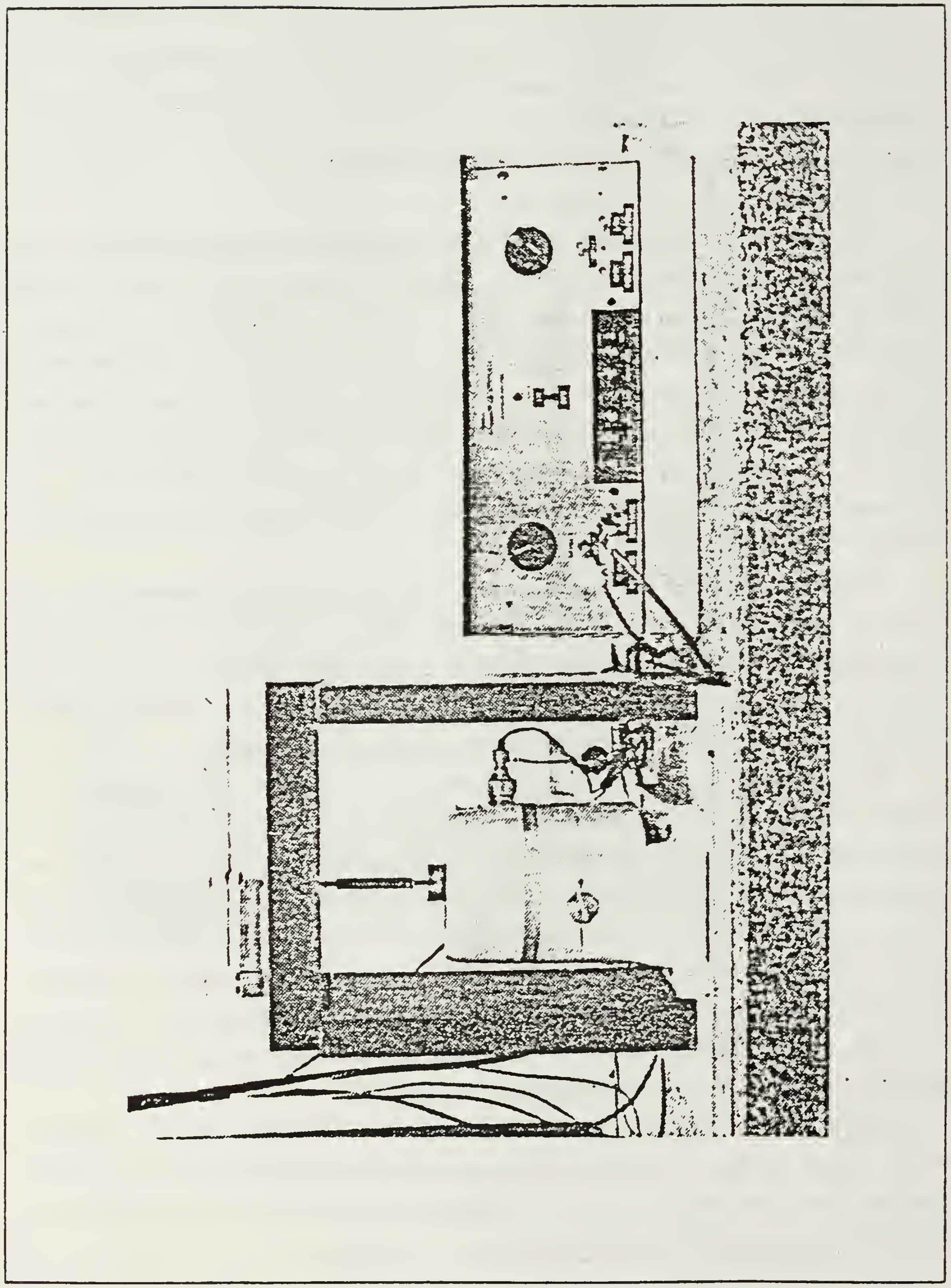

Figure 2.4   Cantilever Beam Test Fixture

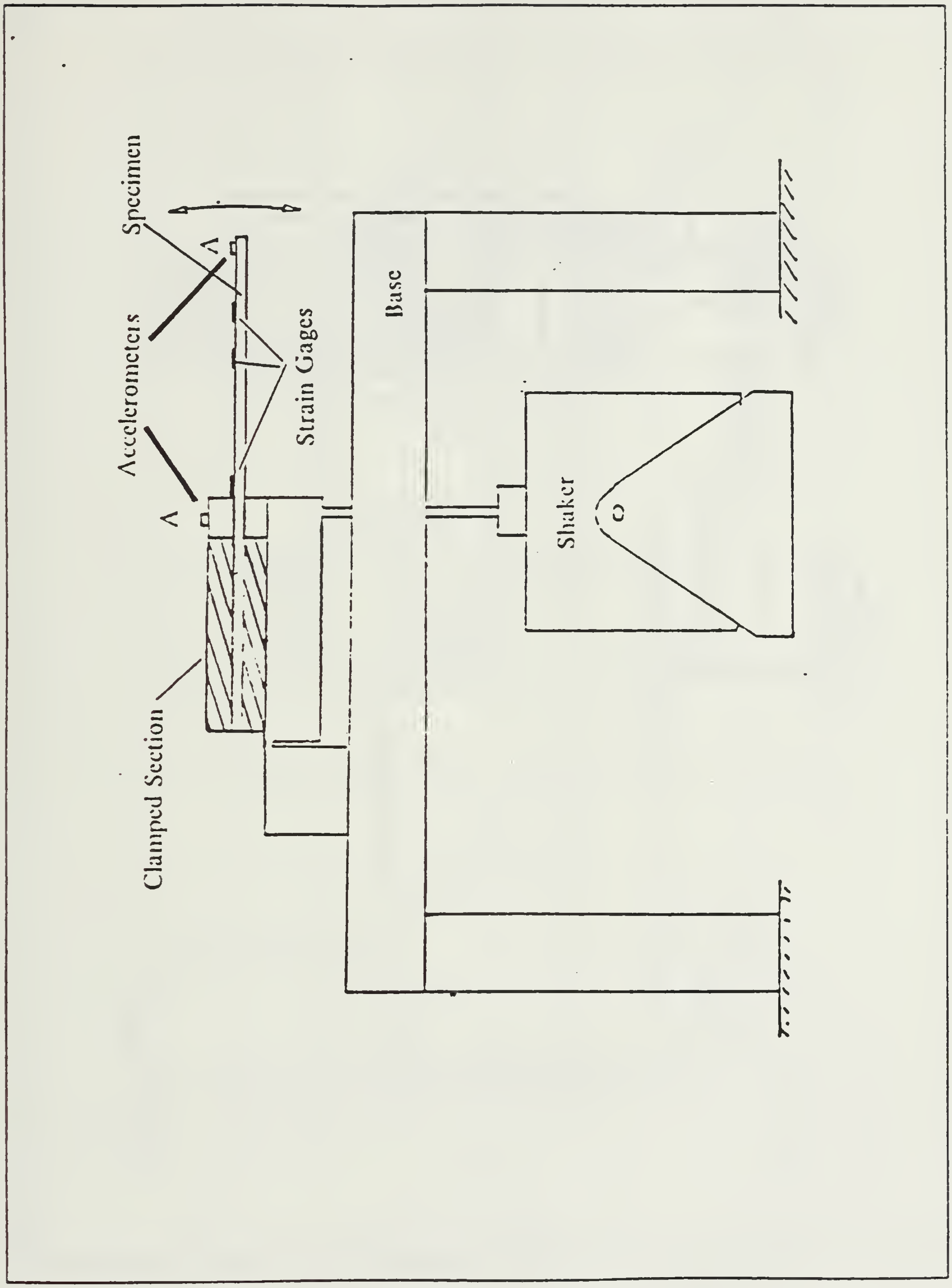

Figure 2.5 Accelerometer Location

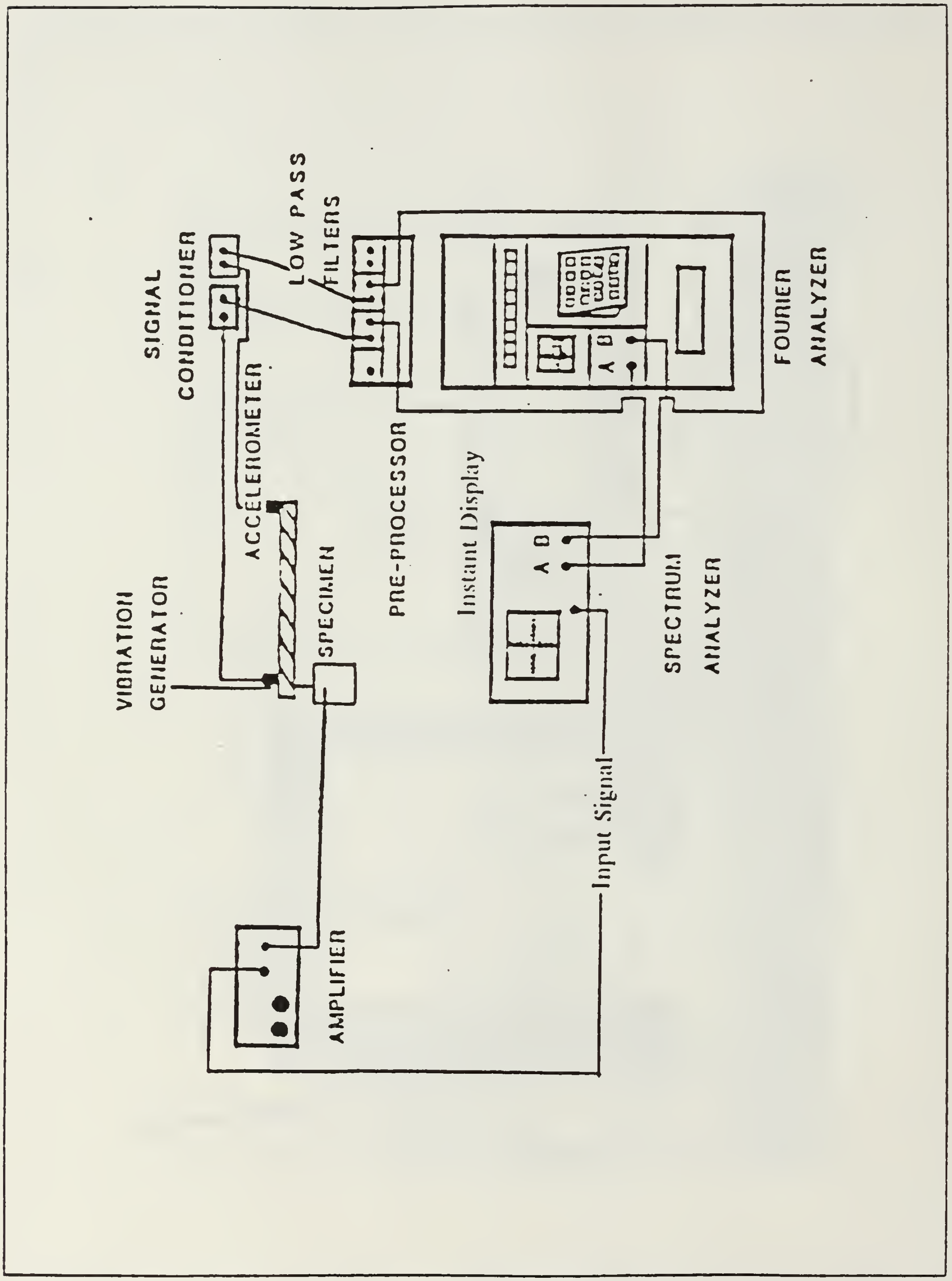

Figure 2.6 Equipment Line Diagram

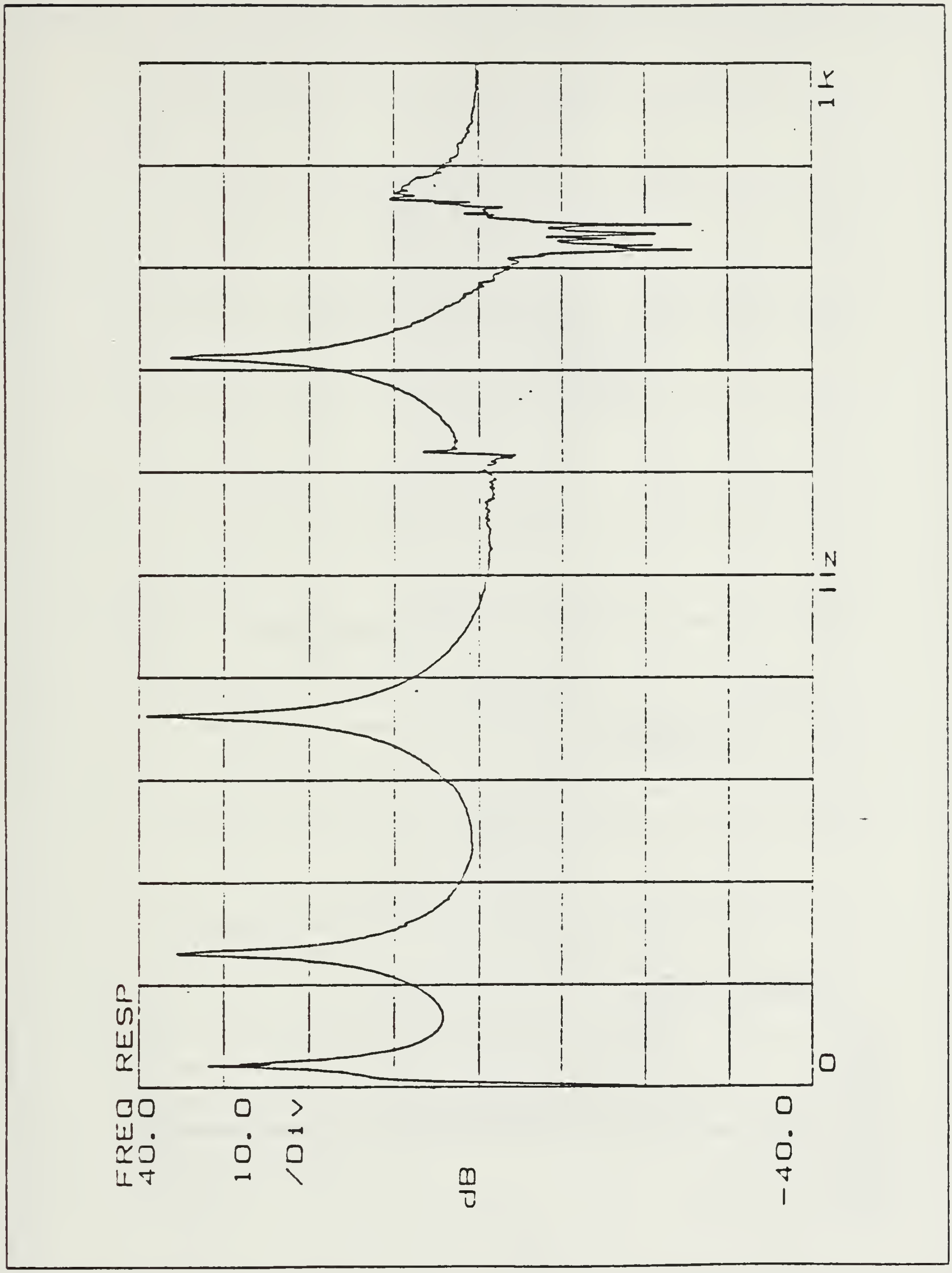

Figure 2.7 Baseband Measurement of the Solution Annealed Sample

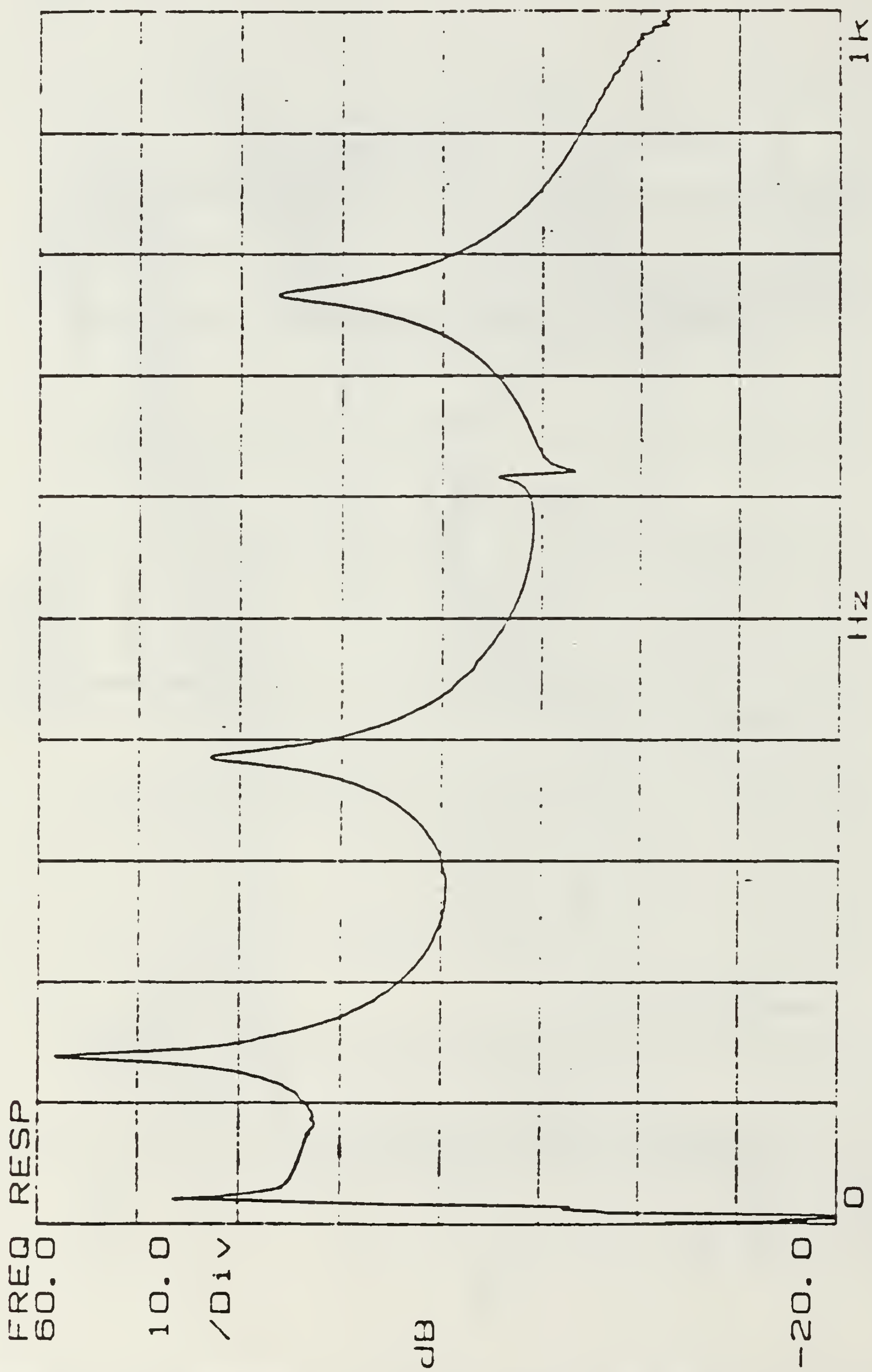

Figure 2.8 Baseband Measurement of the 1-Hour Aged Sample

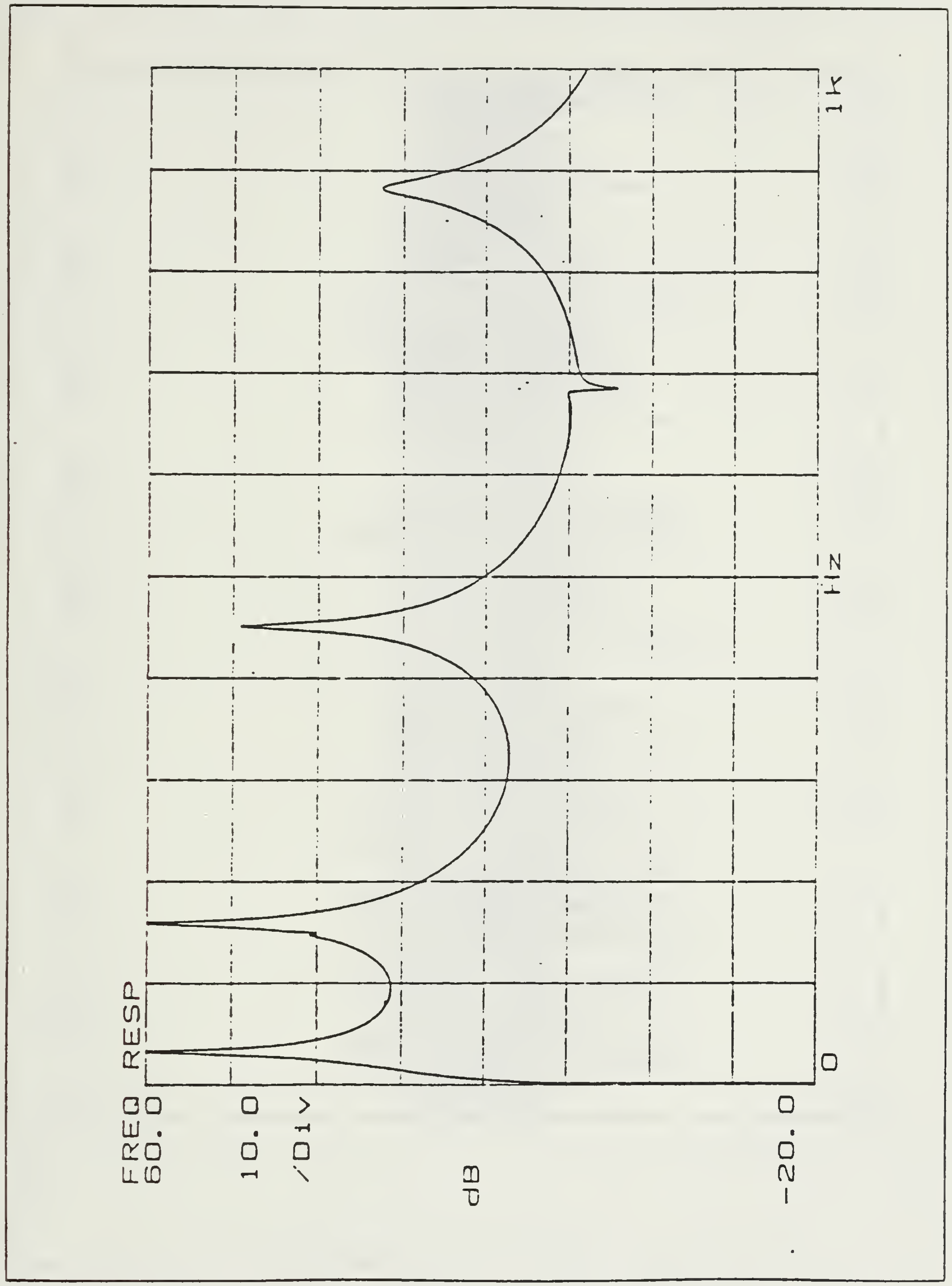

Figure 2.9 Baseband Measurement of the 2-Hour Aged Sample

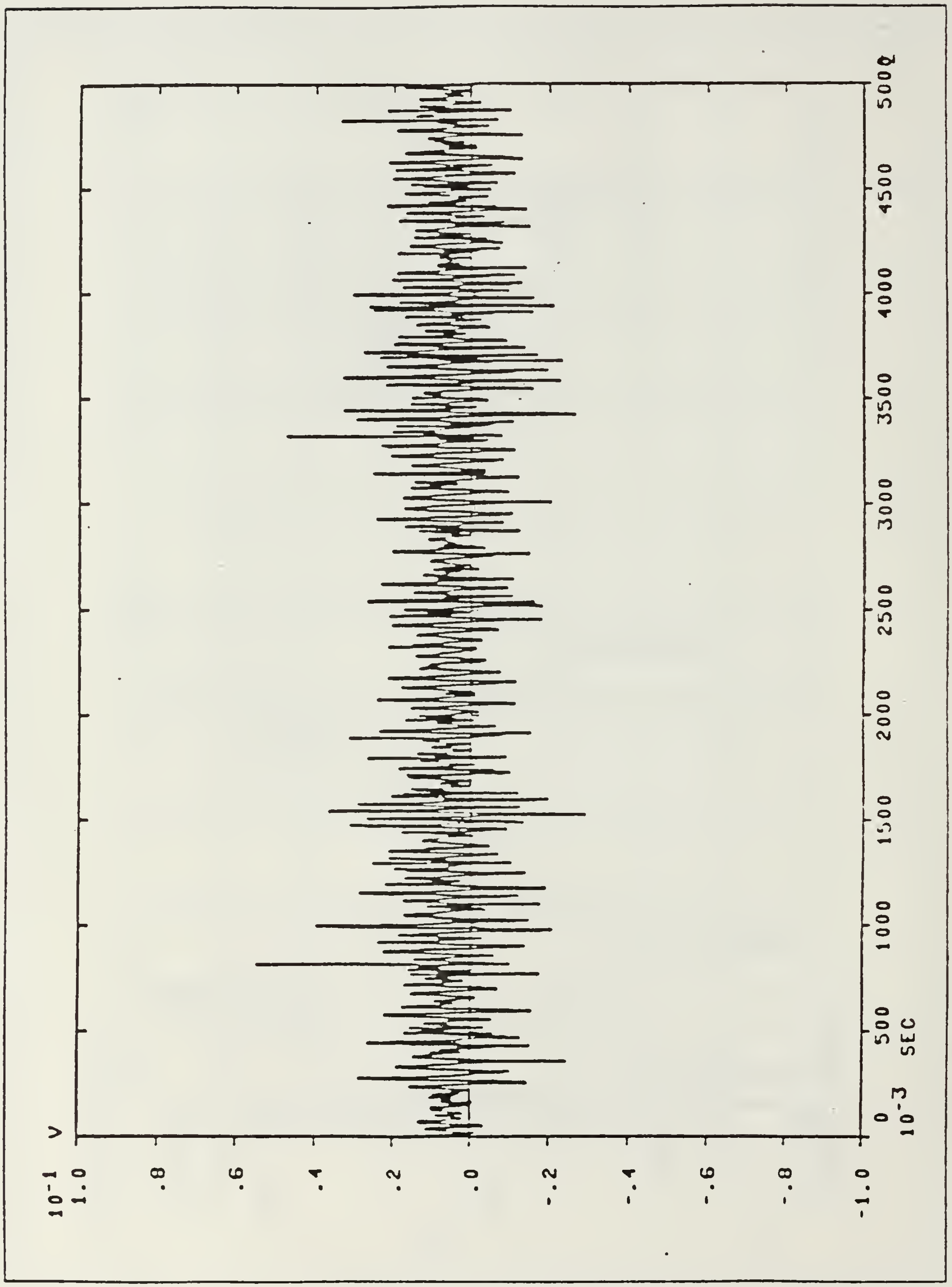

Figure 2.10 Time Sample of the Input Accelerometer

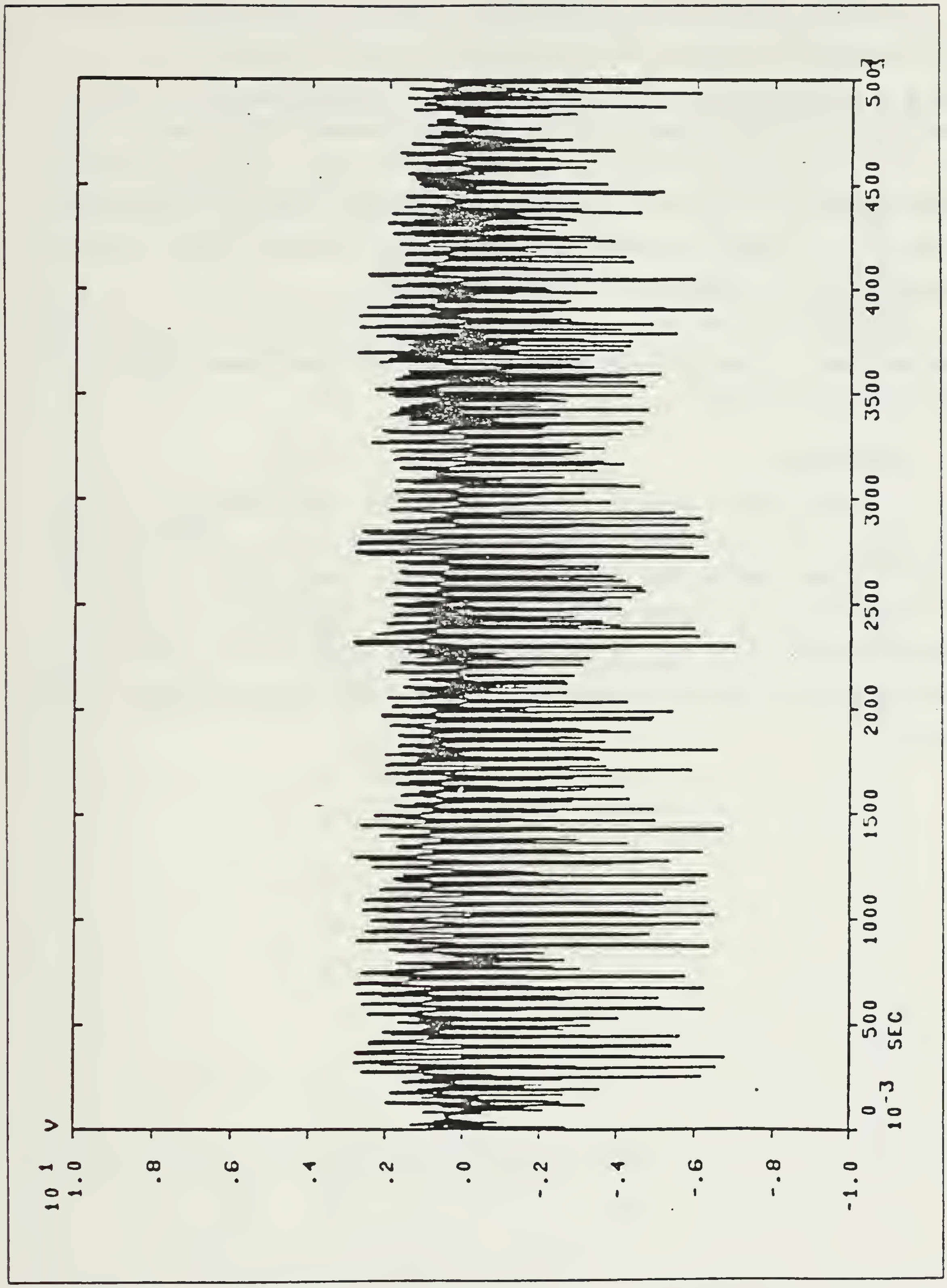

Figure 2.11 Time Sample of the Root Strain Gage

During the random input tests the output accelerometer was removed and the root strain gage was used as the output device in order to test the effect of mass loading of the beam by the 4 mg accelerometer. The resulting transfer function corresponded to that obtained by using two accelerometers. Both had the same resonant frequency and very similar loss factors but different function amplitudes (Figures 2.12 and 2.13). Since there is no mass loading effect due to the accelerometer at the tip of the beam, transfer functions could be obtained using either two accelerometers or one accelerometer and the strain gage.

Each mode was analyzed at six different amplification levels with two transfer functions being obtained at each level. Random noise tests were analyzed first followed by swept sine tests.

C. CALIBRATION

The accelerometers used in the experiment were calibrated by a drop test (free-fall) to obtain the value of mv/g associated with each accelerometer. The HP-3562A Signal Analyzer was used to record the time signal trigger delay. Figures 2.14 and 2.15 show the results of one calibration run. Figure 2.15 is a blown up portion of Figure 2.14 showing just the free-fall voltage difference due to gravity. The voltage difference between the initial state and the first peak corresponds to 1g acceleration.

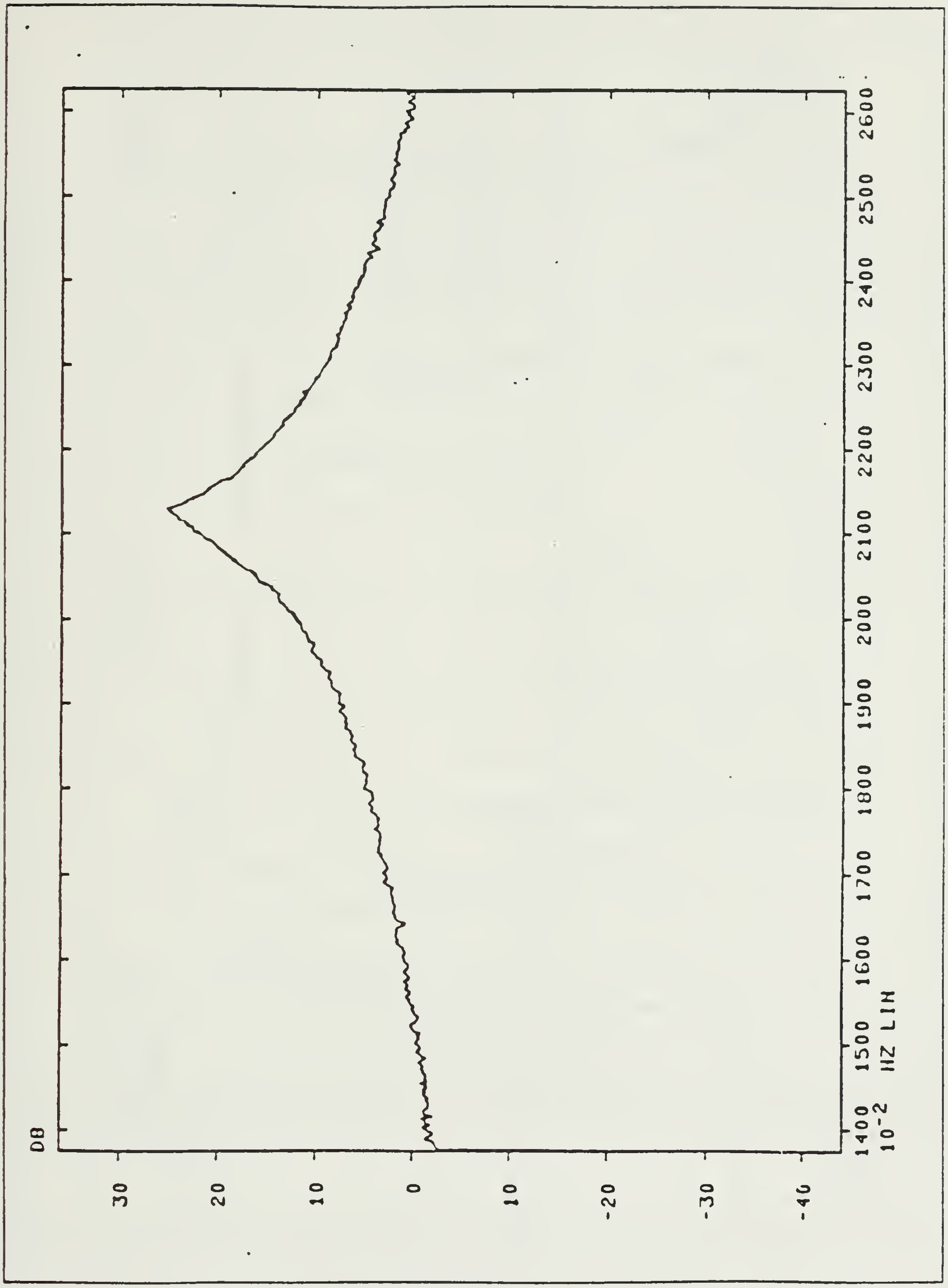

Figure 2.13 Accelerometer/Strain Gage Transfer Function

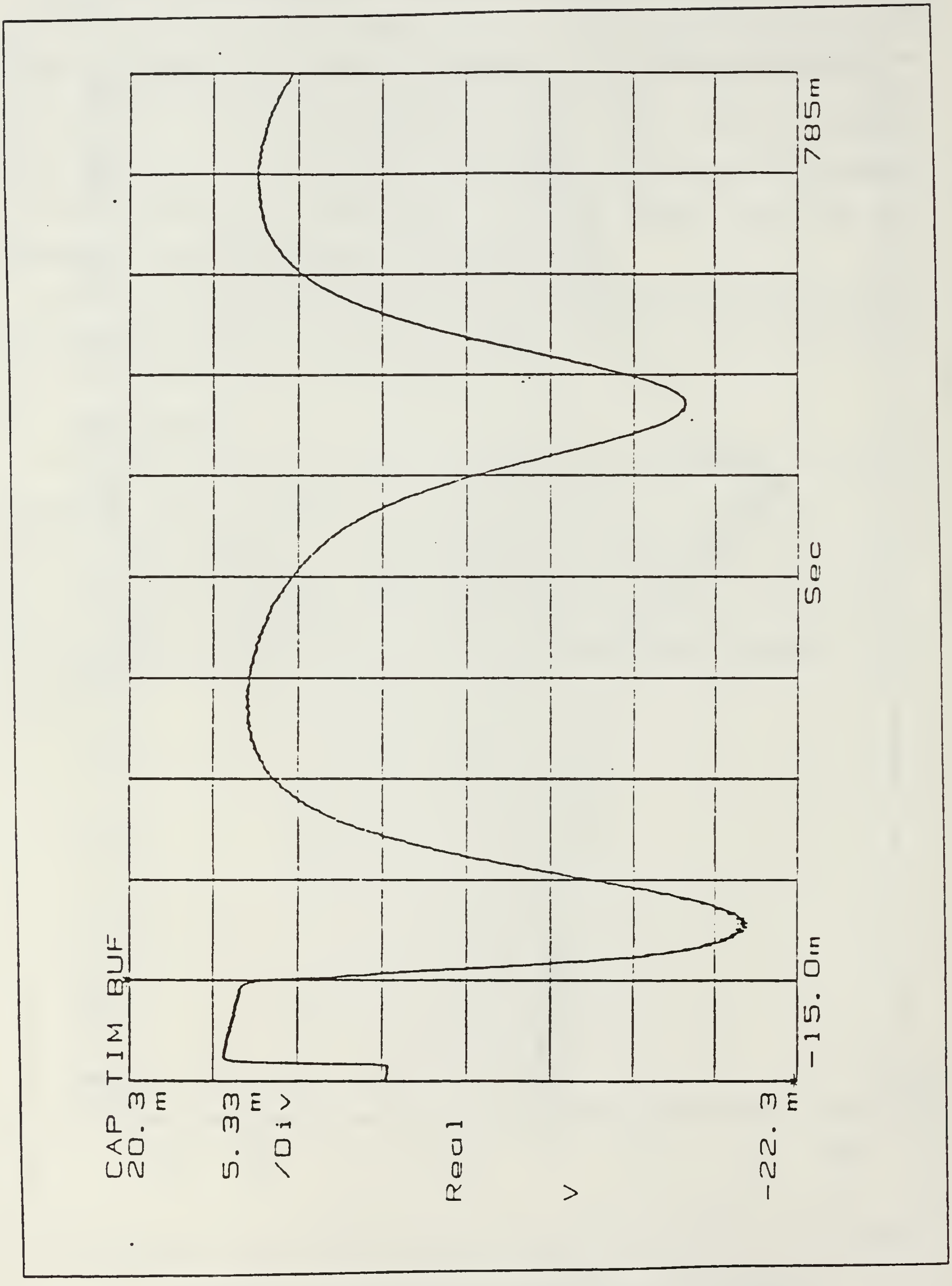

Figure 2.14 Calibration Curve

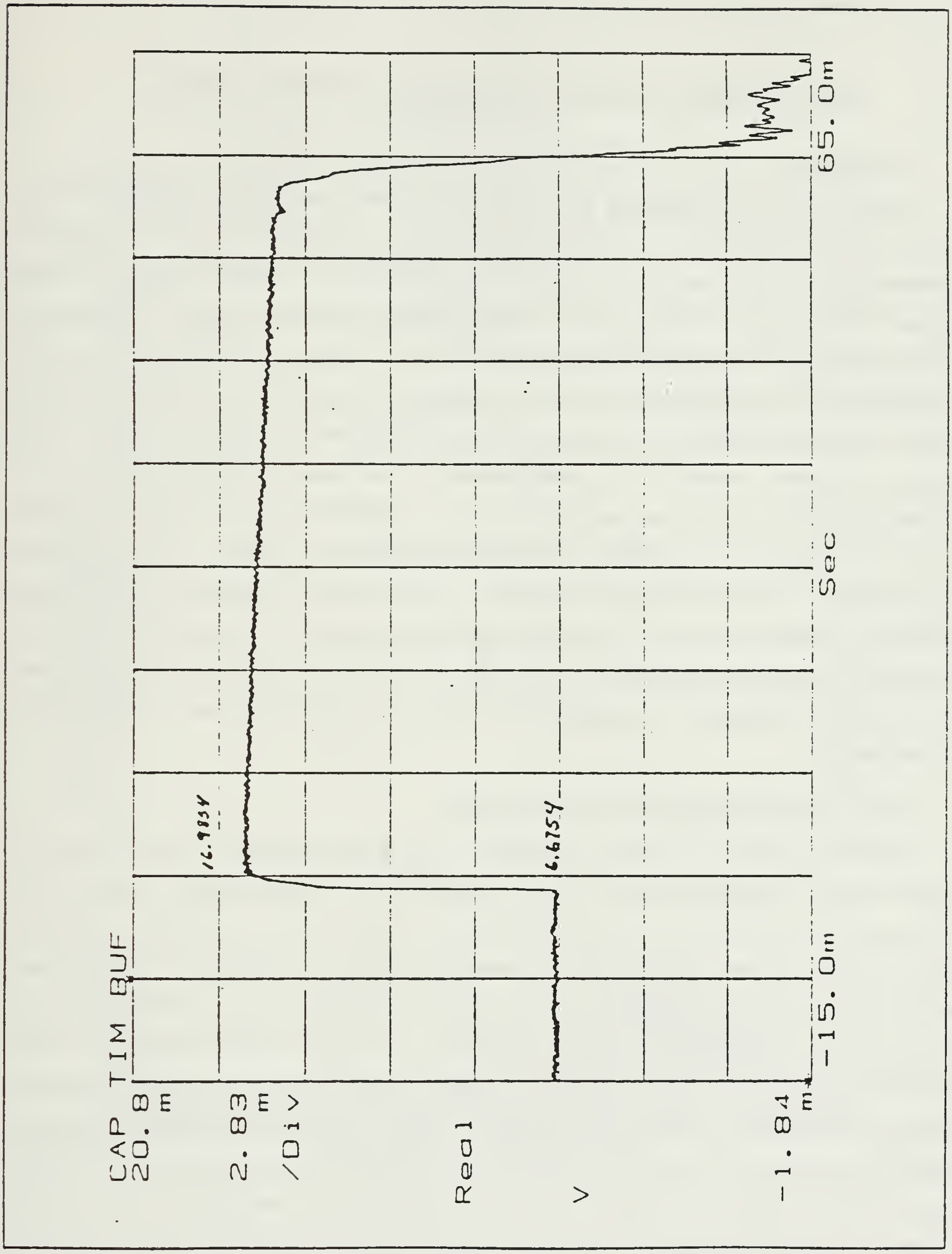

Figure 2.15 Free-fall Section

III. CANTILEVER BEAM RESULTS AND DISCUSSION

A. GENERAL

The cantilever beam samples give results in the frequency ranges 20-25 Hz (Mode 1); 130-160 Hz (Mode 2); and 360-445 Hz (Mode 3). Appendix D (part 1) shows a representative transfer function, in both log magnitude and linear scales, that was obtained after 32 time averages using a random input excitation source. A graph of the associated 180^{o} phase shift, characteristic of a two complex pole system, is also in the appendix. The phase shift can give an indication of the loss factor when compared to other phase shift graphs since a gradual slope is indicative of a high loss factor. The coherence function, which is a measurement of the noise contamination and/or nonlinearity in the transfer function indicates how much of the system output is caused by the system input. A representative graph of the coherence function is also included in Appendix D. The dip in the coherence at the resonant frequency is due to the impedance mismatch between the output and input signals. The collected data from the random input and swept sine tests are listed in part 1 of Appendix E. These tables list the resonant frequency, computed loss factor, average strain, and average input acceleration.

B. INPUT ACCELERATION -VS- STRAIN

Figure 3.1 shows the Input Acceleration -vs- RMS Strain for Mode 1 using a random input. This RMS Strain value is determined from the average of ten 5mSec time samples taken from the root strain gage. The input acceleration value is determined in the same manner. Each sample was tested at six different amplification levels and shows that the strain increases with an increase in input acceleration in a linear fashion. It appears that the unaged and 1 hour aged samples follow the same trend while the strain for the 2 hour aged sample increases faster for smaller increases in input acceleration. Figure 3.2 is a graph of Input Acceleration -vs- Strain using a swept sine excitation source. The swept sine test was performed using the HP-3562 Signal Analyzer. The HP-3562 was set for 8 averages and a resolution of 400 points per sweep. The strain value in this case is obtained at the resonant frequency as is the input acceleration. In both tests, random and swept sine, the strain increases with input acceleration as expected. Figures 3.3 to 3.6 are graphs of Input Acceleration -vs-Strain for modes 2 and 3. In both mode 2 and mode 3 the strain increases as the input

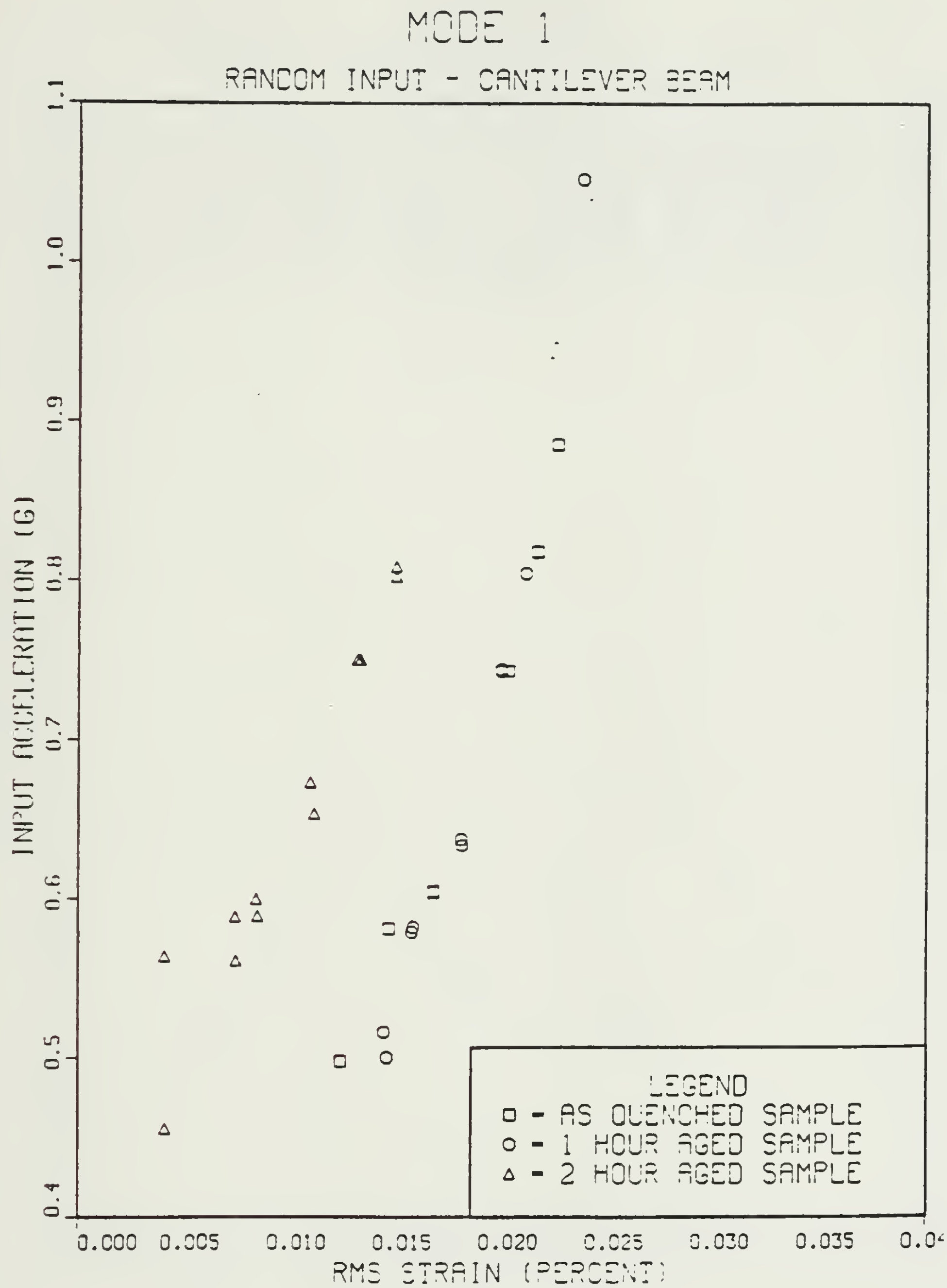

Figure 3.1 Mode 1 - Input Acceleration -vs- Strain
(Random Input)

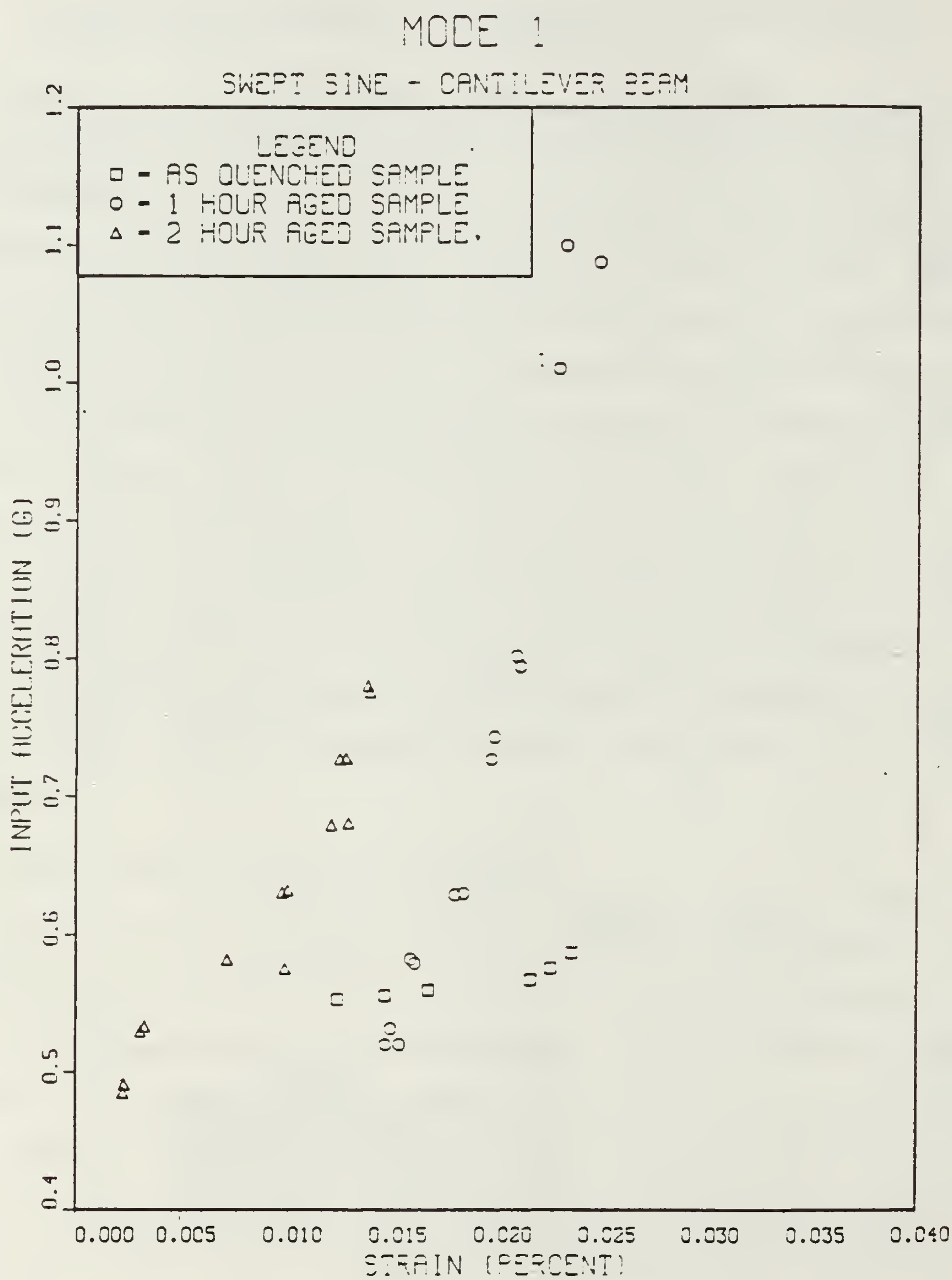

Figure 3.2 Mode 1 - Input Acceleration -vs- Strain
(Swept Sine)

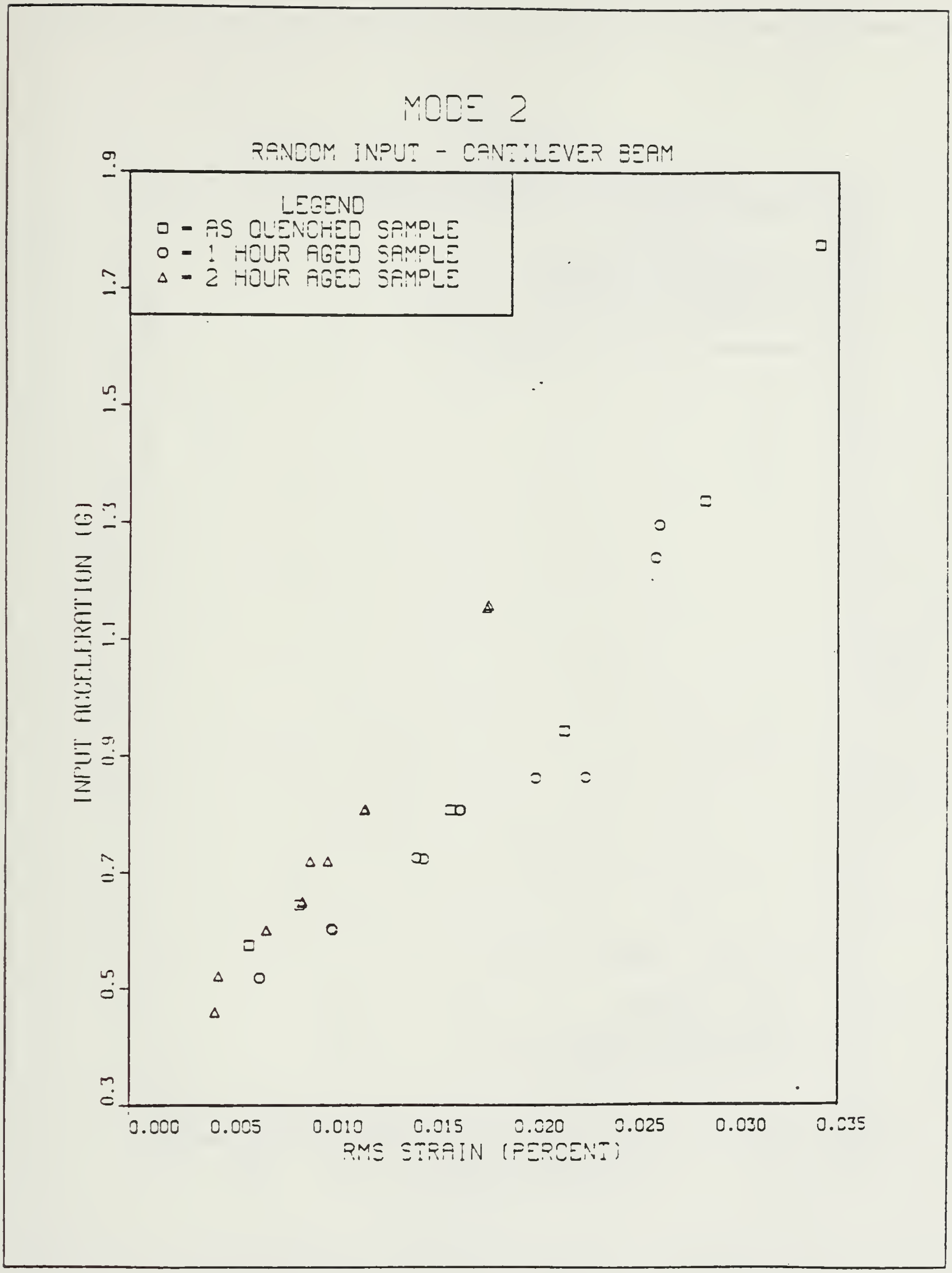

Figure 3.3 Mode 2 - Input Acceleration -vs- Strain (Random Input)

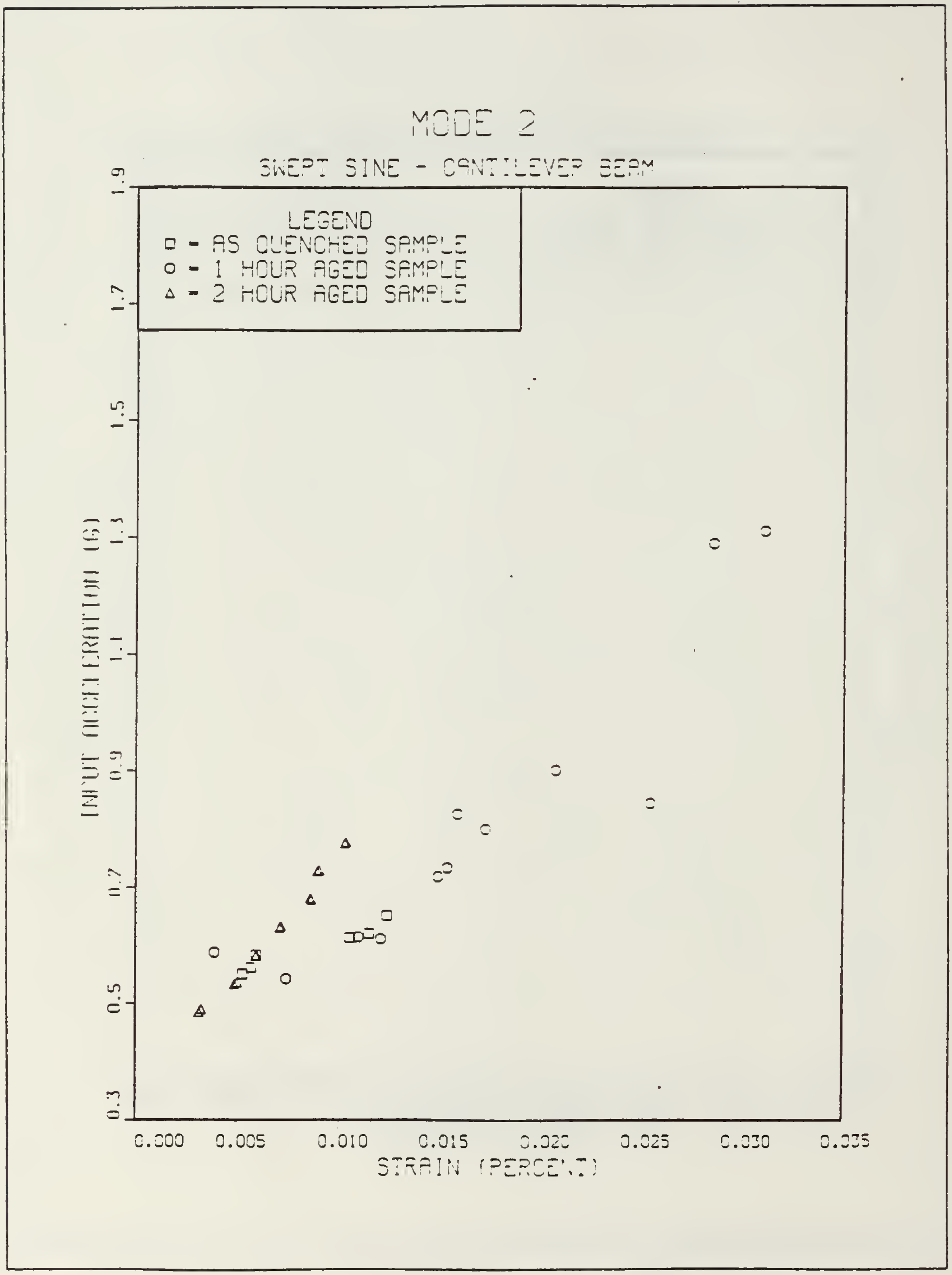

Figure 3.4 Mode 2 - Input Acceleration -vs- Strain (Swept Sine)

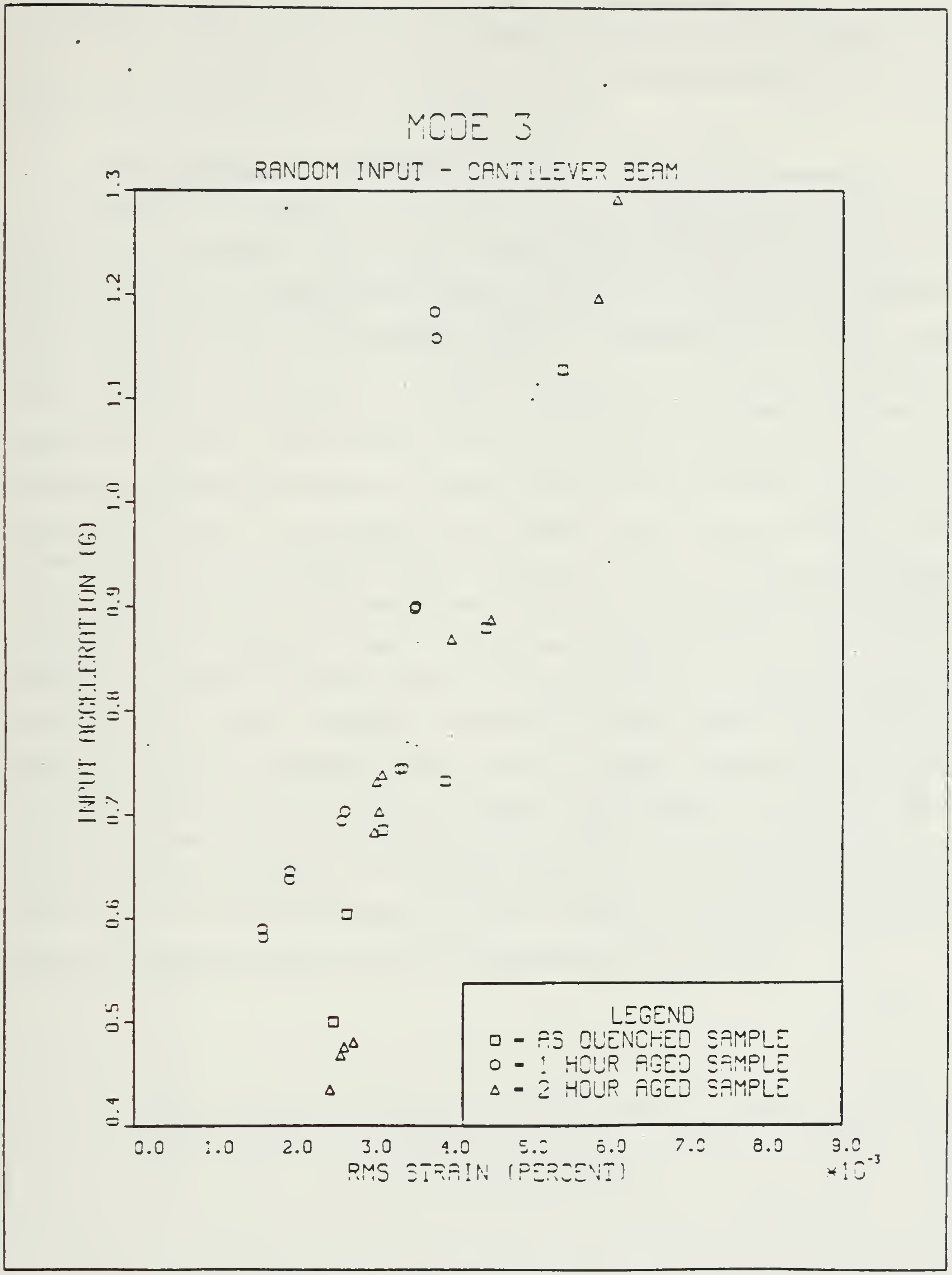

Figure 3.5 Mode 3 - Input Acceleration -vs- Strain
(Random Input)

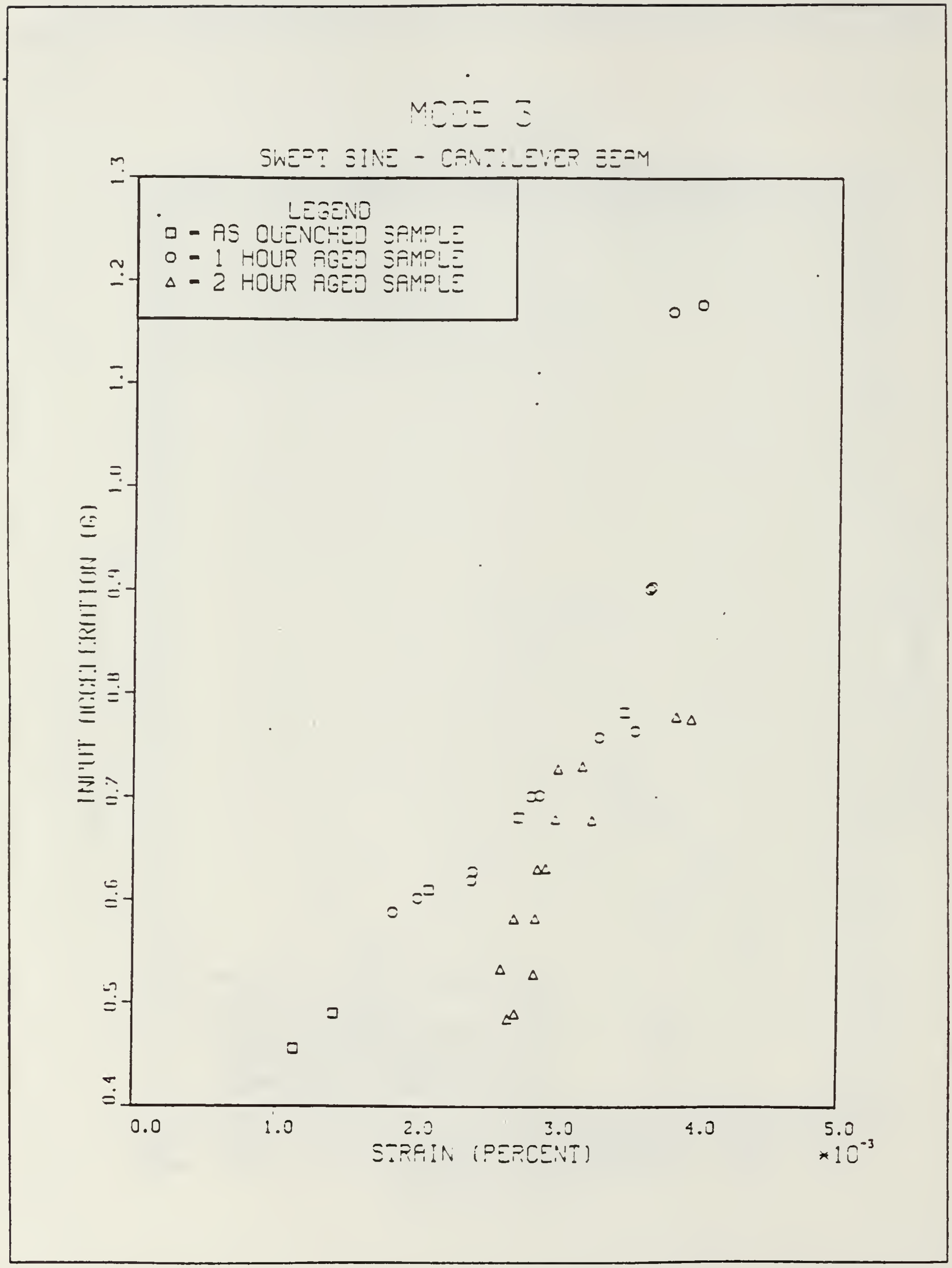

Figure 3.6 Mode 3 - Input Acceleration -vs- Strain (Swept Sine)

acceleration increases and seems to be consistent between the random tests and the swept sine tests. The root strain gage was used for all measurements as it gave the highest value of strain for all three modes.

C. LOSS FACTOR -VS- STRAIN

Figure 3.7 is a graph of Loss Factor -vs- RMS Strain for mode 1 random input. As the strain increases the loss factor increases. The aging time also plays a factor in the loss factor. As the aging time increases the loss factor increases. It appears that the loss factor of the 2 hour aged sample increases significantly at the 0.015% strain level. This could be due to the non-linearities in the material. Figure 3.8 is the mode 1 swept sine results of Loss Factor -vs- Strain. The results are very similar to those from random input tests. Both excitation sources give quite consistant results for tests repeated under similar conditions. Figures 3.9 and 3.10 are the mode 2 results. The trends seen in mode 1 are repeated here in mode 2 except that the loss factor has a lower value for all of the mode 2 samples. Figures 3.11 and 3.12 are the mode 3 results. As in modes 1 and 2, the loss factor increases with both increasing strain and increased aging time. The damping of mode 3 seems to be comparable with that of mode 2 but both are less than that found in mode 1. From looking at the baseband curves for each of the three heat treatments (Chapter 2), it would appear that the highest damping occurs in the second mode. However, actually measuring the loss factor shows that the first mode is the mode of highest energy dissipation. In all three modes, the random input and swept sine input tests give similar results. For all of the tests the geometry of the sample plays an important part in determining the level of bending strain and its associated loss factor. In order to compare the physical properties of different materials the geometry of the test samples must be the same.

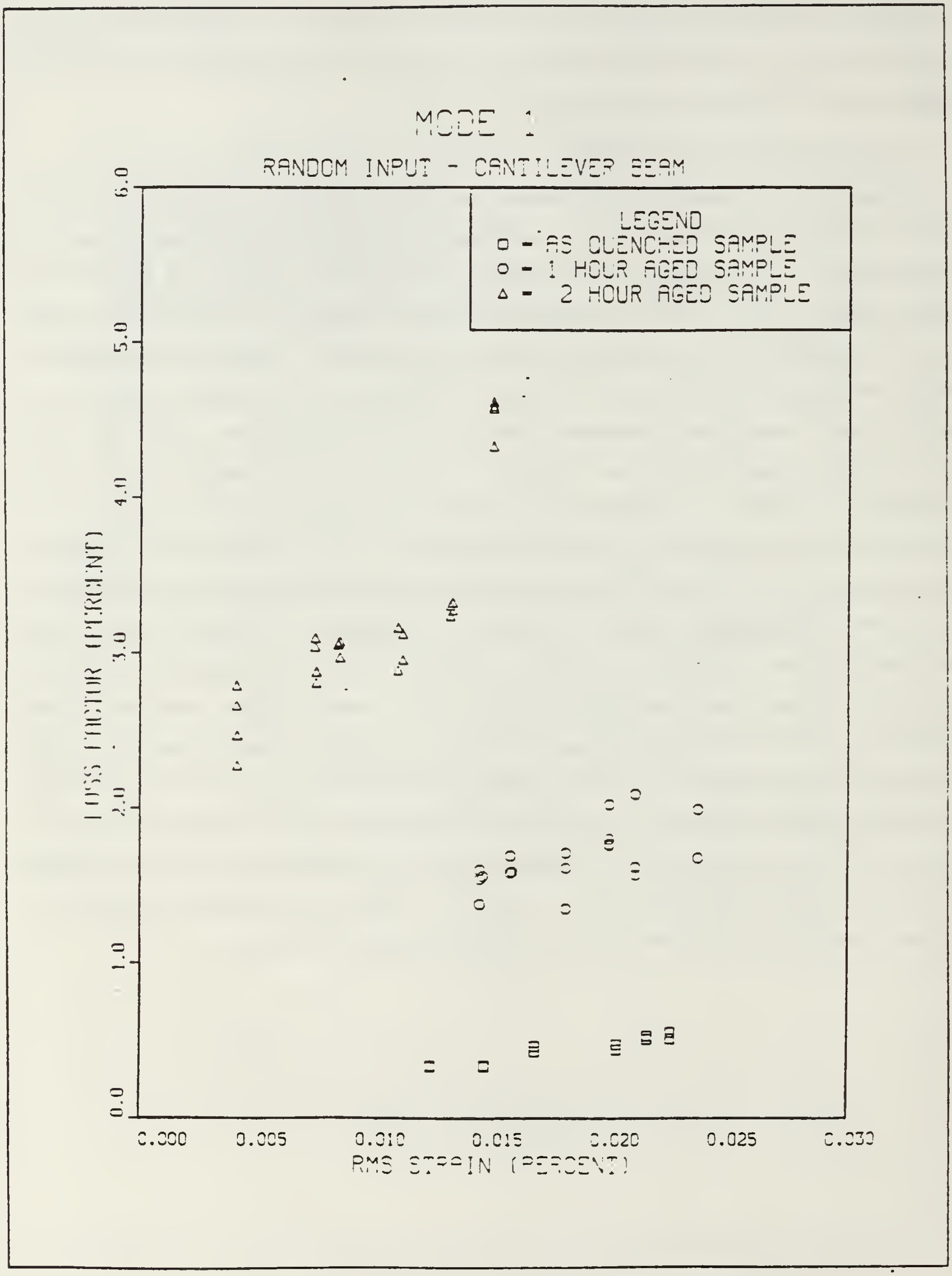

Figure 3.7 Mode 1 - Loss Factor -vs- Strain (Random Input)

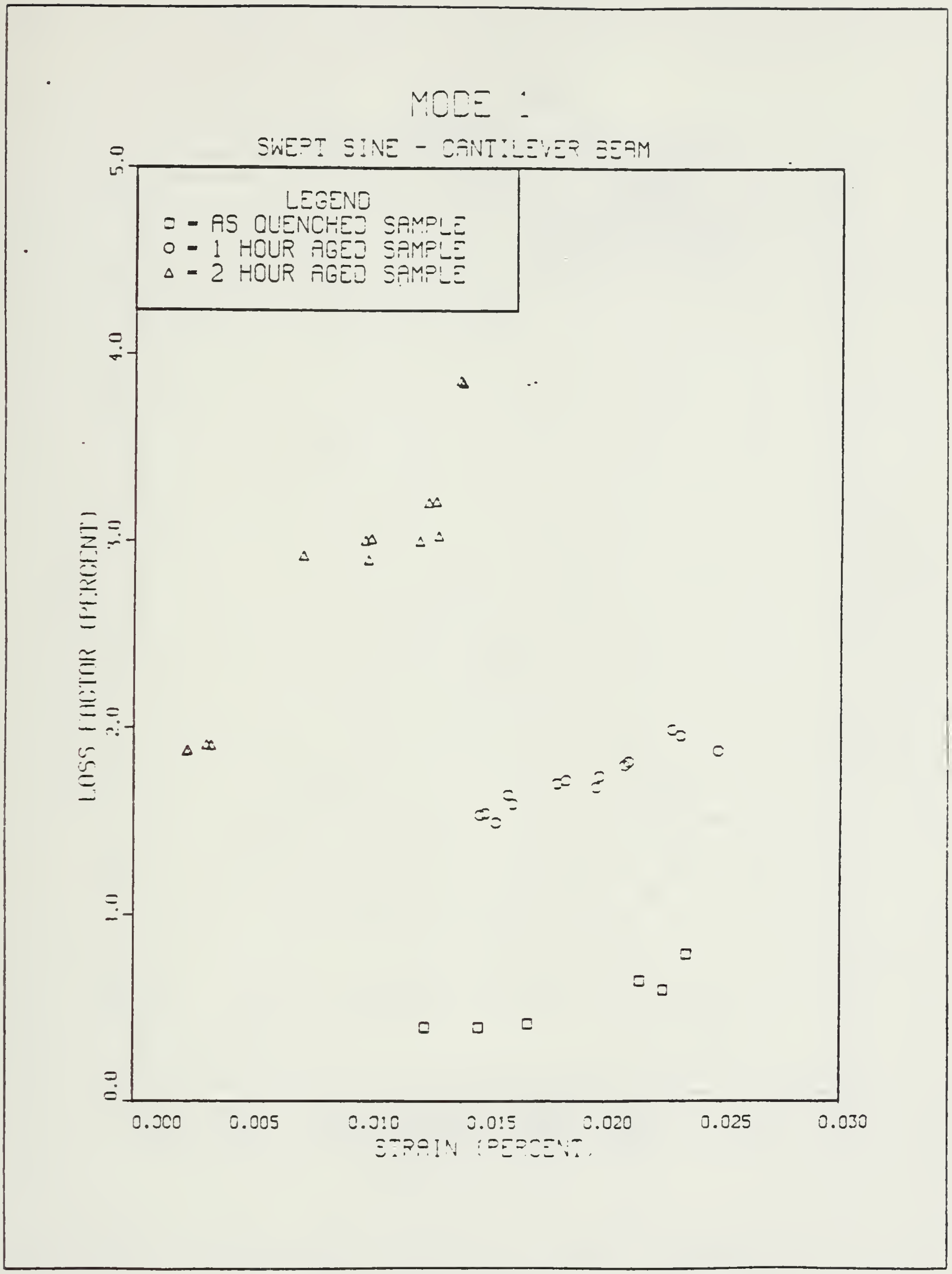

Figure 3.8 Mode 1 - Loss Factor -vs- Strain
(Swept Sine)

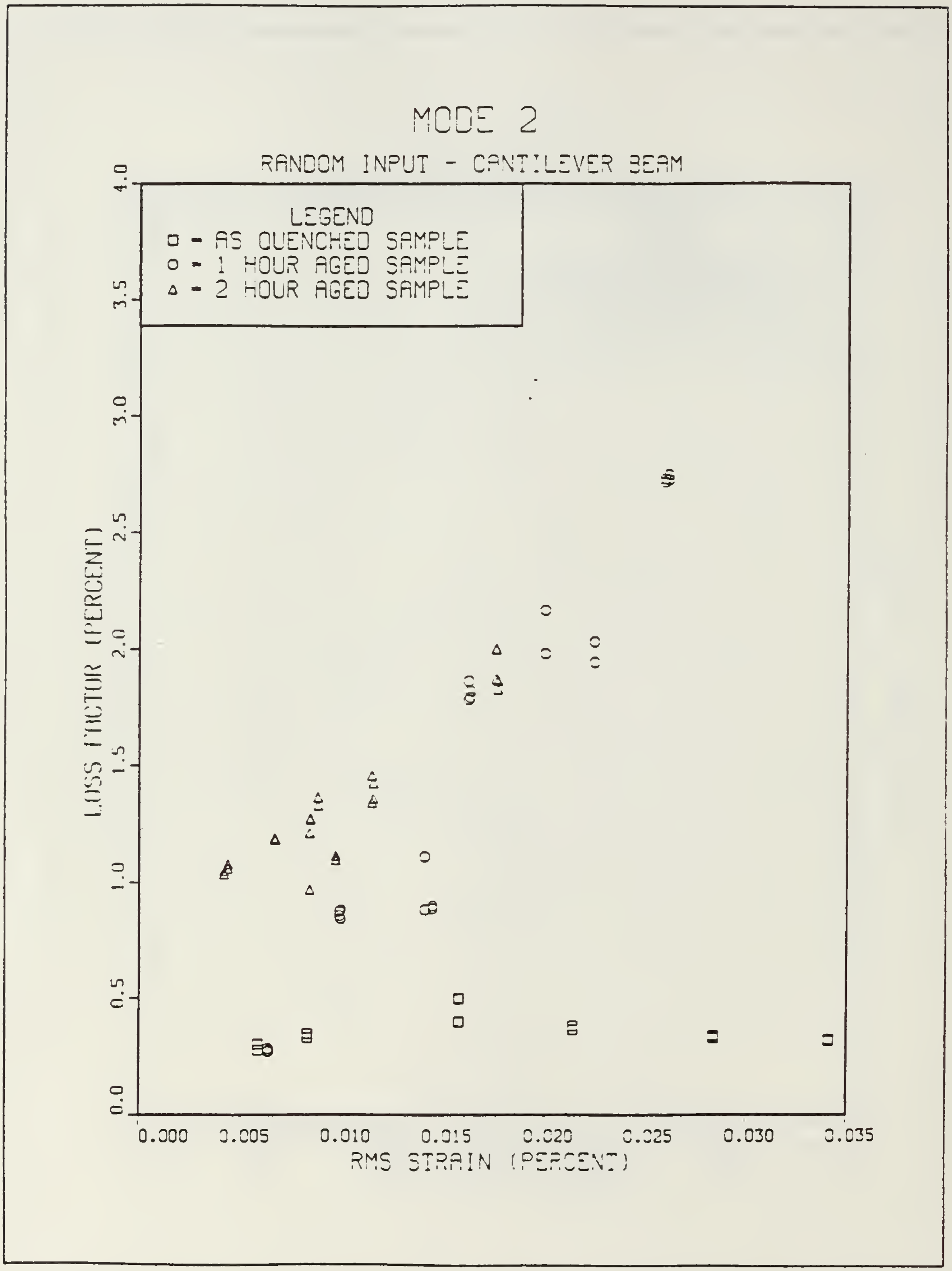

Figure 3.9 Mode 2 - Loss Factor -vs- Strain (Random Input)

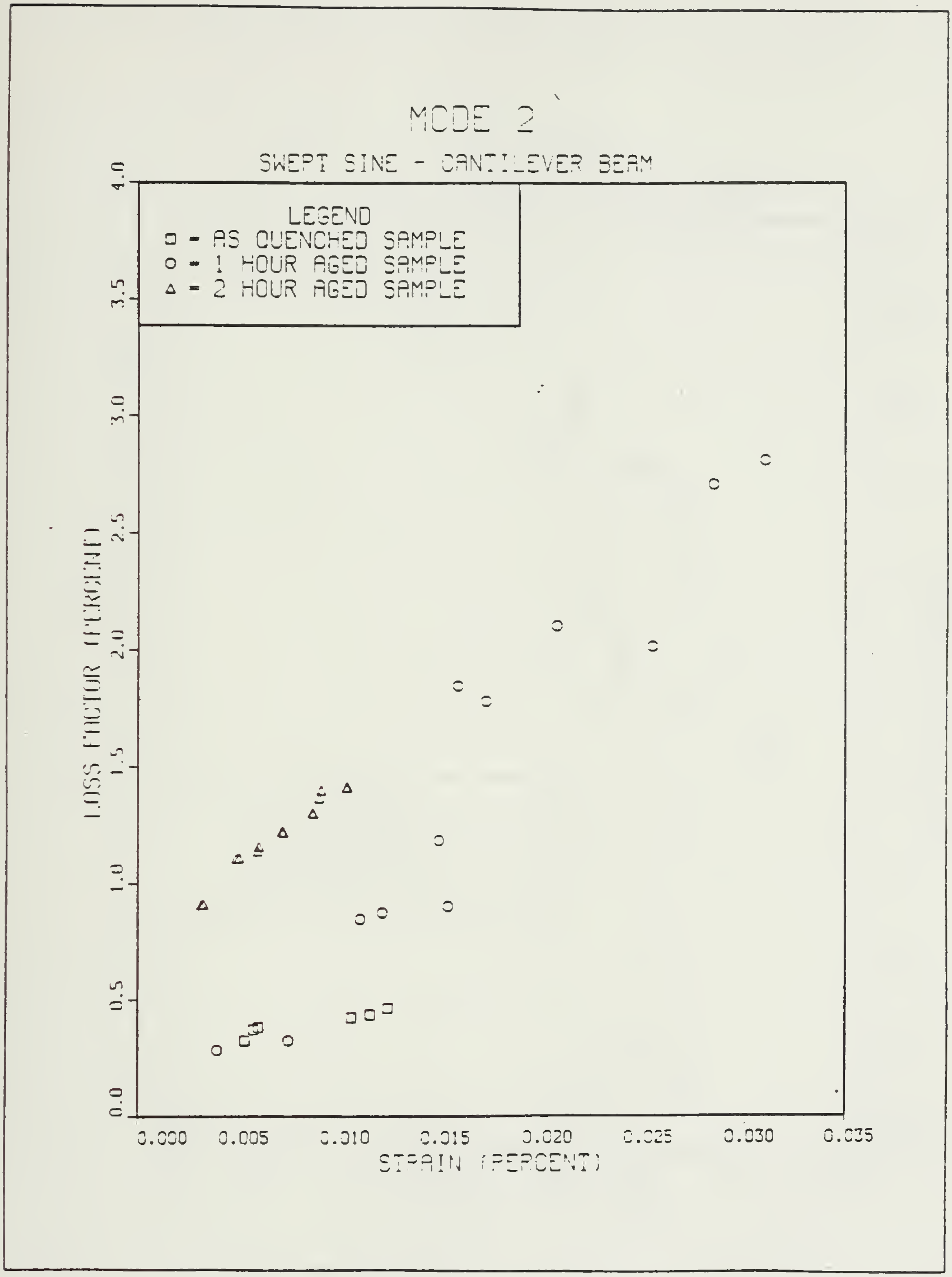

Figure 3.10 Mode 2 - Loss Factor -vs- Strain
(Swept Sine)

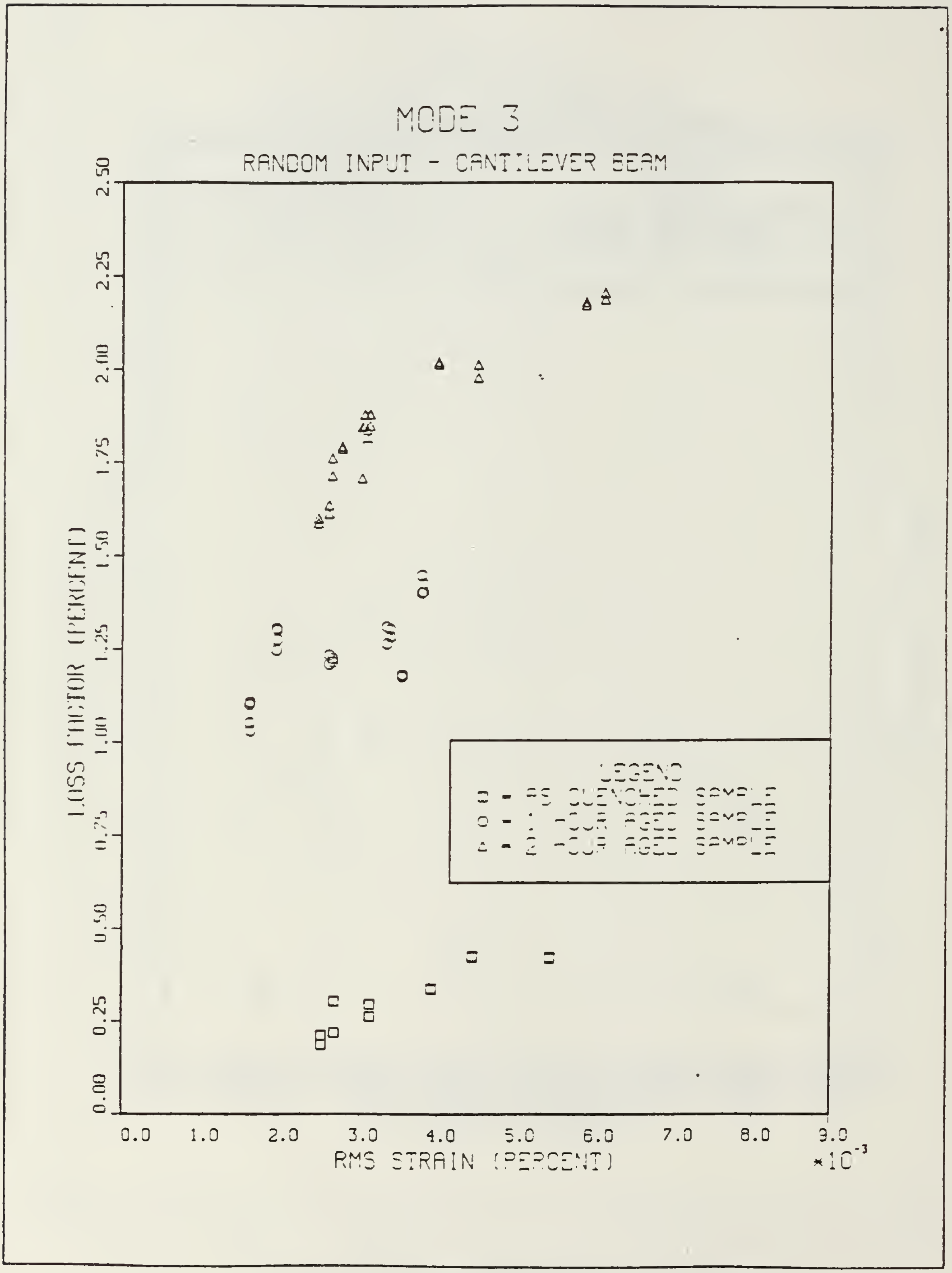

Figure 3.11 Mode 3 - Loss Factor -vs- Strain (Random Input)

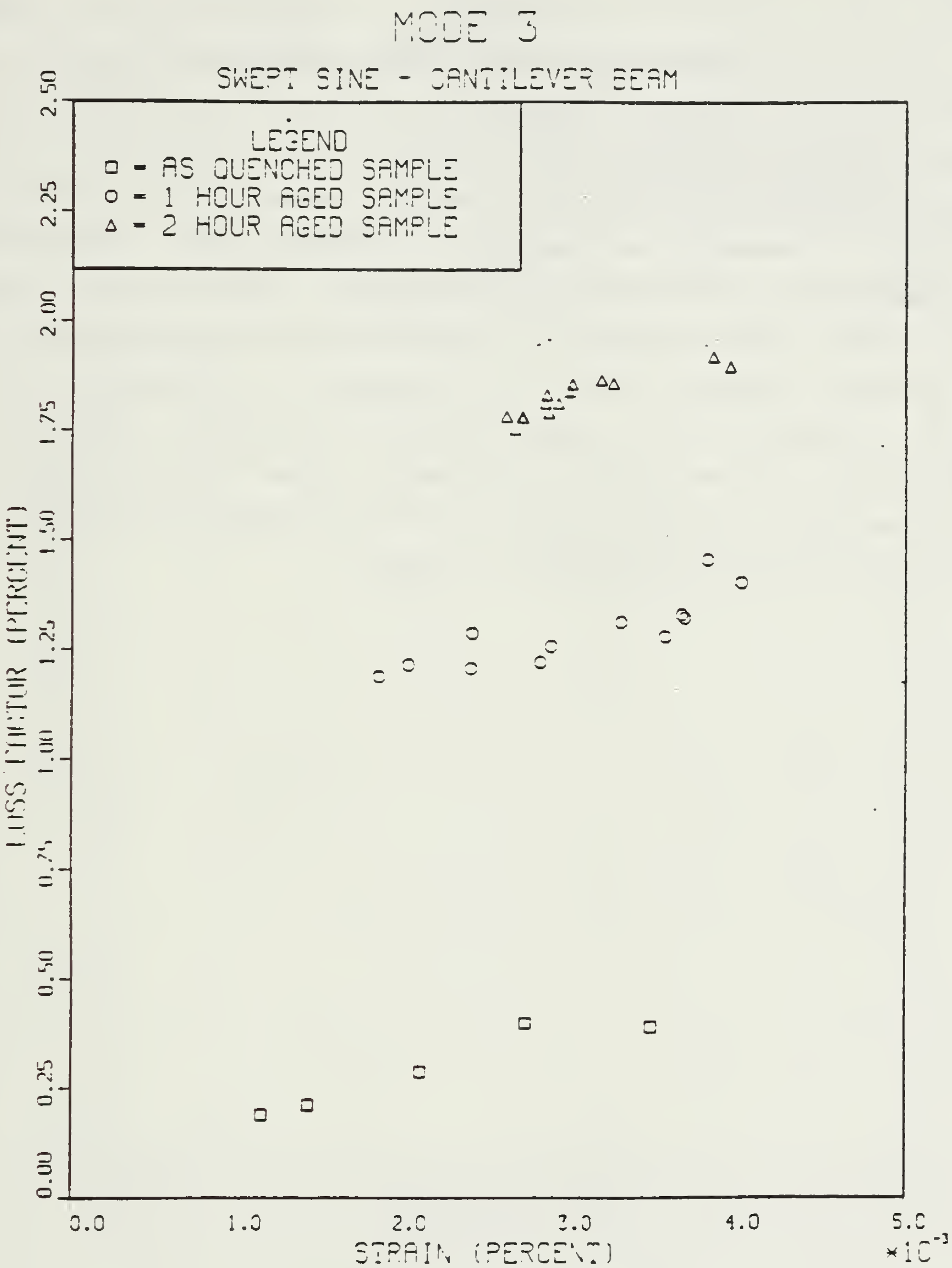

Figure 3.12 Mode 3 - Loss Factor -vs- Strain
(Swept Sine)

D. STRAIN -VS- FREQUENCY

Figure 3.13 is a graph of the RMS Strain -vs- Frequency for mode 1 random input. For all of the samples as the strain increases the resonant frequency shifts downward. This increase in strain corresponds to a decrease in the Young's Modulus (see stress/strain curve in Chapter 2). Since Young's Modulus is needed in calculating the resonant frequency a decrease in E will result in a decrease in resonant frequency (Appendix B). As the aging time increases the downward shift in the resonant frequency becomes more pronounced as the strain increases. Figure 3.14 is the mode 1 swept sine results. Again, the results are comparable with those obtained from the random input tests. Figures 3.15 and 3.16 are the Strain -vs- Frequency results for mode 2. In both figures the 1 hour aged samples show the greatest frequency shift. The results between the two graphs are comparable. Mode 3 results are shown in Figures 3.17 and 3.18. The same downward shift of the resonant frequency as the strain increases appears here as in the other two modes.

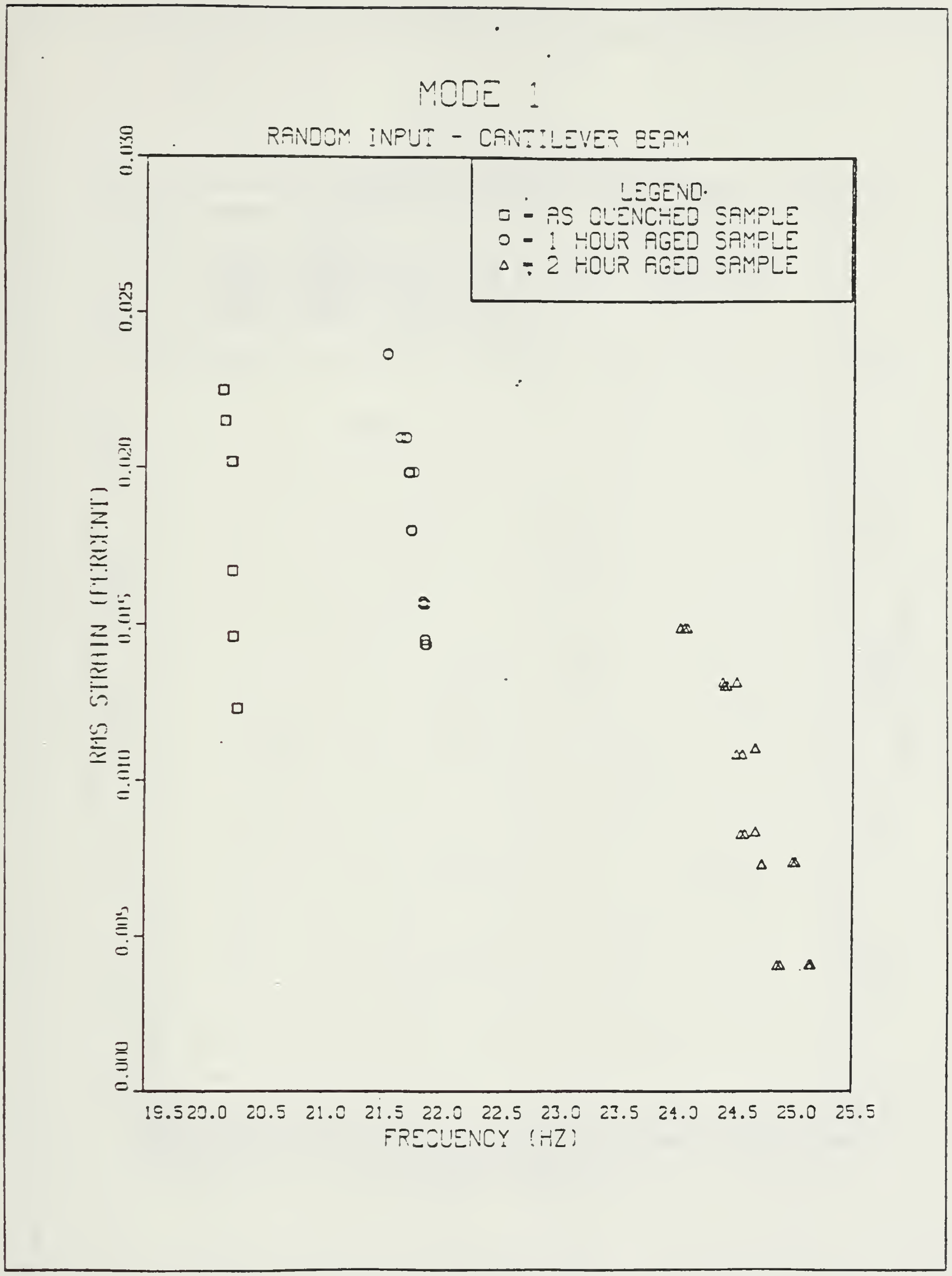

Figure 3.13 Mode 1 - Strain -vs- Frequency
(Random Input)

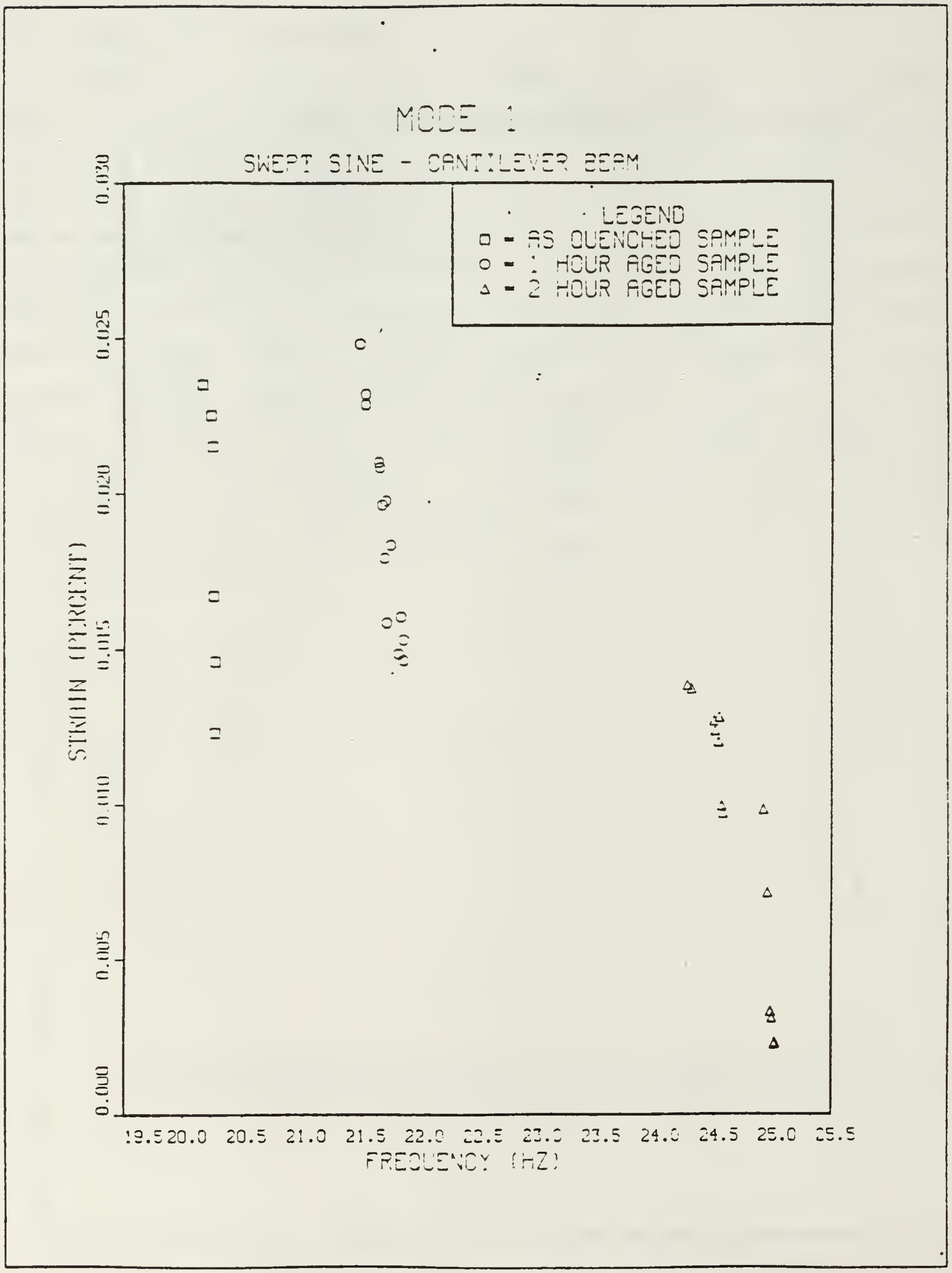

Figure 3.14 Mode 1 - Strain -vs- Frequency (Swept Sine)

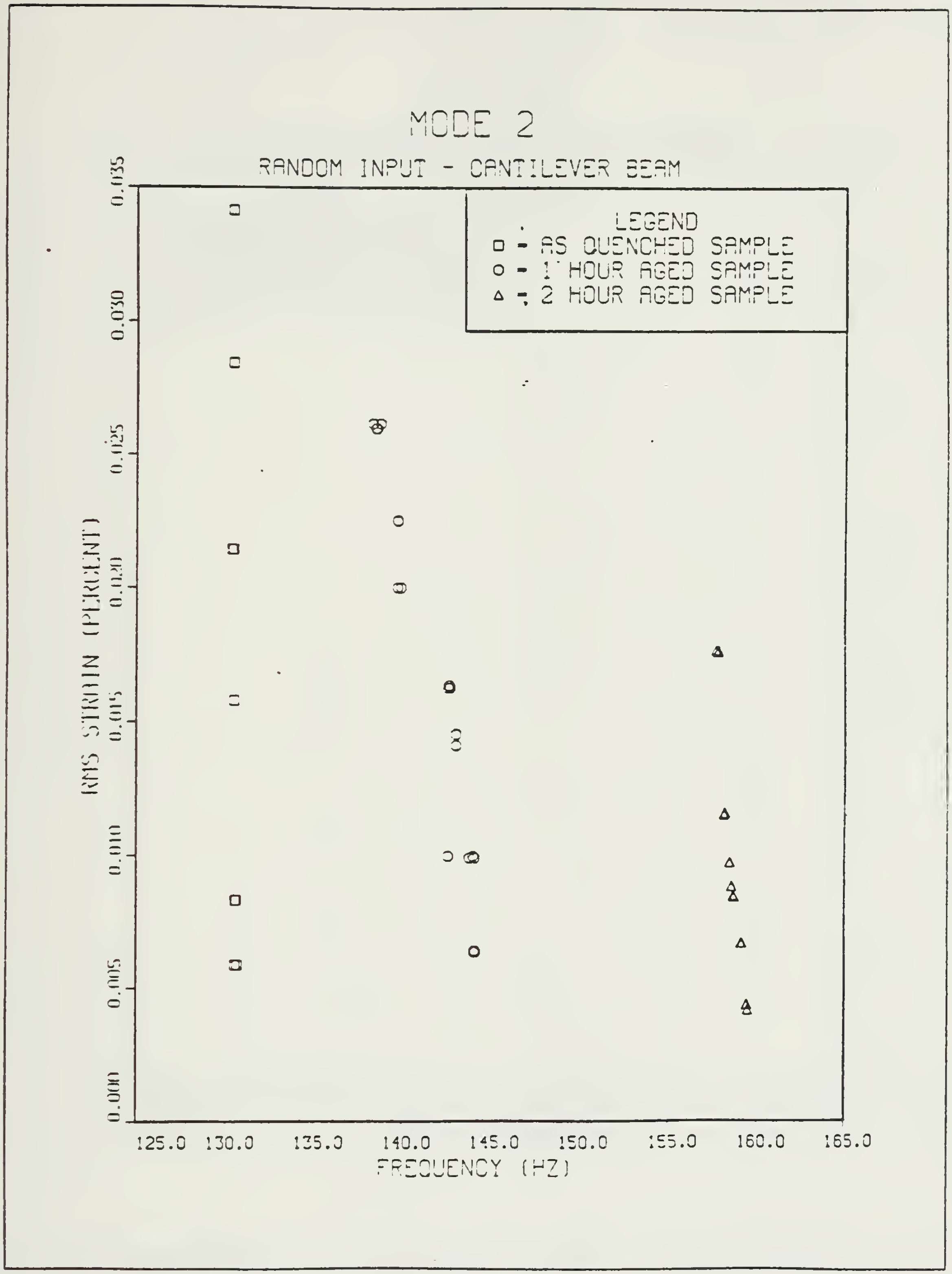

Figure 3.15 Mode 2 - Strain -vs- Frequency
(Random Input)

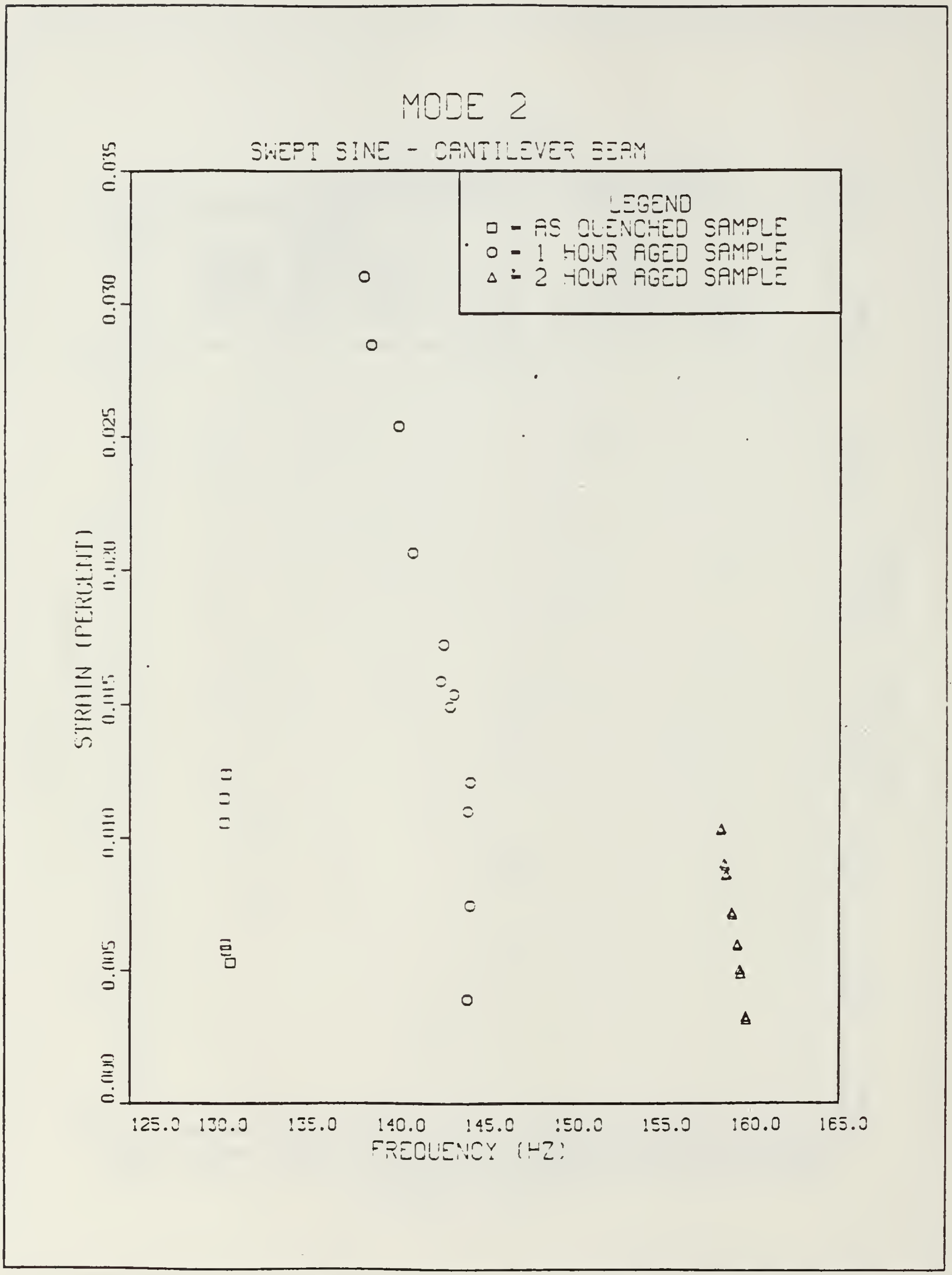

Figure 3.16 Mode 2 - Strain -vs- Frequency (Swept Sine)

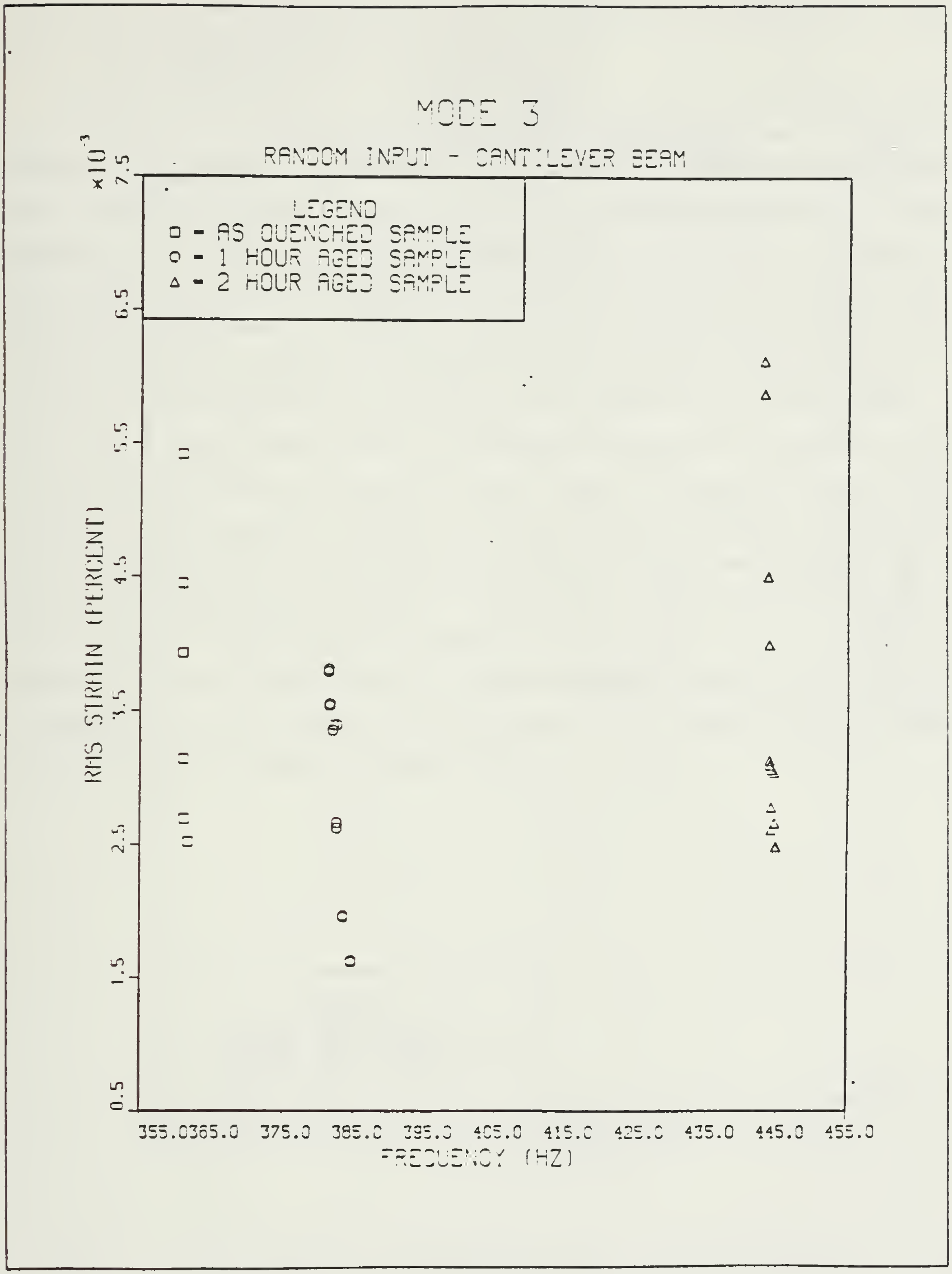

Figure 3.17 Mode 3 - Strain -vs- Frequency
(Random Input)

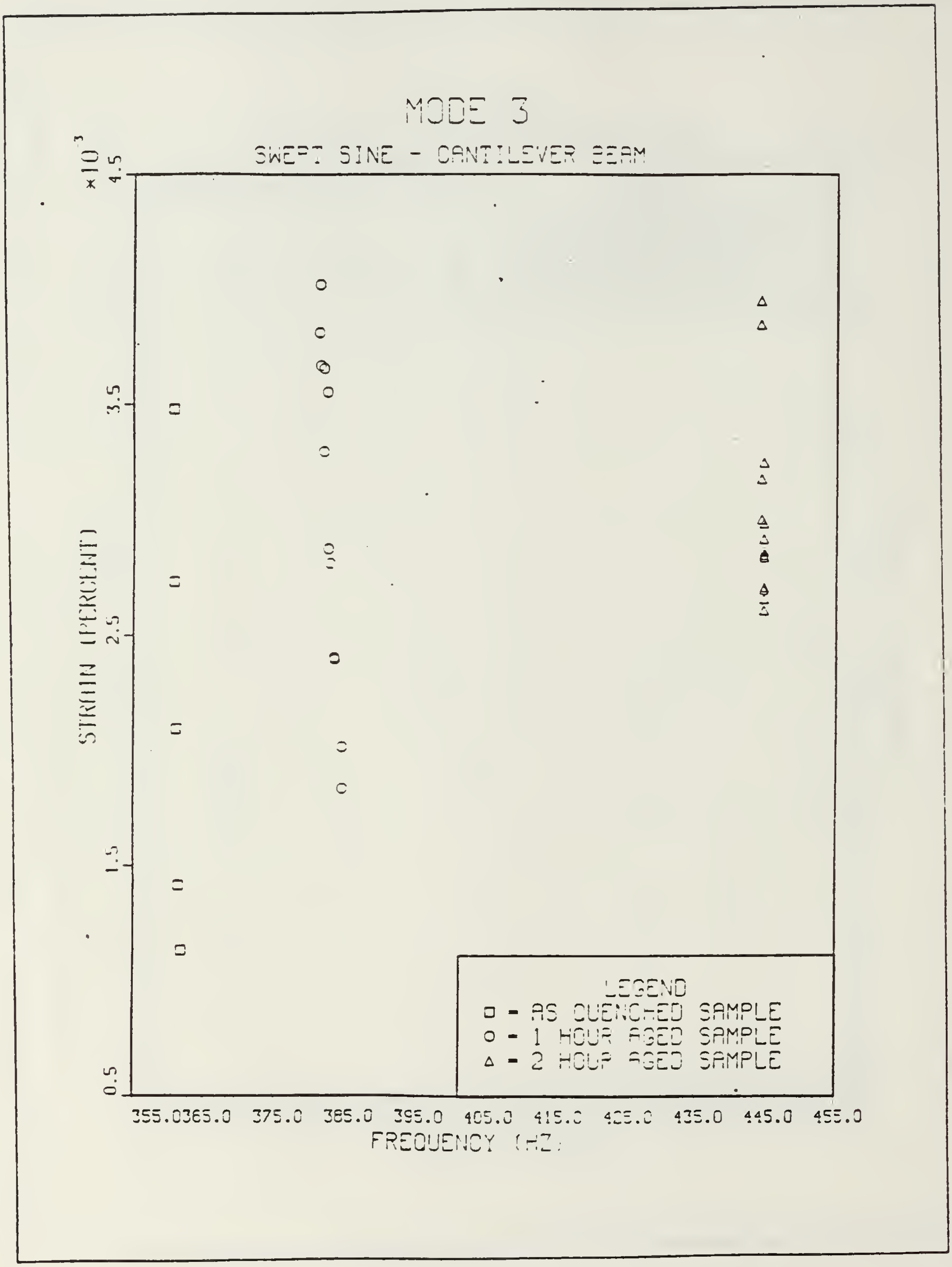

Figure 3.18 Mode 3 - Strain -vs- Frequency (Swept Sine)

E. INPUT ACCELERATION -VS- FREQUENCY

Figure 3.19 is a graph of the mode 1 Input Acceleration -vs- Frequency for a random input. In this graph as the input acceleration level increases the resonant frequency shifts downward in the same manner as seen in the Strain -vs- Frequency graphs. Since it was found (Figures 3.1 to 3.6) that the input acceleration and strain increase in a linear fashion and that an increase in strain corresponds to a decrease in resonant frequency, the downward shift of the resonant frequency with increasing input acceleration should occur in a similar fashion as it does with increasing strain. This downward shift does in fact occur. Figure 3.20 is the mode 1 Input Acceleration -vs- Frequency results using the swept sine input. This graph shows the same trend. In both cases, as aging time increases, the resonant frequency shifts downward faster. Figures 3.21 and 3.22 are the mode 2 results. Again, the resonant frequency shifts downward with an increase in the input acceleration level. In mode 2 it appears that the 1 hour aged sample makes the fastest frequency shift. This was seen earlier in the Strain -vs- Frequency graphs (Figures 3.15 and 3.16). Figures 3.23 and 3.24 are the mode 3 results. These results are comparable to the mode 3 results of Strain -vs- Frequency as they should be given the linear relationship between strain and input acceleration. As the excitation level is increased the resonant frequency shifts downward due to the change in Young's Modulus.

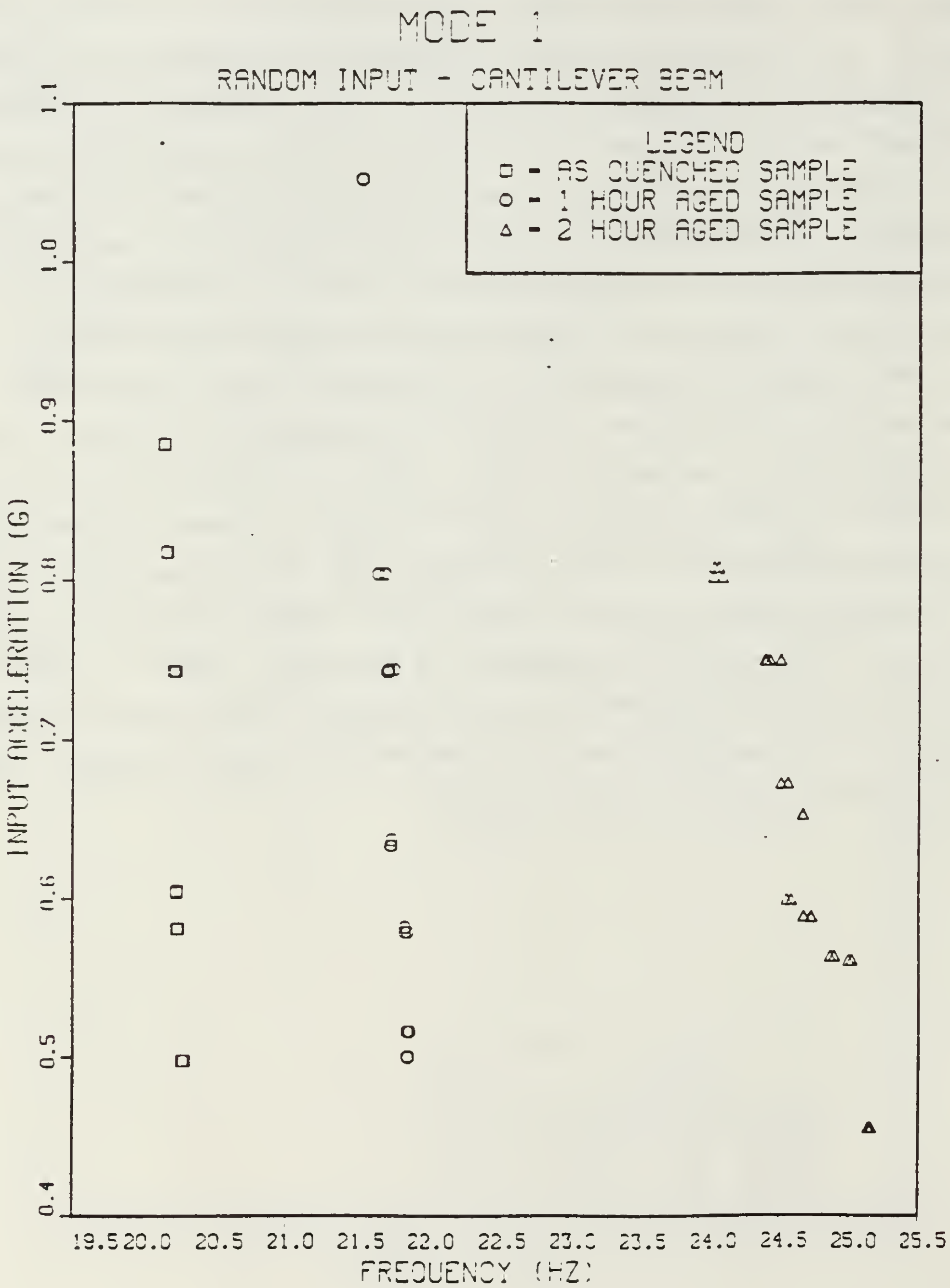

Figure 3.19 Mode 1 - Input Acceleration -vs- Frequency
(Random Input)

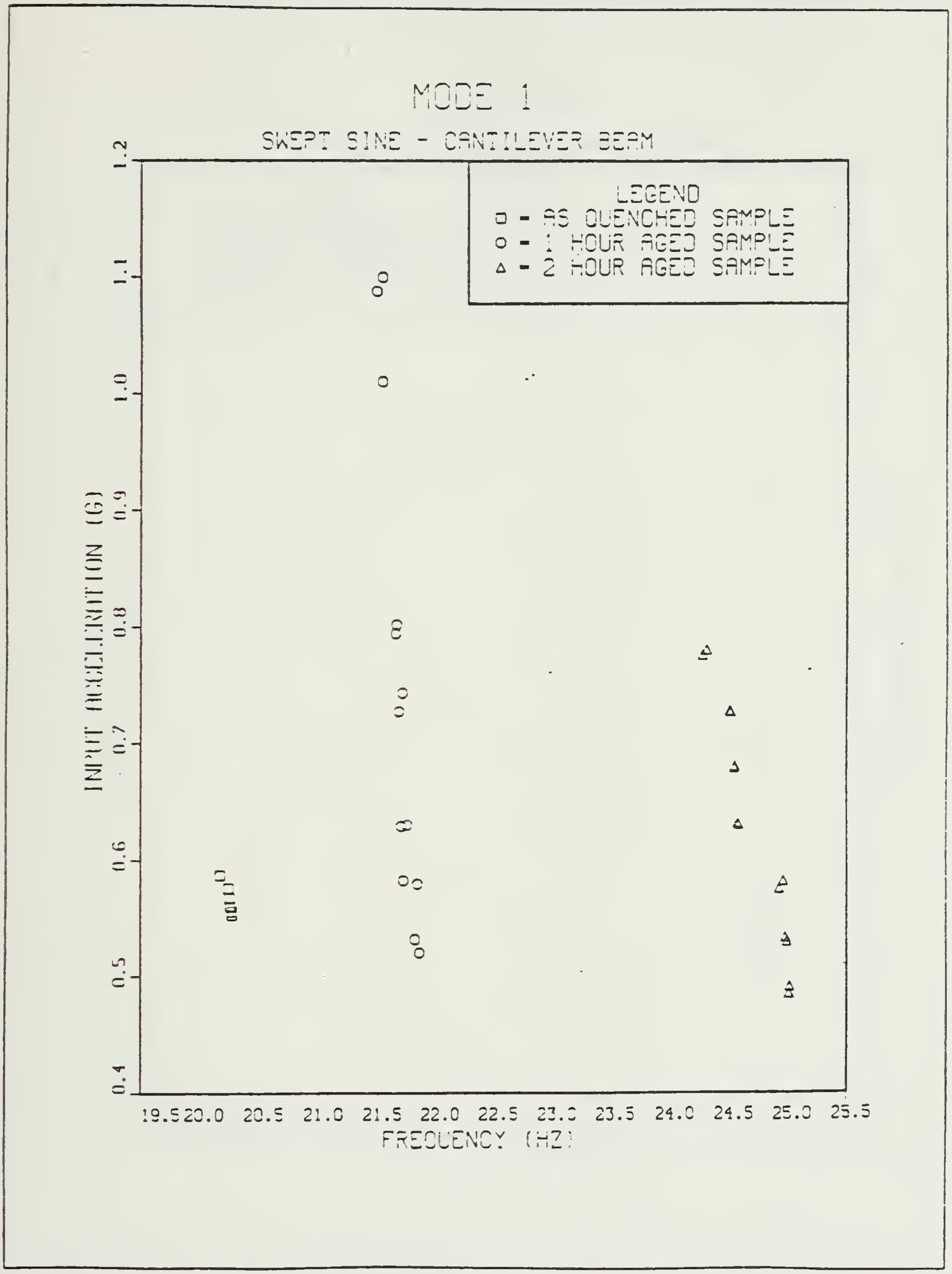

Figure 3.20 Mode 1 - Input Acceleration -vs- Frequency
(Swept Sine)

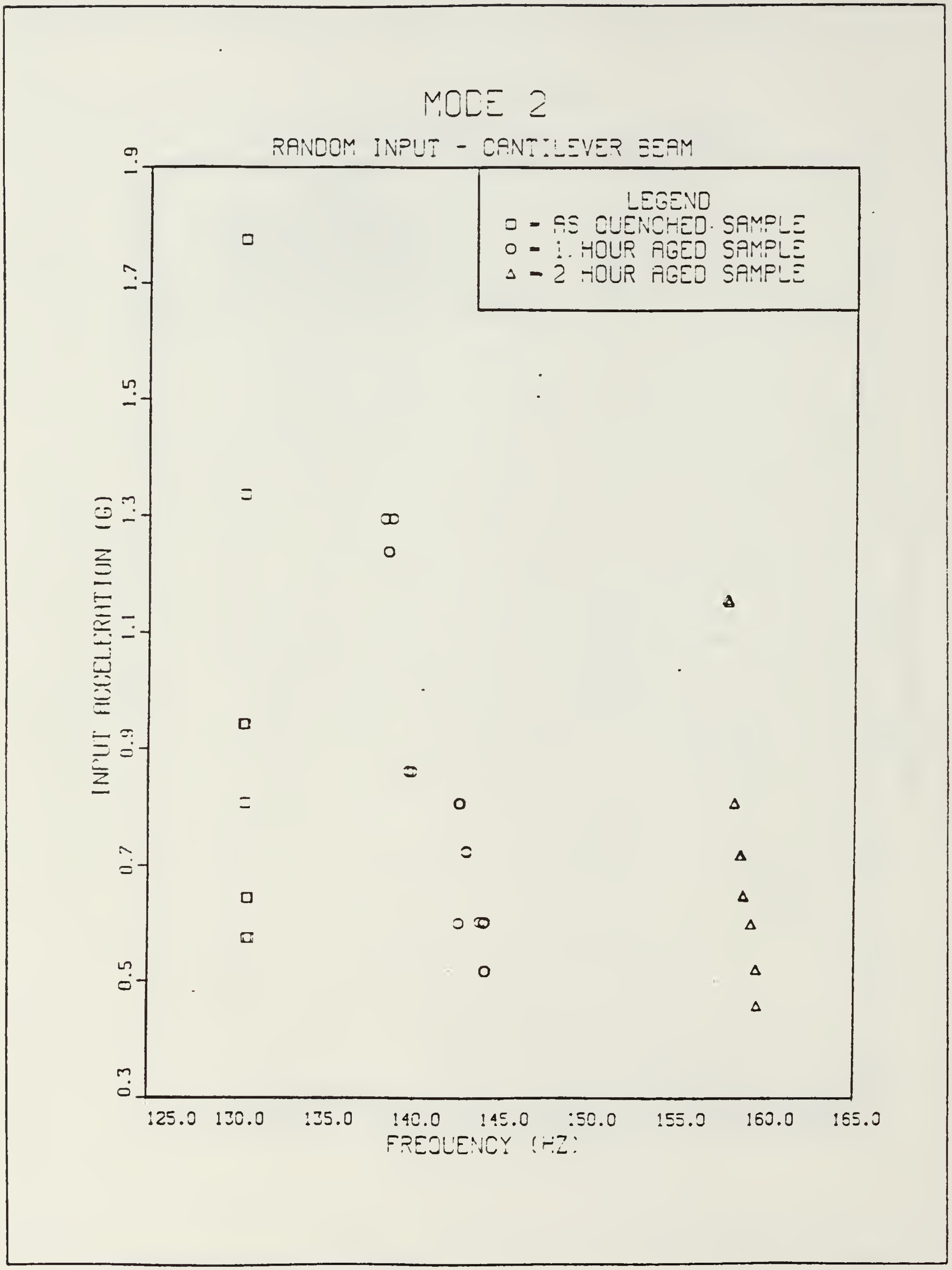

Figure 3.21 Mode 2 - Input Acceleration -vs- Frequency (Random Input)

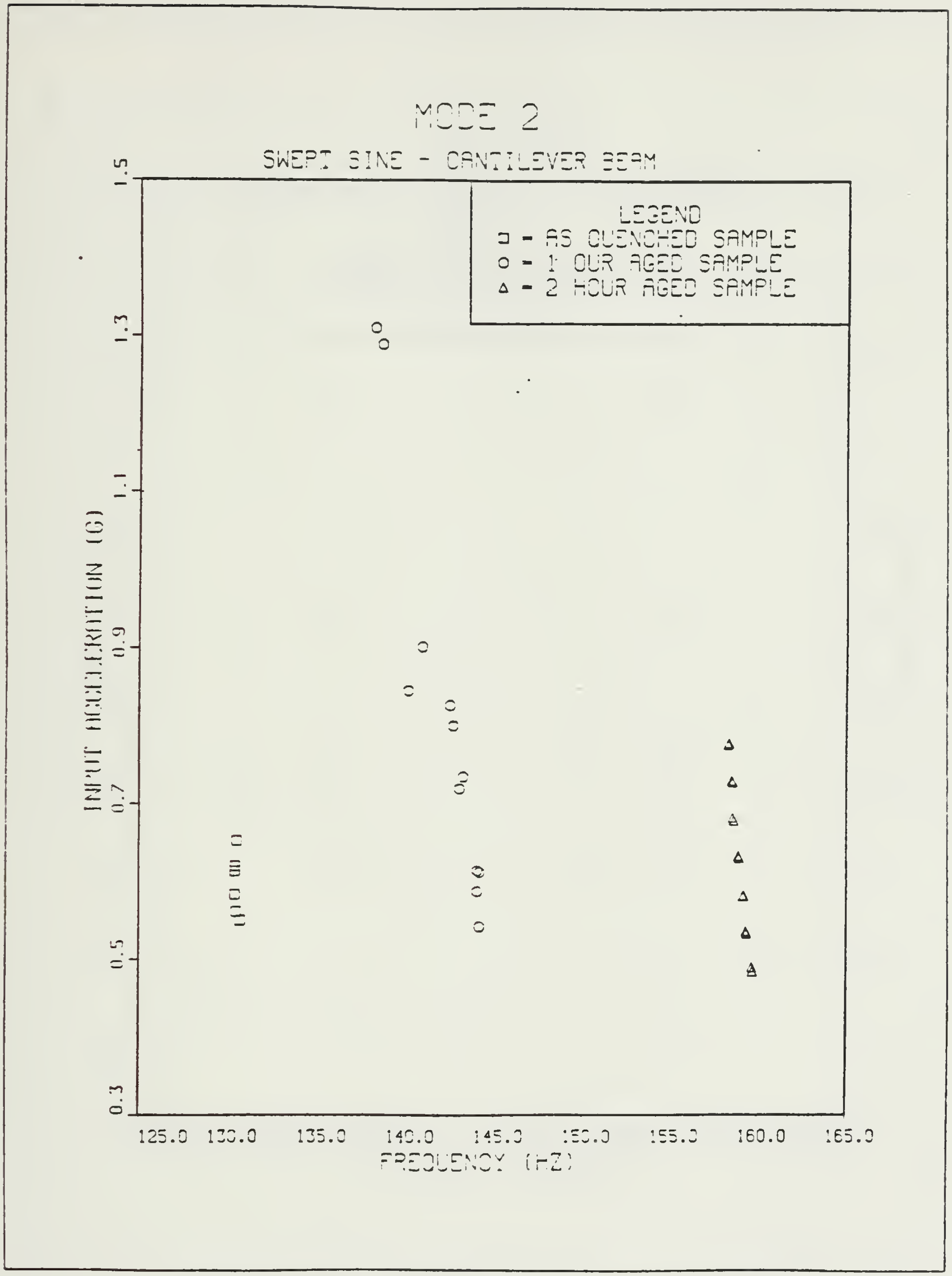

Figure 3.22 Mode 2 - Input Acceleration -vs- Frequency (Swept Sine)

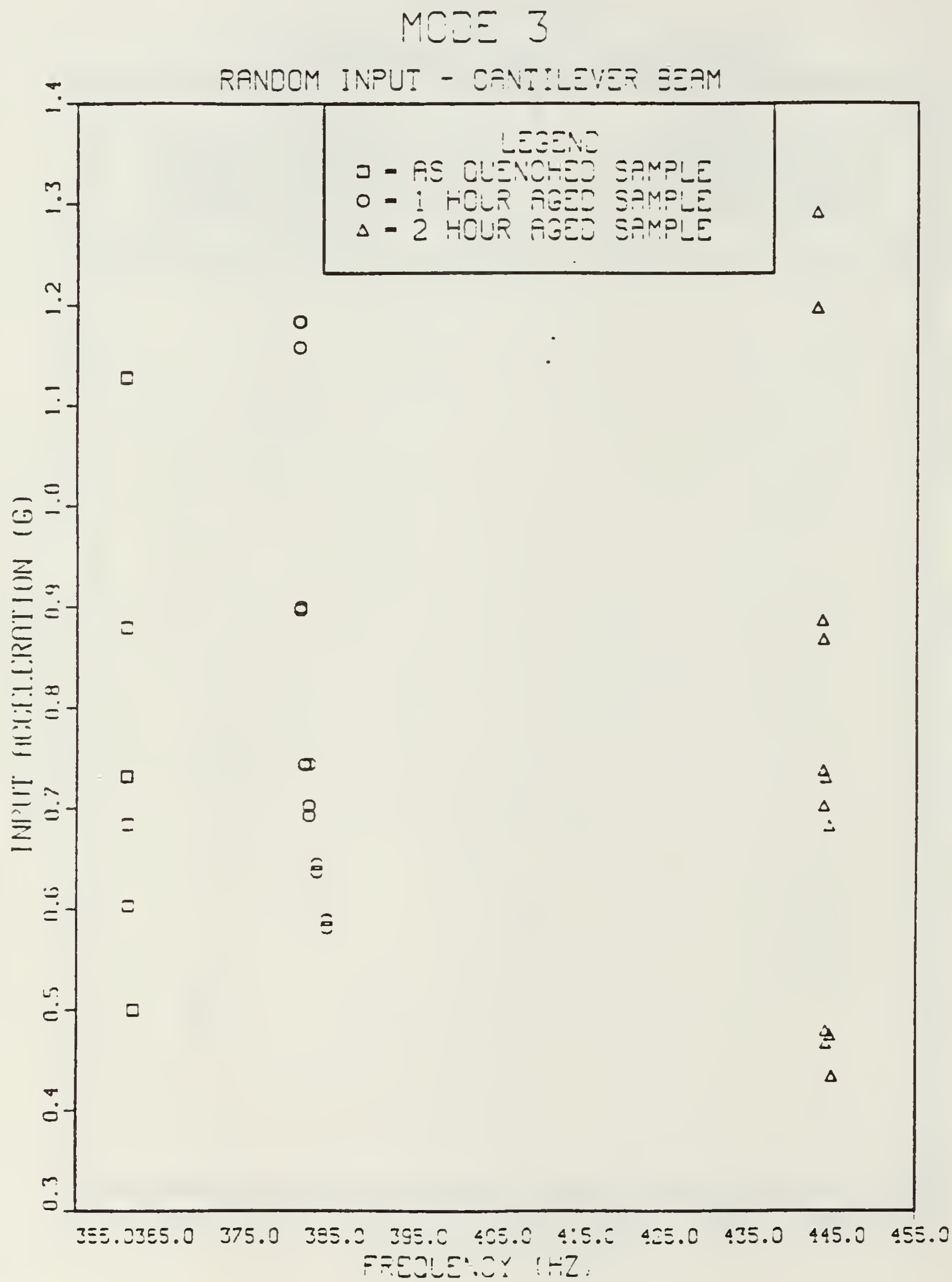

Figure 3.23 Mode 3 - Input Acceleration -vs- Frequency (Random Input)

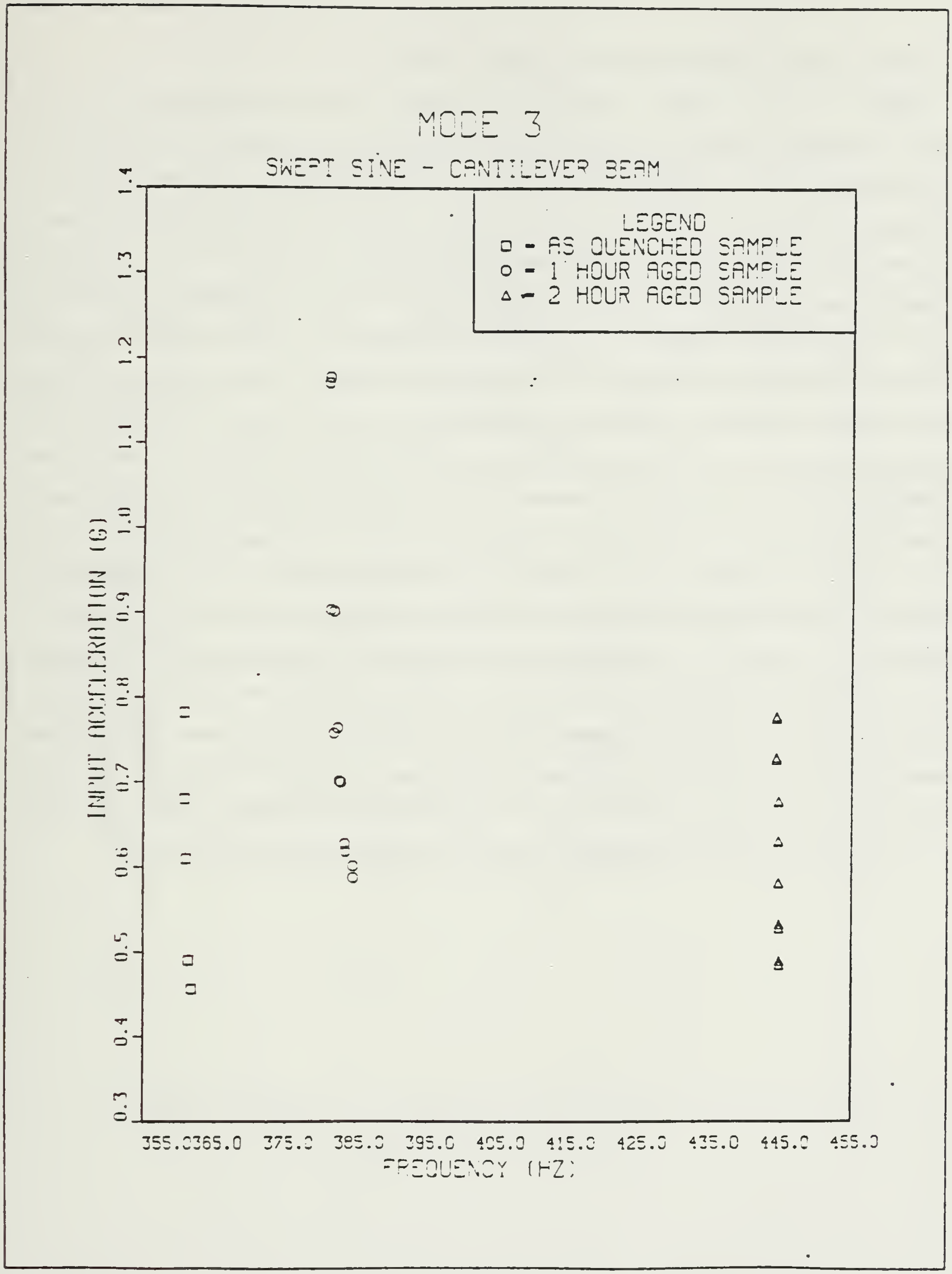

Figure 3.24 Mode 3 - Input Acceleration -vs- Frequency
(Swept Sine)

F. INPUT ACCELERATION -VS- LOSS FACTOR

Figure 3.25 is the mode 1, random input graph of Input Acceleration -vs- Loss Factor. This graph shows that as the input acceleration is increased the loss factor of the material increases. Also, as the aging time increases the loss factor increases significantly. These two trends are exactly the same as the trends found in the Strain -vs- Loss Factor graphs. Once again this should occur since the strain and input acceleration can be related. The 2 hour aged sample shows a significant increase in loss factor as the input acceleration level reaches the 0.8g level. This could be a result of the non-linearities in the material. As mentioned in Chapter 1 the loss factor of the Mn-Cu material increases as aging time increases up to about 8 hours. Figure 3.26 is the swept sine graph of the input acceleration and loss factor for mode 1. As with the random input test, the loss factor increases with both increased input acceleration and increased aging time. The 2 hour aged samples show the same rapid increase in loss factor at an input acceleration level of 0.8g as it did in the random test. For complete analysis of the material this would involve further investigation but for this paper what is significant is the fact that the trend was occured in both the random input and swept sine tests. Figure 3.27 and 3.28 are the mode 2 results while Figures 3.29 and 3.30 are the mode 3 results. In mode 2 it appears that the loss factor of the 1 hour aged sample increases faster than the 2 hour aged sample. However, the general trend, that the loss factor increases with both increased input acceleration and increased aging time still holds. It can be seen that the highest loss factors are obtained in the first mode.

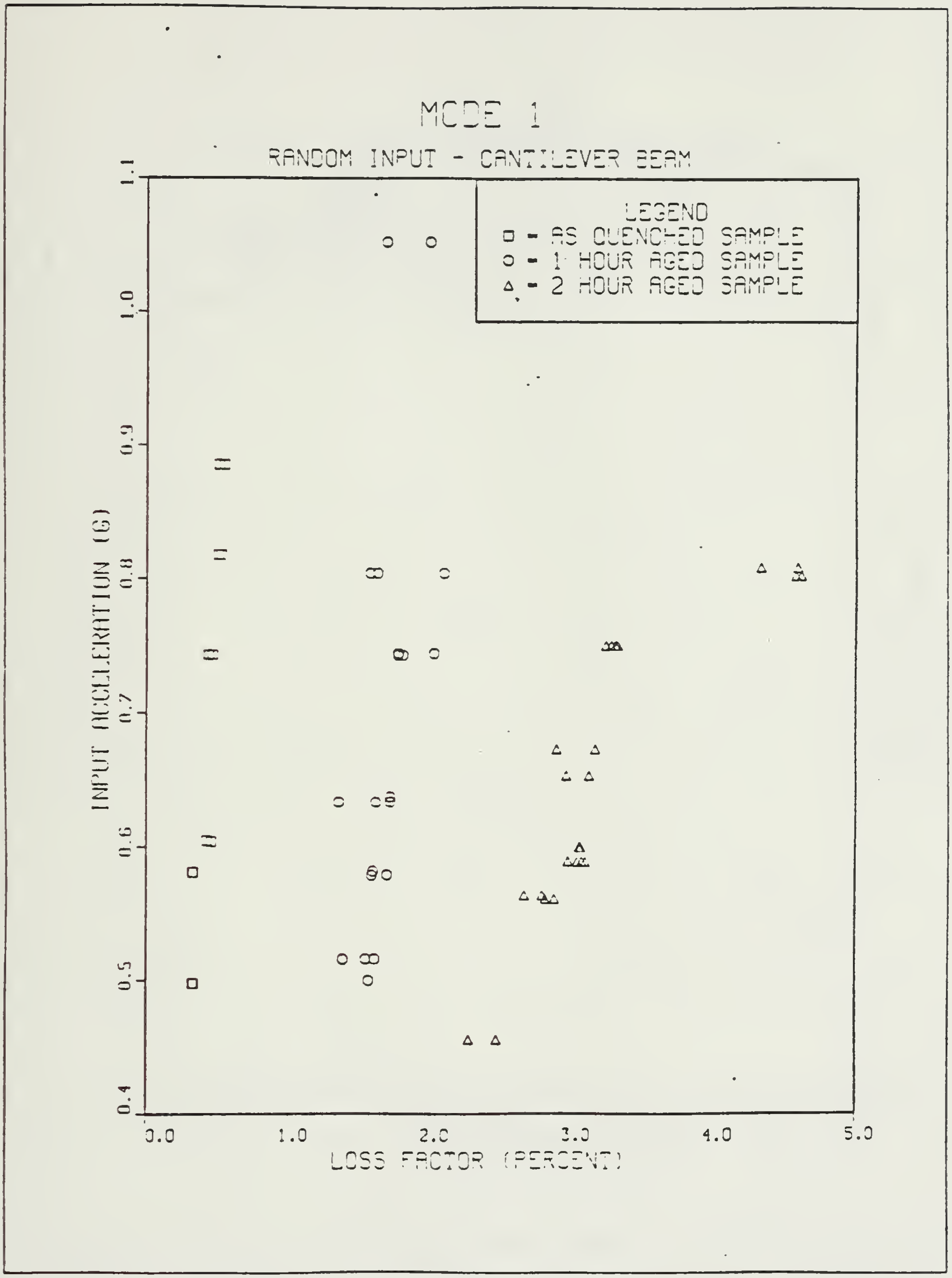

Figure 3.25 Mode 1 - Input Acceleration -vs- Loss Factor
(Random Input)

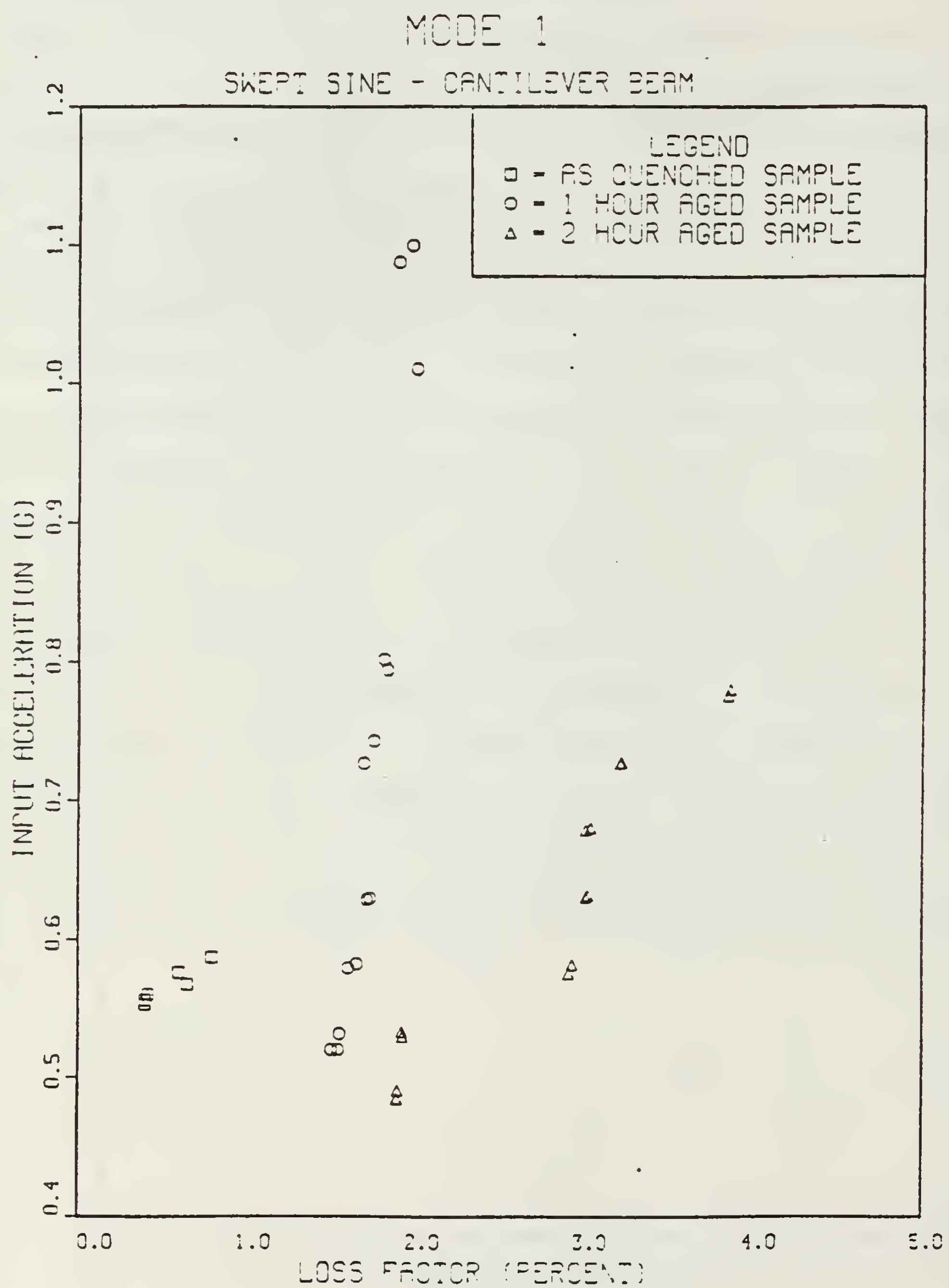

Figure 3.26 Mode 1 - Input Acceleration -vs- Loss Factor (Swept Sine)

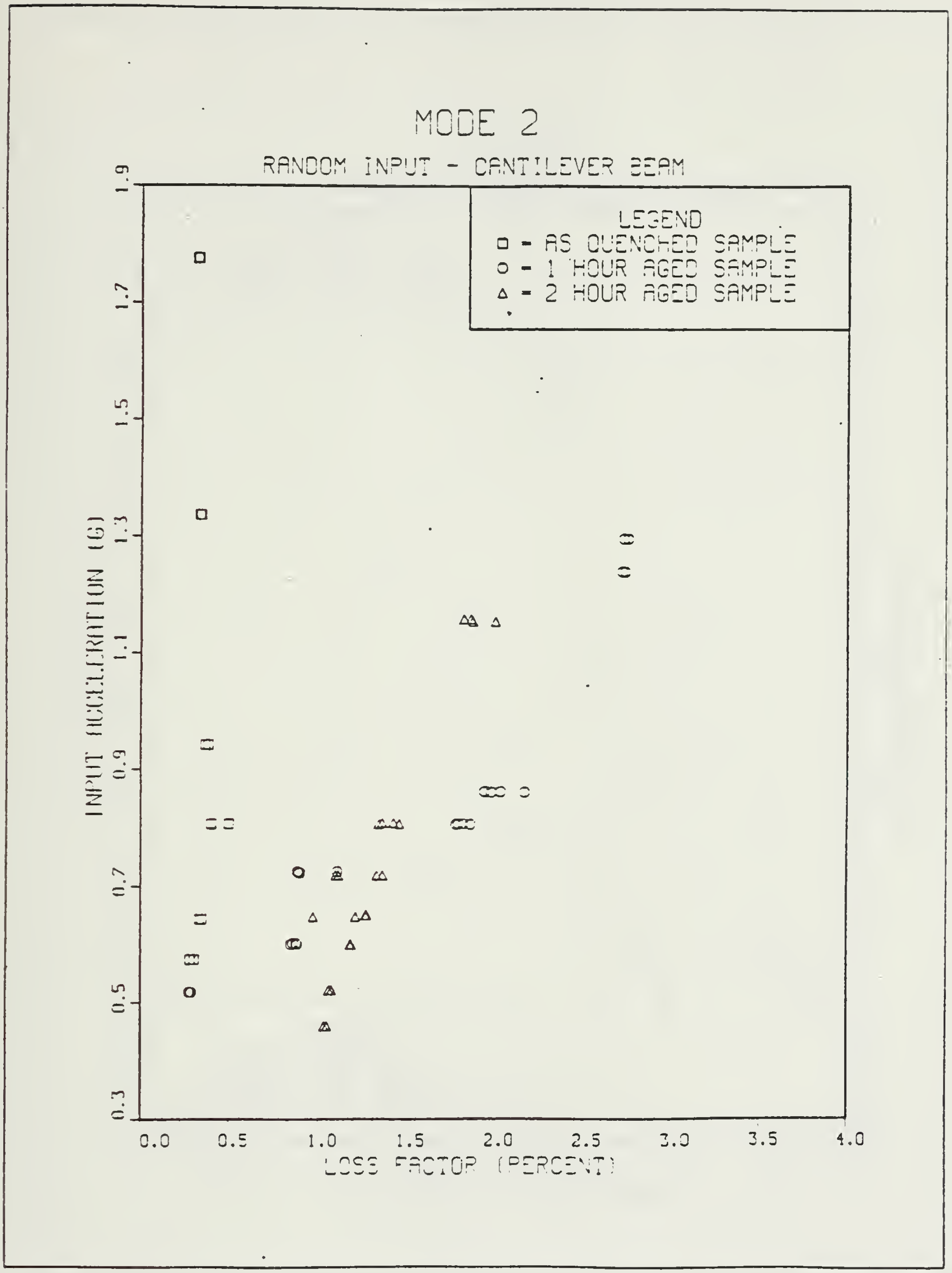

Figure 3.27 Mode 2 - Input Acceleration -vs- Loss Factor (Random Input)

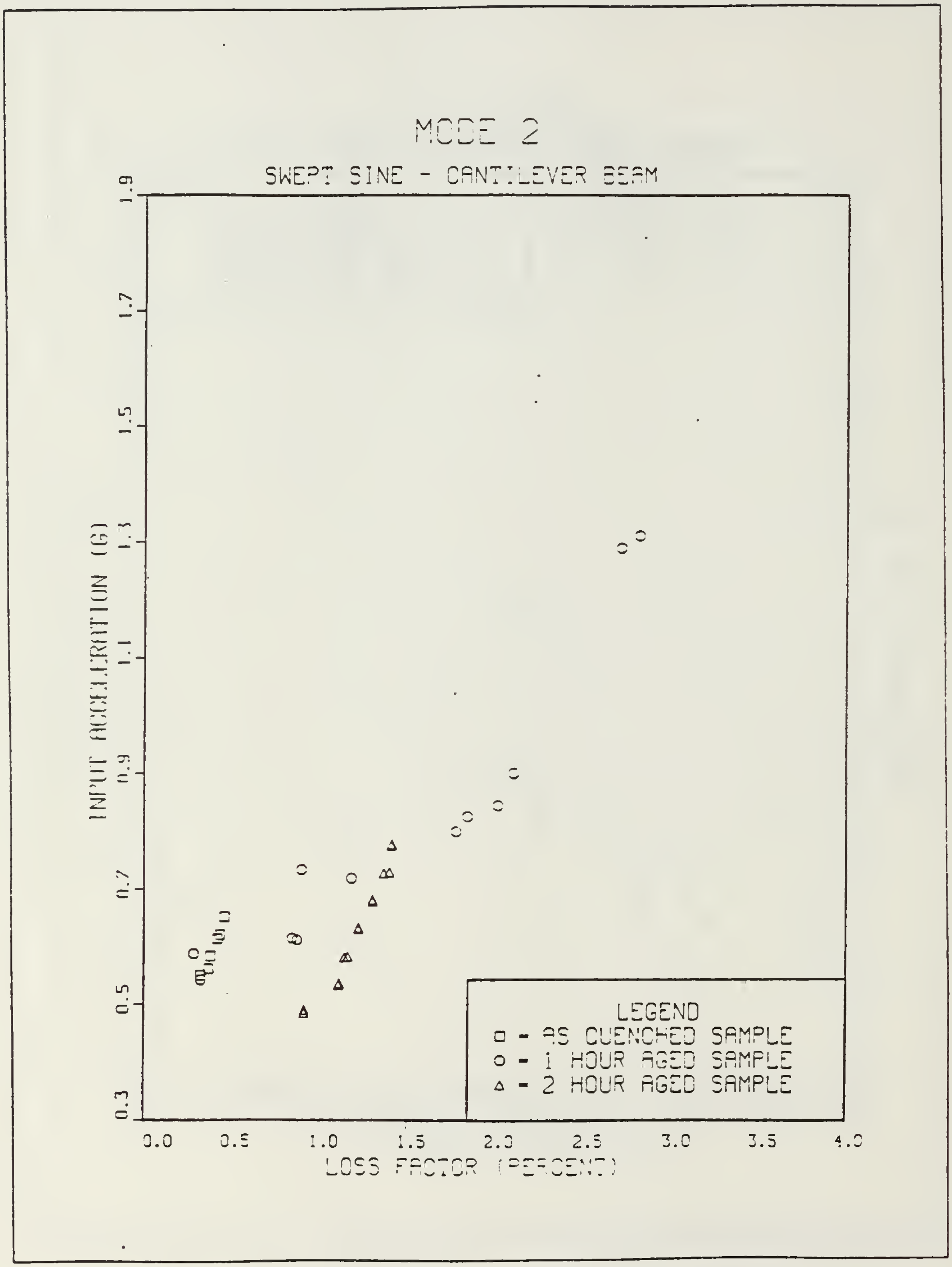

Figure 3.28 Mode 2 - Input Acceleration -vs- Loss Factor (Swept Sine)

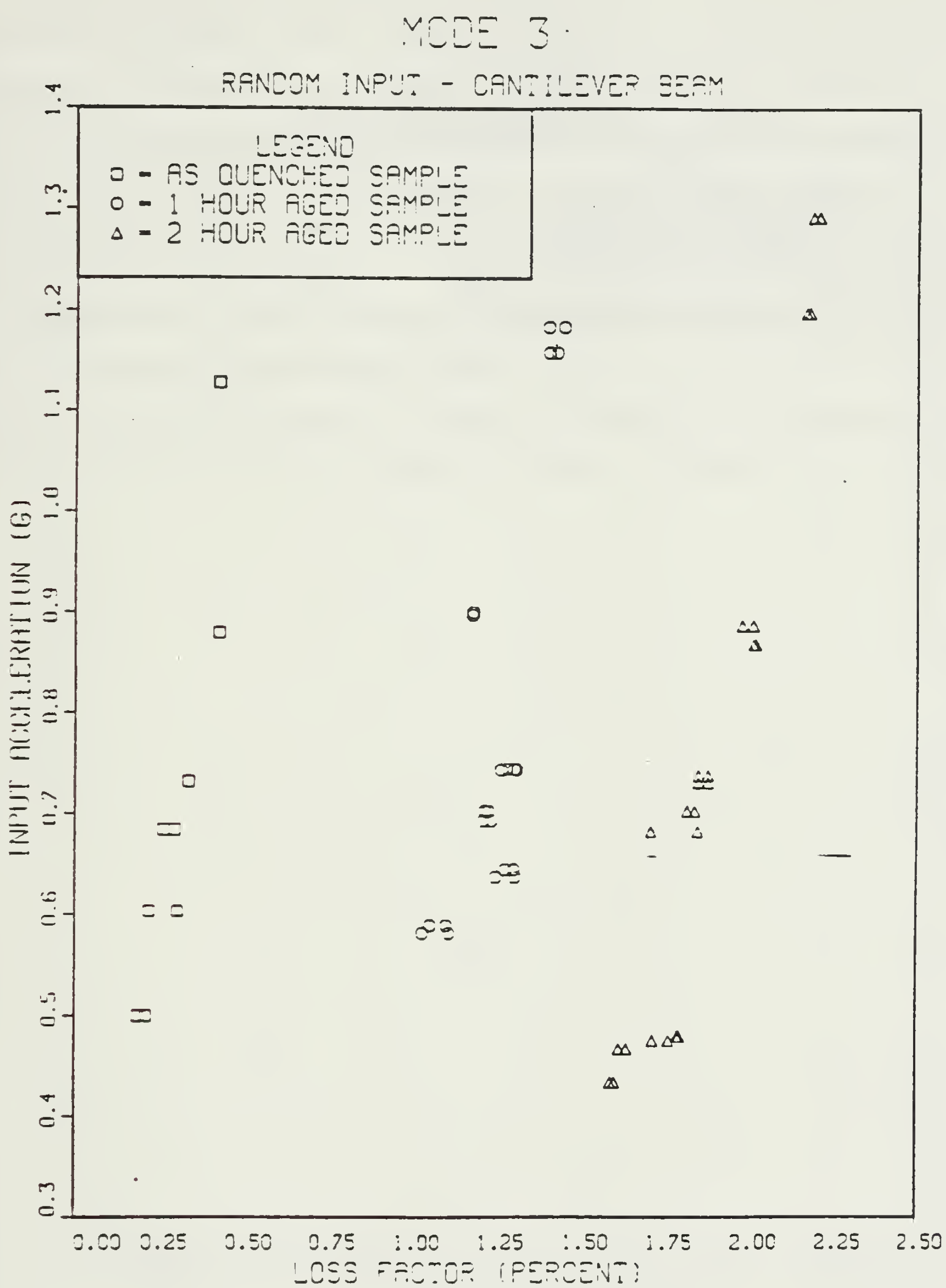

Figure 3.29 Mode 3 - Input Acceleration -vs- Loss Factor (Random Input)

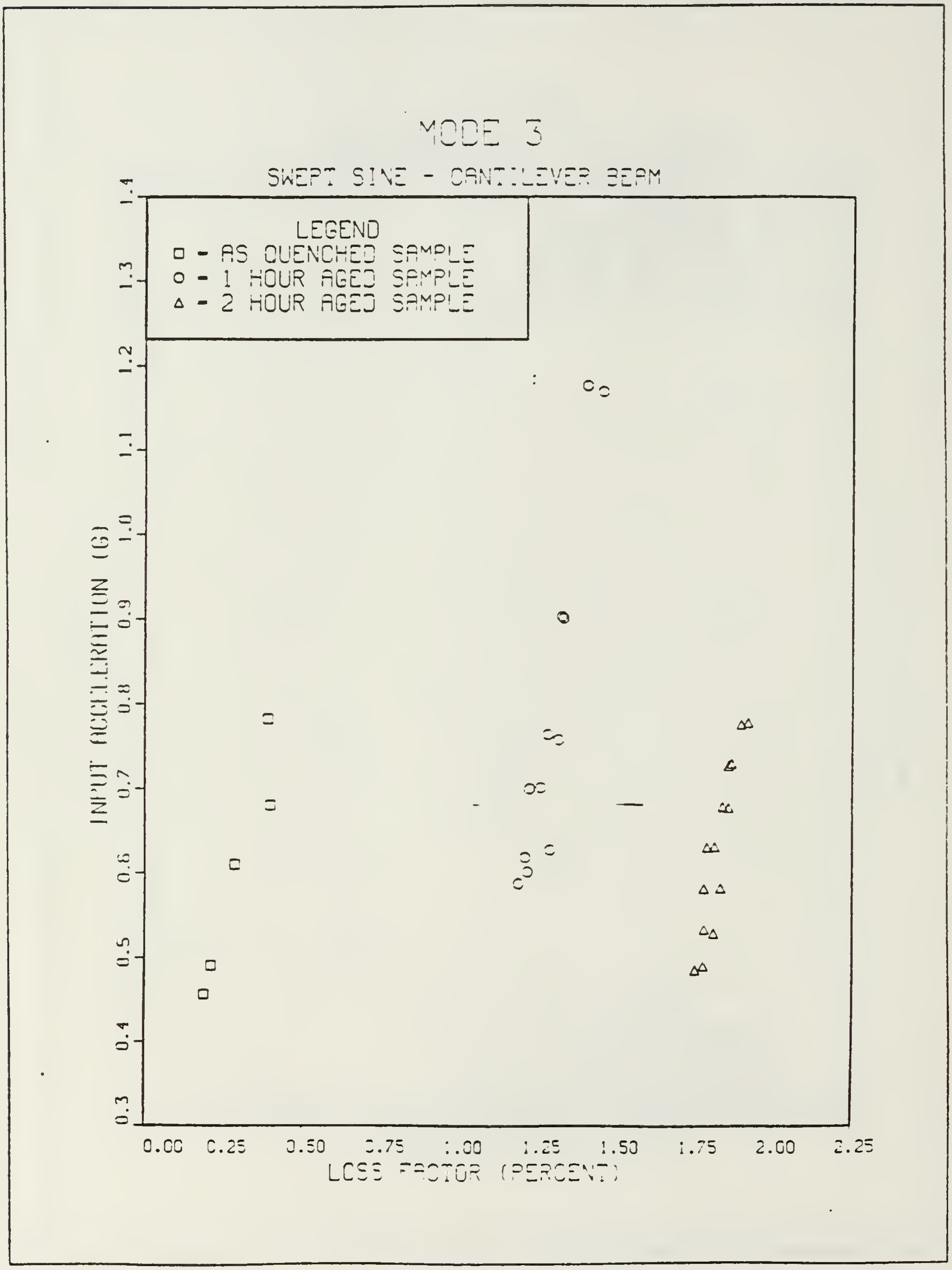

Figure 3.30 Mode 3 - Input Acceleration -vs- Loss Factor (Swept Sine)

G. LOSS FACTOR -VS- FREQUENCY

Figure 3.31 is a graph of the mode 1 random input results of the Loss Factor -vs-Frequency. This graph shows a linear relationship between the loss factor and the frequency. As the loss factor increases the resonant frequency shifts downward. This makes sense since an increase in the loss factor corresponds to an increase in the the amount of strain that the sample undergoes. As mentioned previously, an increase in the strain results in a decrease in the Young's Modulus of the material with a resulting decrease in the resonant frequency. Figure 3.32 is the mode 1 swept sine results. The two graphs are very similar indicating that either way of testing (using random input or swept sine input) will obtain good results. Figures 3.33 and 3.34 are the mode 2 results. In both of these graphs the relationship between the loss factor and frequency appears to be linear as it does in Figures 3.35 and 3.36 which are the mode 3 results.

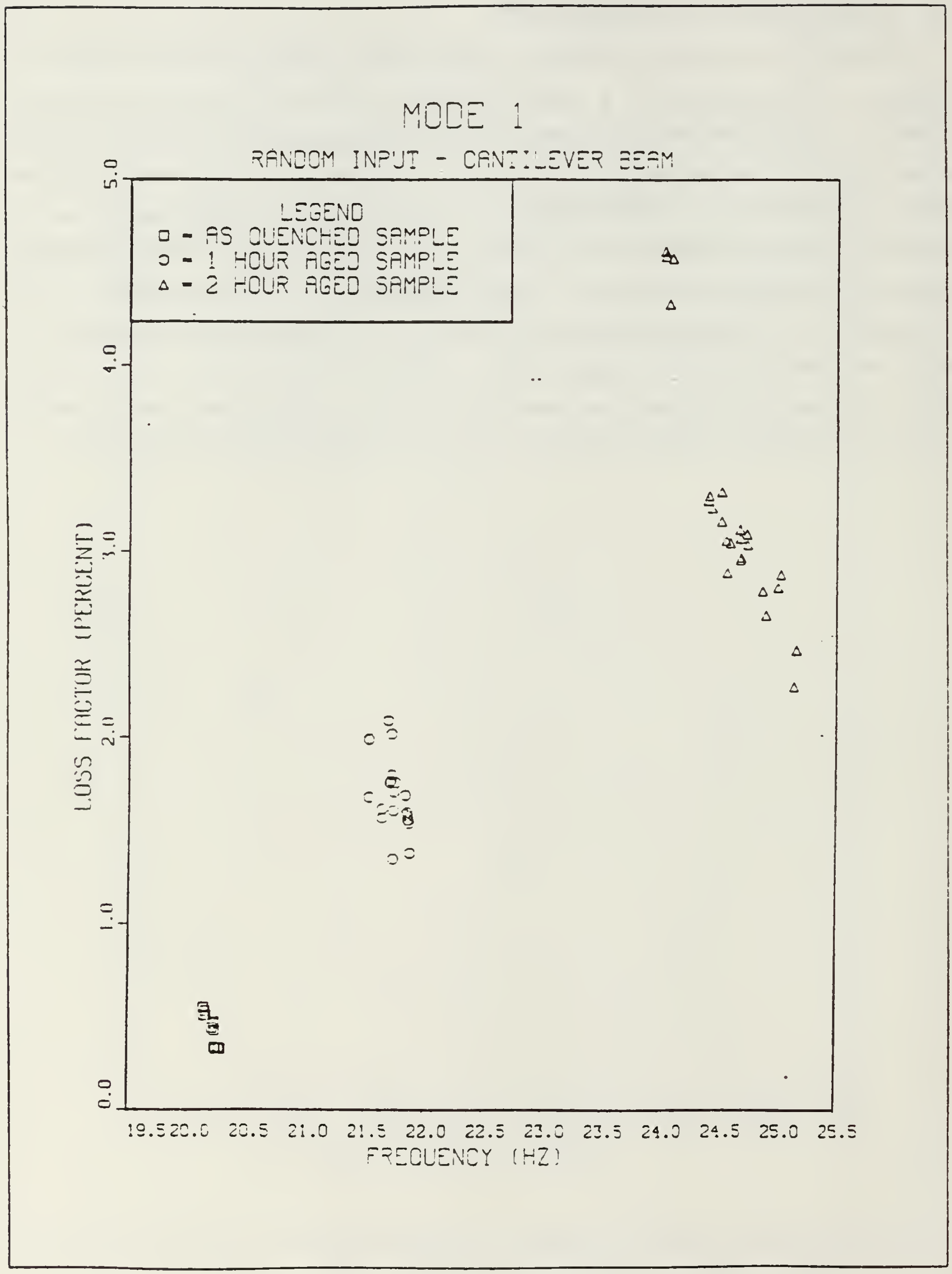

Figure 3.31 Mode 1 - Loss Factor -vs- Frequency (Random Input)

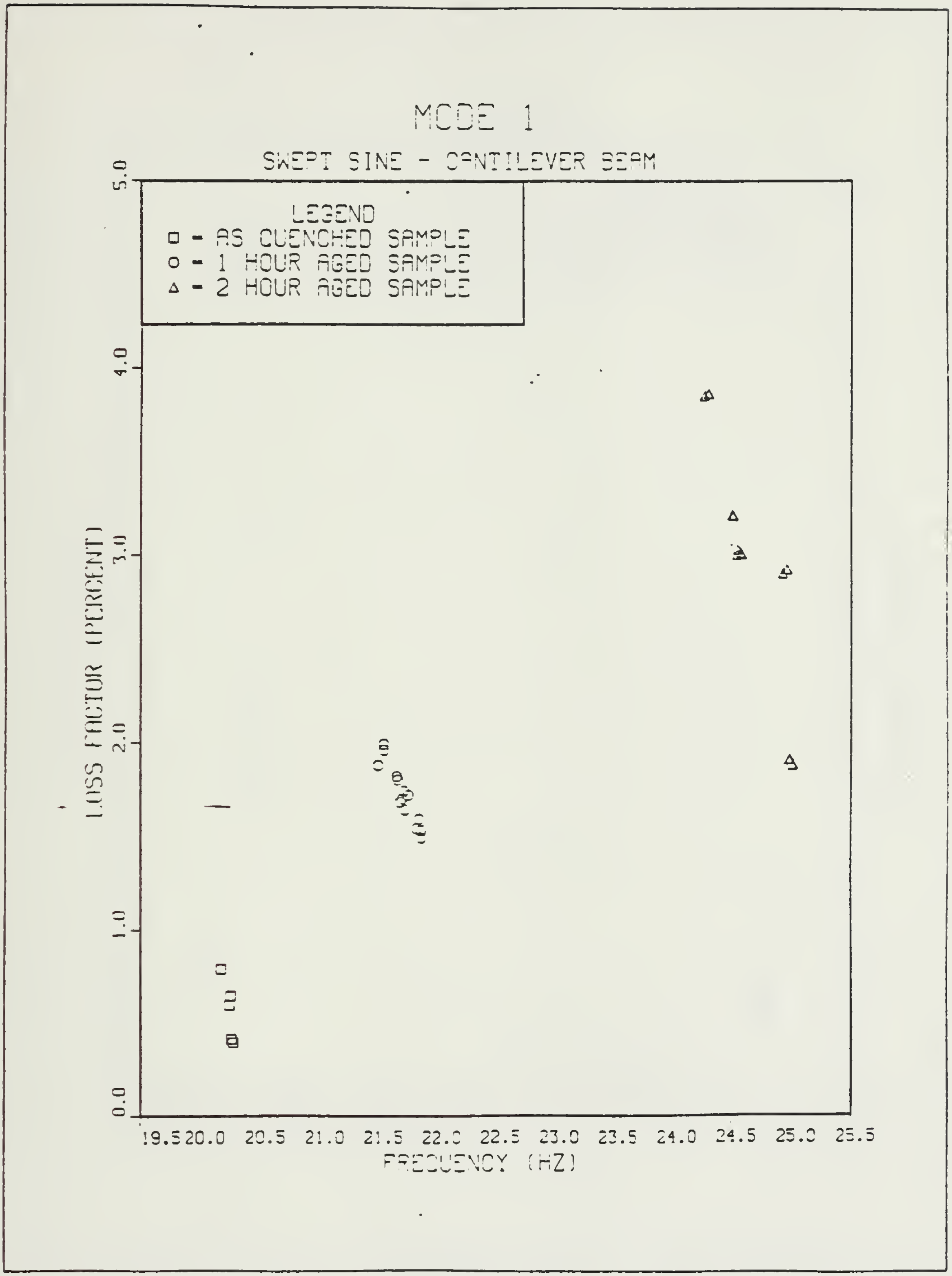

Figure 3.32 Mode 1 - Loss Factor -vs -Frequency (Swept Sine)

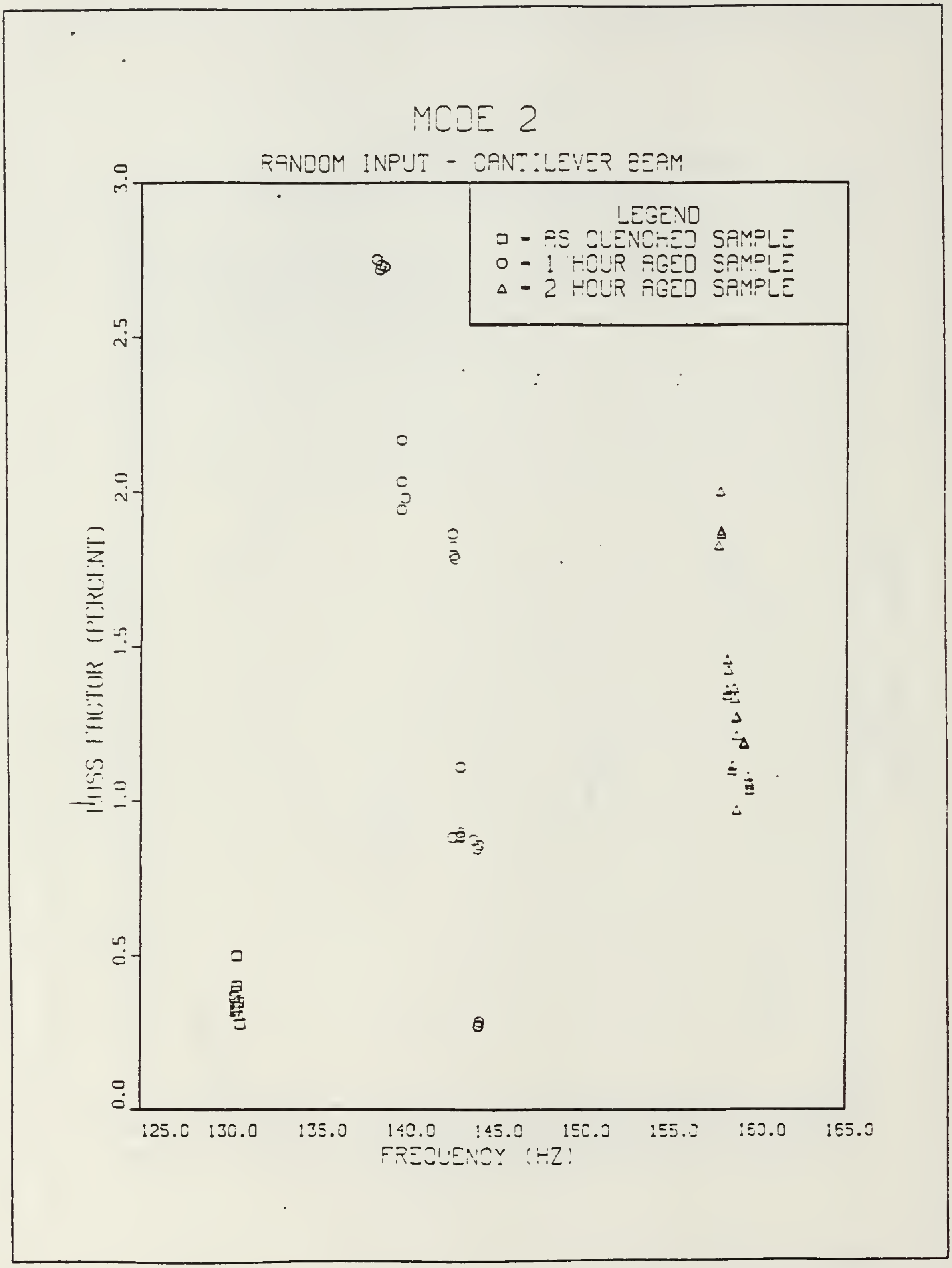

Figure 3.33 Mode 2 - Loss Factor -vs- Frequency (Random Input)

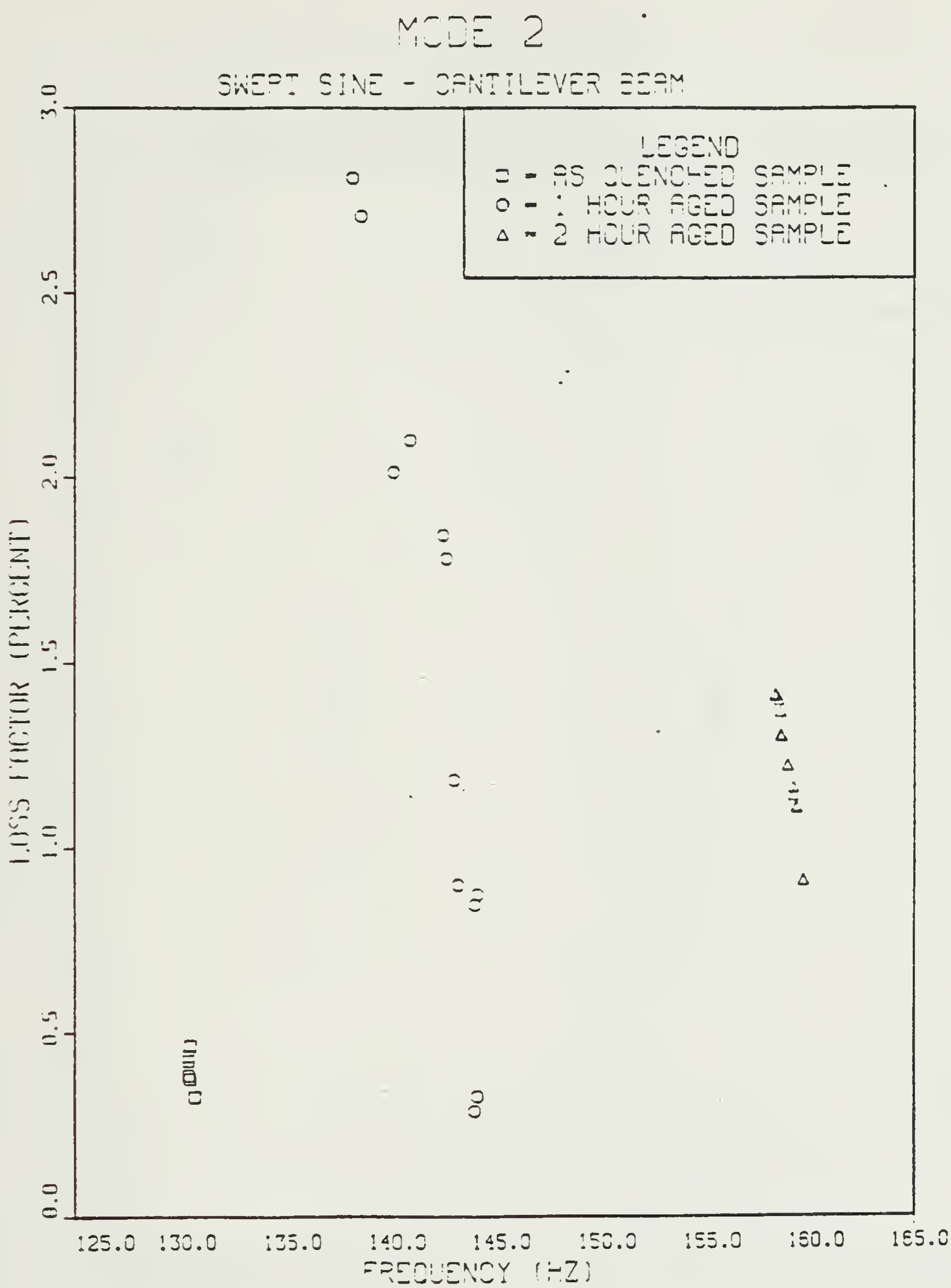

Figure 3.34 Mode 2 - Loss Factor -vs- Frequency (Swept Sine)

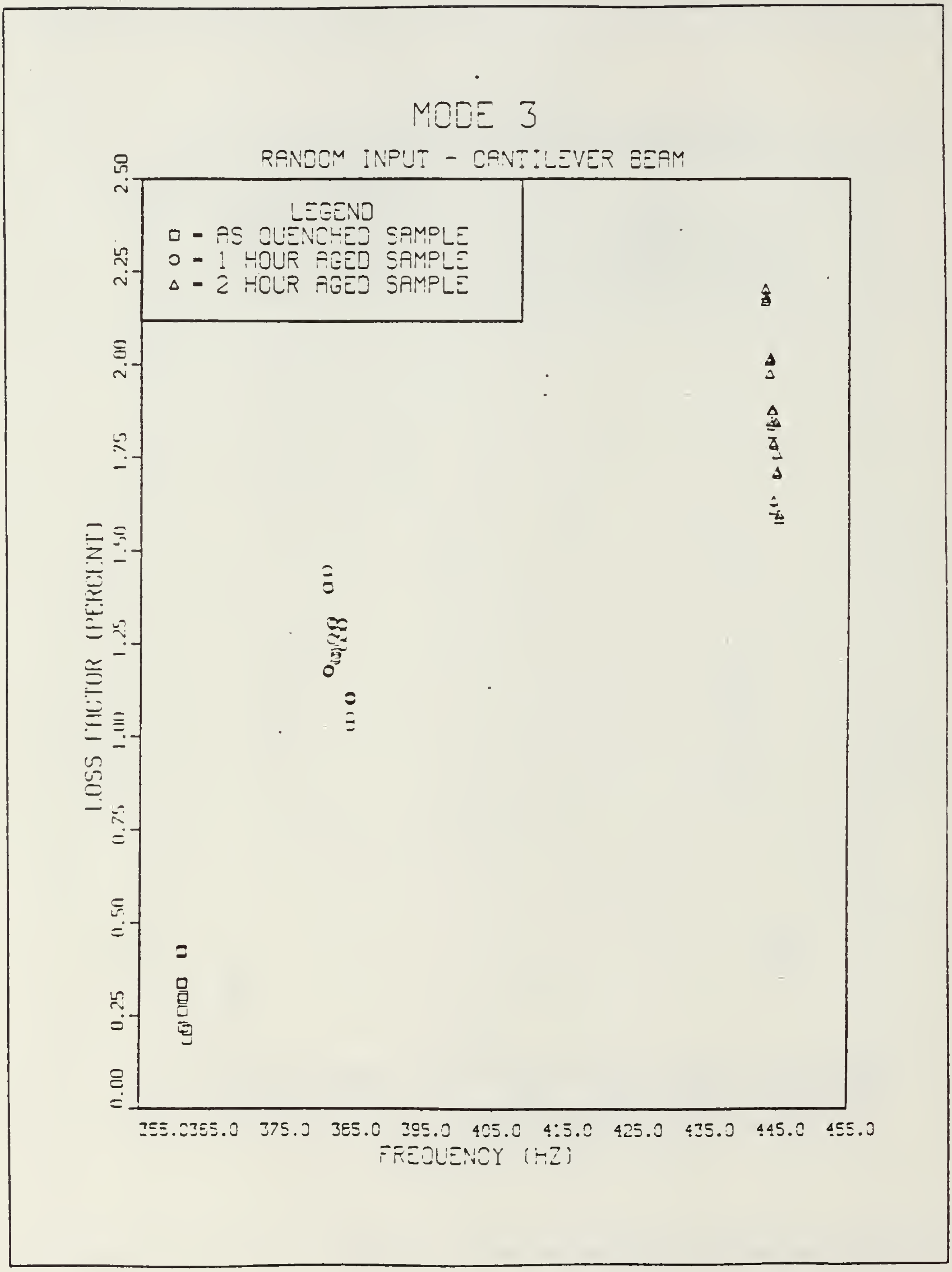

Figure 3.35 Mode 3 - Loss Factor -vs- Frequency (Random Input)

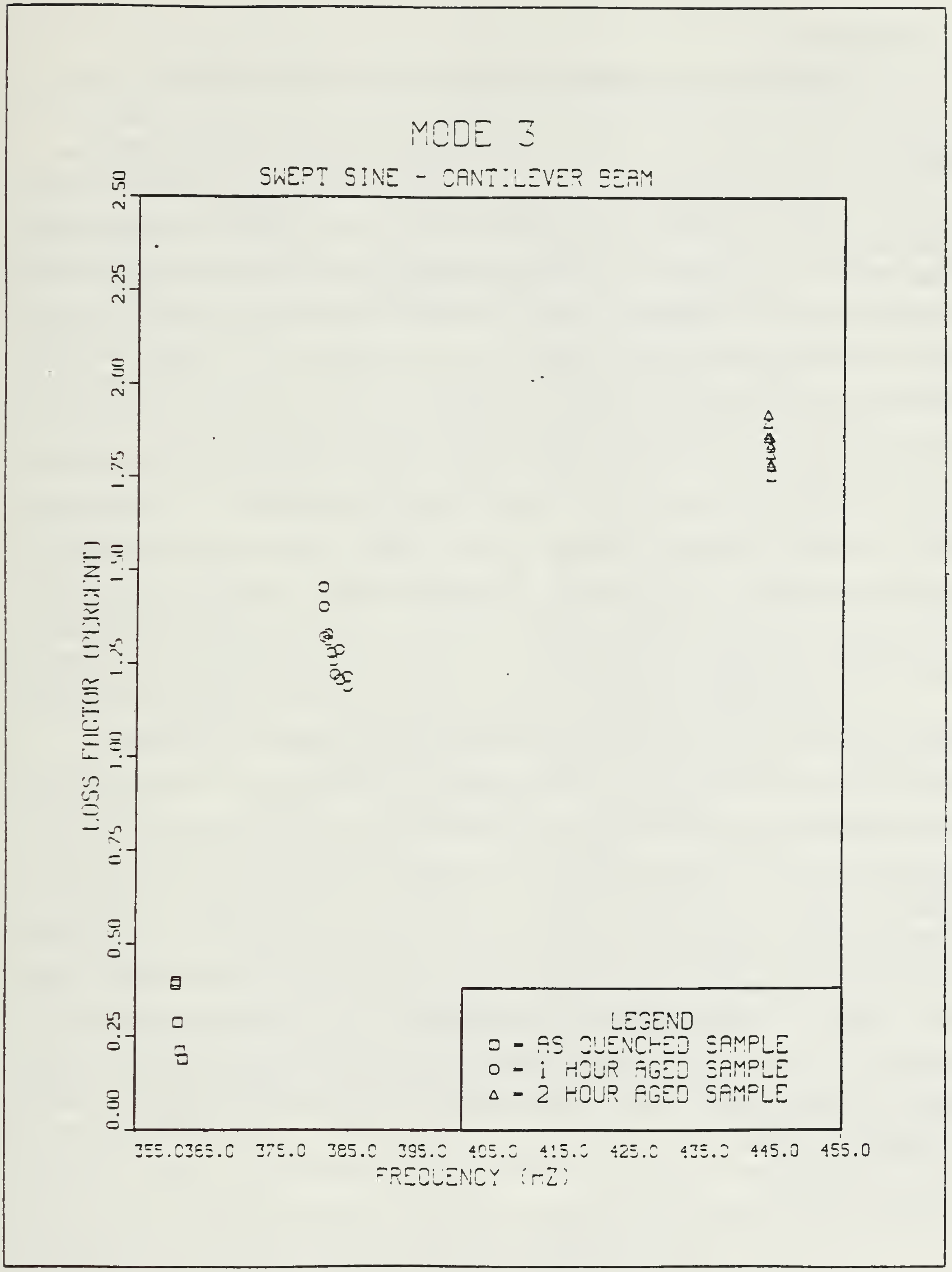

Figure 3.36 Mode 3 - Loss Factor -vs- Frequency (Swept Sine)

H. DISCUSSION

In running the tests some problems were encountered. The strain gages have a fatigue life of approximately 10^5 cycles. The fatigue is a function of the solder joint formation. Since the first mode has the highest tip deflection it is recommended that this mode be tested after the third and second modes. To prevent inadvertent joint damping the sample should be securely tightened and once it is placed in the test stand it should not be removed until after all desired testing has been performed. Both the strain gages and the accelerometers can be a source of extraneous noise if their associated wiring is allowed to repeatedly hit the beam sample as it vibrates. In this investigation the accelerometer coaxial cable (tip accelerometer only) was taped along the cantilever beam. Also the strain gage wiring was taped to the beam right after the gage solder connection. The wire was then looped to allow free vibration of the beam without any interference. This scotch tape could have an effect on the damping, however, considering the small amounts of tape used it was felt that this did not contribute significantly to the damping. Using large accelerometers on the tip will mass load the system, causing the resonant frequency to shift significantly downward (on the order of 5-10 Hz). The time to run the tests varied greatly between the random input and swept sine input tests. For one cantilever beam, to investigate all three modes, required almost 25 hours using the random input source. This compared to 5 hours using the swept sine source. The coherence for both tests was very good although measuring the strain and input acceleration for the swept sine tests was more difficult since the strain and acceleration are constantly changing. The swept sine tests compare favorably with the random tests. Therefore, either test could be used when comparing different materials, provided that the test samples have the same geometry. For lower levels of strain the random input tests give better results since the swept sine signal-to-noise ratio is very small making measurements of strain and damping difficult. Higher levels of strain can be obtained using the swept sine input method. Using swept sine input for higher strain levels and random input for lower strain levels would give satisfactory results.

IV. TORSION SAMPLE EXPERIMENTAL METHOD

A torsion testing apparatus was constructed to enable testing of the Sonoston specimen in torsion (Appendix C). The specimens were designed such that they form a single degree of freedom system under base excitation. Therefore, unlike the cantilever beam, where the strain varies along the beam length, the shear strain is constant at the outer radius along the length of the sample shaft. Appendix B delineates how the natural frequency of such a system can be calculated. In this test the sample was a 12 cm. long cylinder with a 0.8 cm. diameter. The same three heat treatments were performed as for the cantilever beams: Solution Annealing at 800°C for 1 hour, water quenching, and then aging one sample for 1 hour at 425°C; aging one sample for 2 hours at 425°C; and leaving one sample unaged. A strain gage was attached to allow for determining the shear strain that the specimen undergoes. Two Endevco accelerometers were used to obtain the transfer function between the base and the end rotation of the cylinder. The first accelerometer was attached to the turning disc while the second was attached to the heavy mass on the end of the sample. Figures 4.1 and 4.2 are photos of the torsion test apparatus and torsion sample respectively.

For random input testing, the RMS Shear Strain level was determined in exactly the same manner as it was for the bending strain (the average of ten 5mSec time samples for each excitation level). Figure 4.3 is a representative time history of one shear strain variation during a random test. The RMS input acceleration level was also obtained by averaging ten 5mSec time samples (Figure 4.4). An initial transfer function from 0-200 Hz using a random input was performed on the unaged sample in order to make sure that the sample was only excited in the torsion mode (Figure 4.5). A 60 Hz spike occurs every time, however. Baseband tests were also run for the 1hour and 2 hour samples. The torsion and bending frequencies were calculated using the values of Young's Modulus obtained from the tensile tests performed (refer to Chapter 2) and compared to the value obtained by zooming the test near the resonant frequency region. The Half-Power Point Method was used for determining the loss factor from the transfer function. In all three cases only the torsion mode was excited. Each sample was analyzed at nine different amplification levels.

For the swept sine tests, measurements of input acceleration and shear strain were made in the same way except that the time domain data was obtained at the peak of the transfer function. Six different amplification levels were used in the swept sine tests.

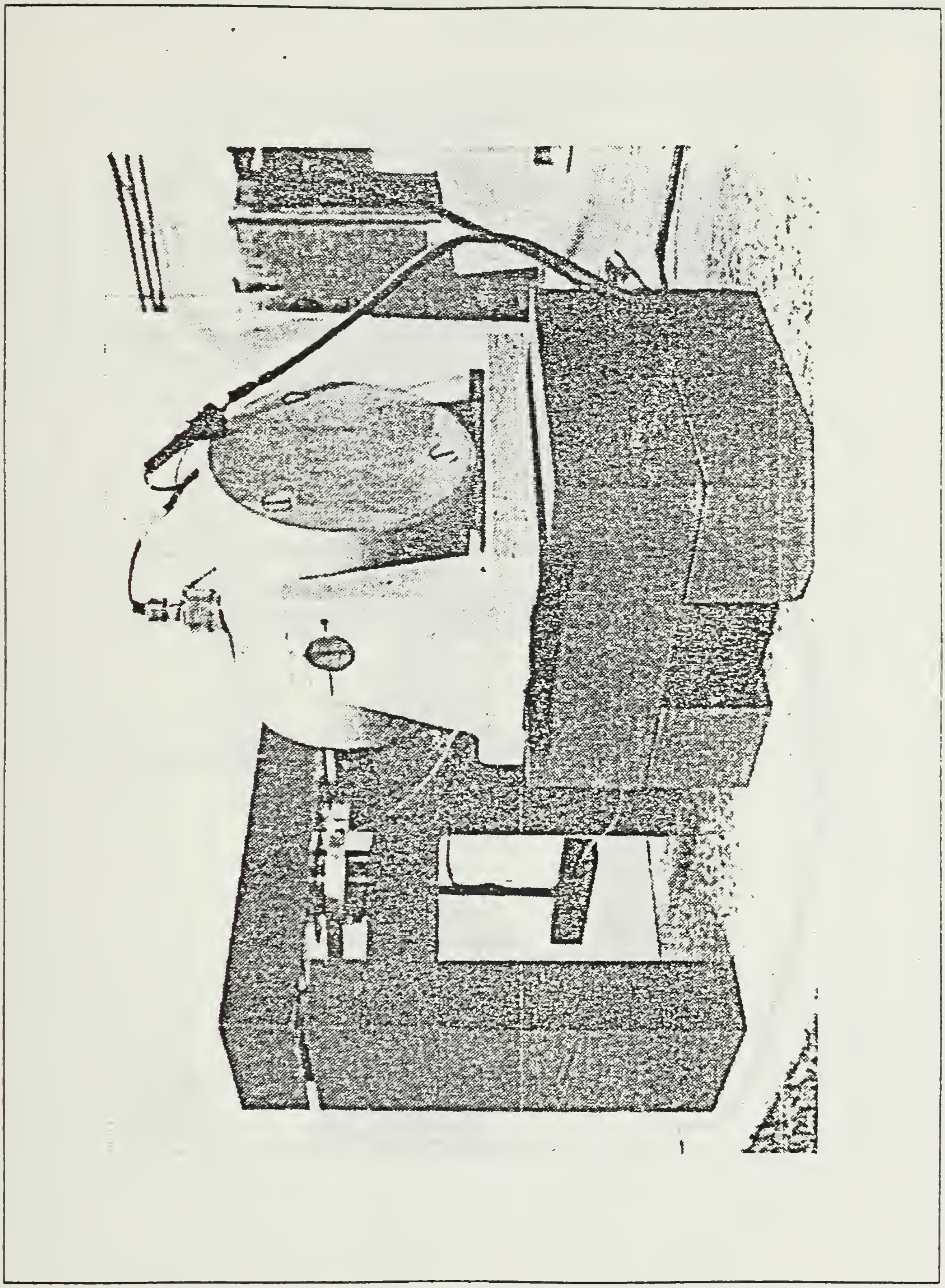

Figure 4.1 Torsion Sample Test Fixture

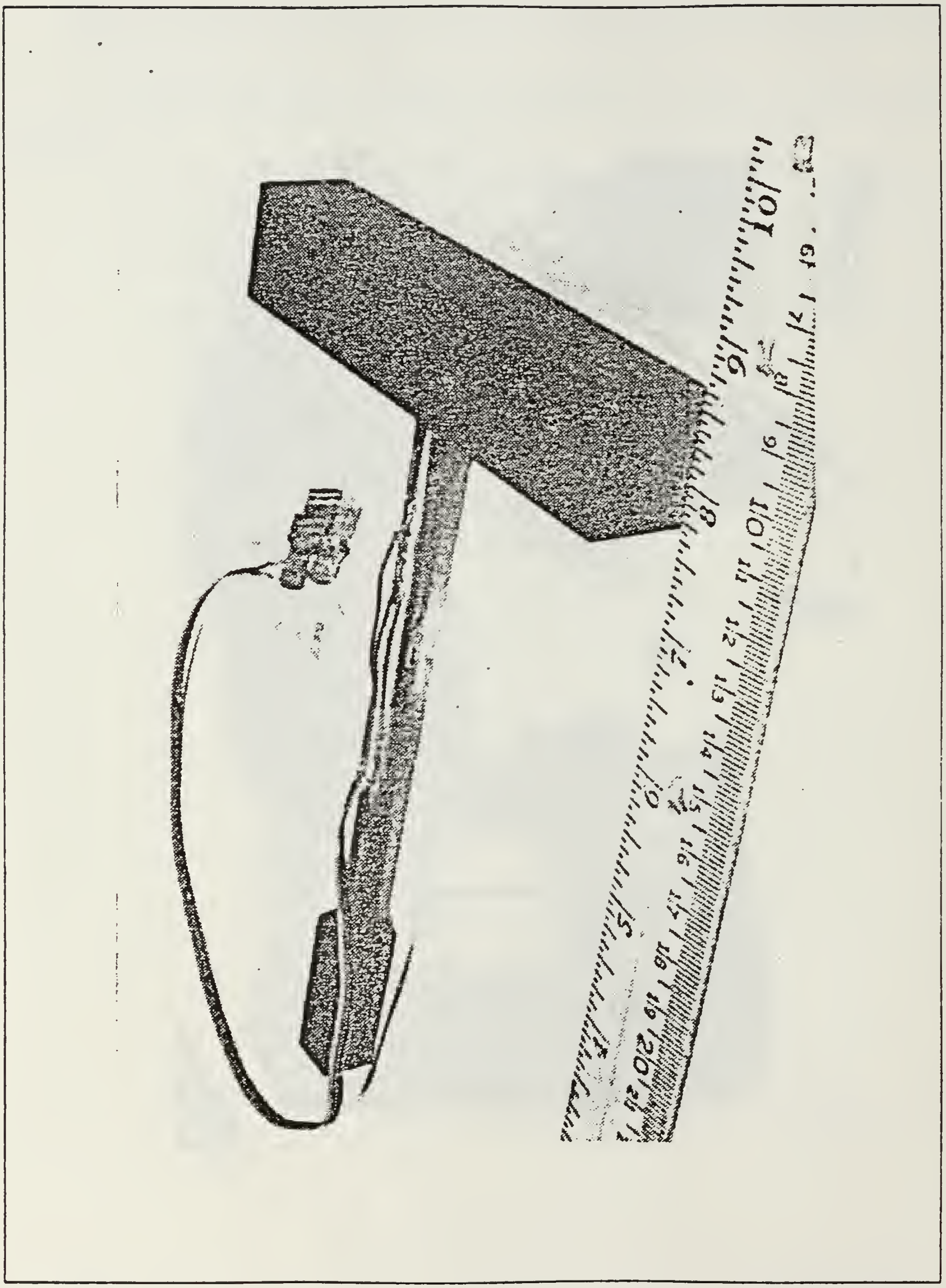

Figure 4.2 Torsion Sample Photograph

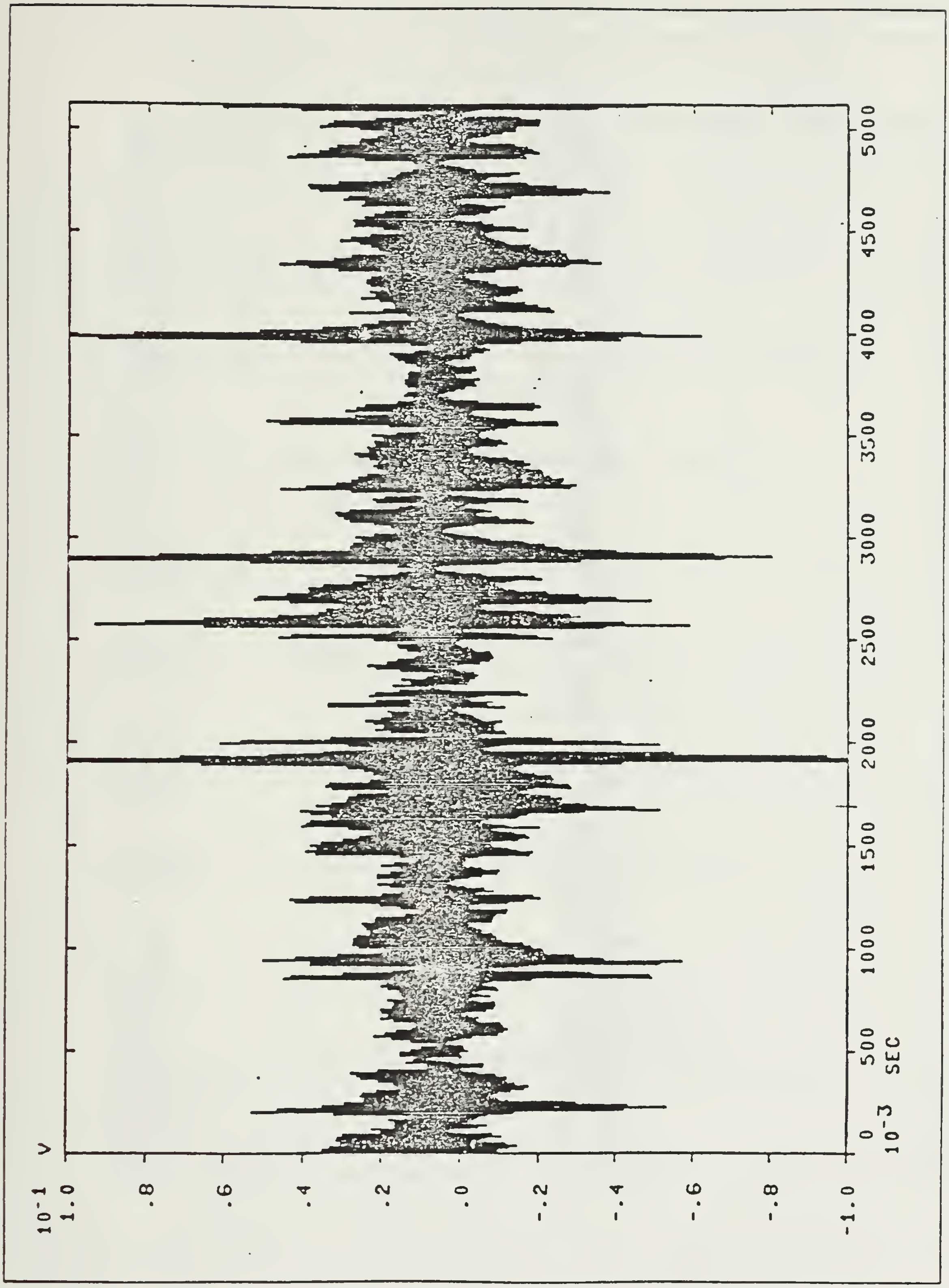

Figure 4.3 Time Sample of Shear Strain Gage

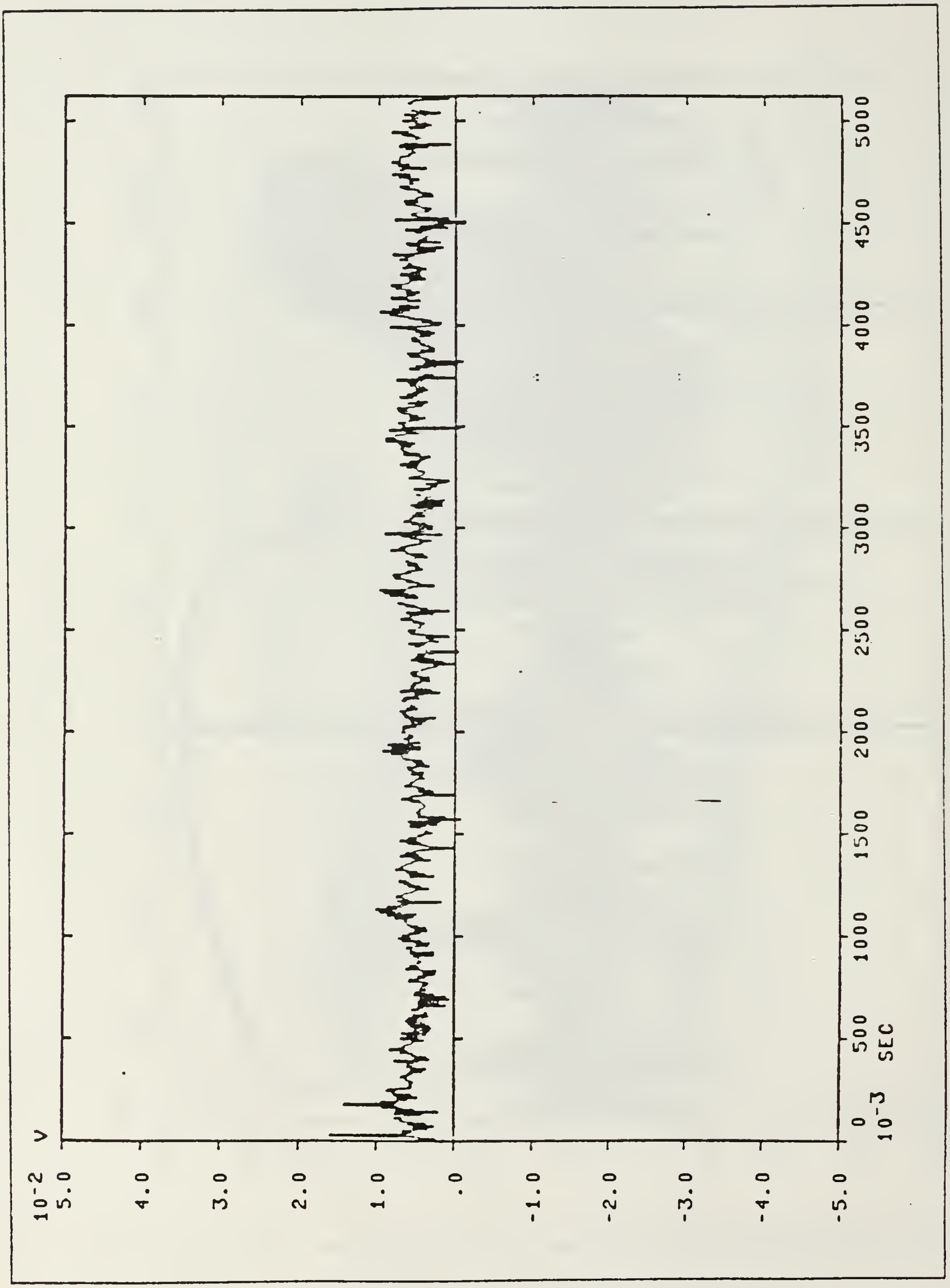

Figure 4.4 Time Sample of Torsion Input Accelerometer

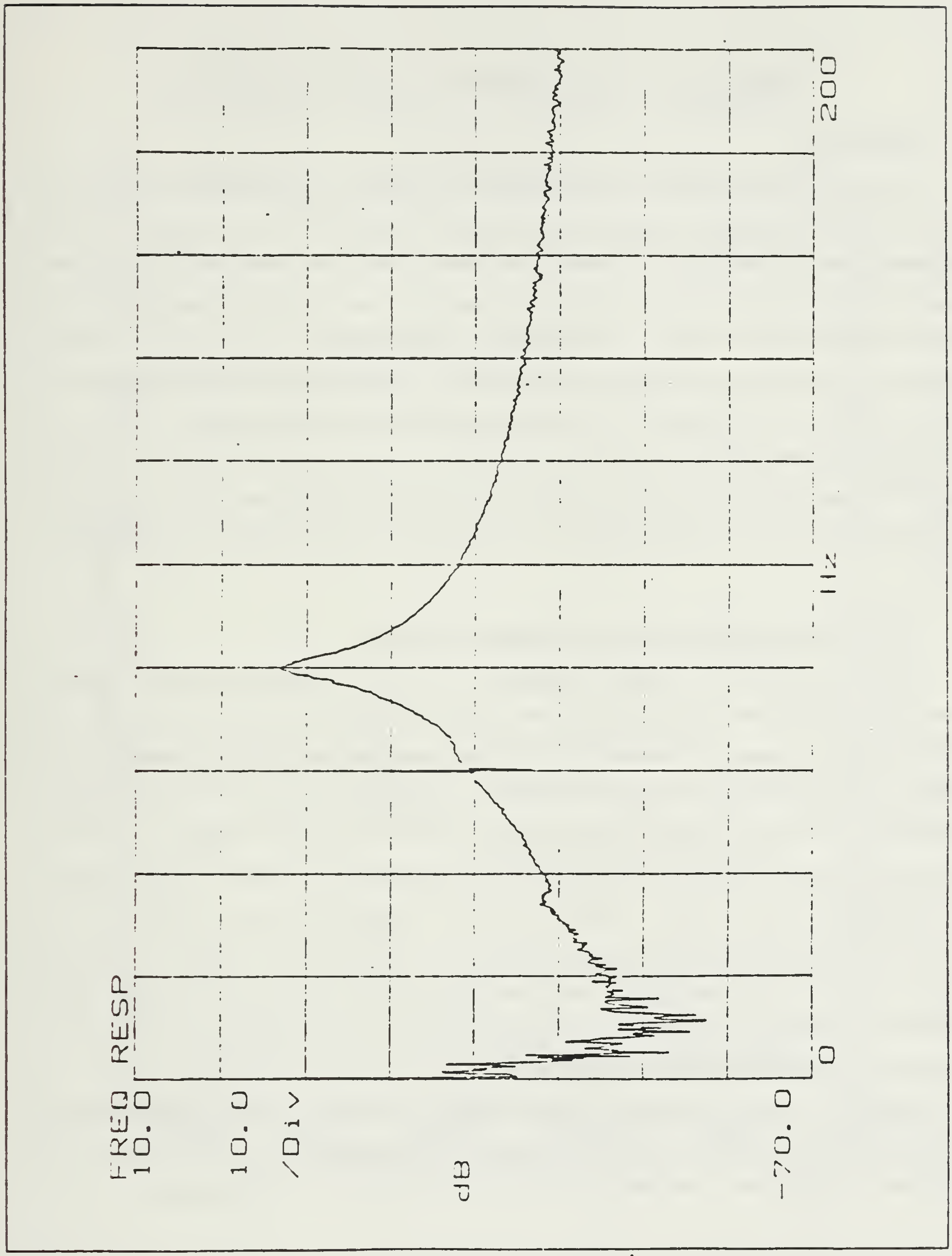

Figure 4.5 Baseband Response for Solution Annealed Sample

V. TORSION SAMPLE RESULTS AND DISCUSSION

A. GENERAL

The torsion samples that were analyzed give results in the frequency range 65-85 Hz. The solution annealed sample has a resonant frequency of 83 Hz compared to the calculated value of 84.5 Hz. For the 1 hour and 2 hour aged samples the calculated values were 89.6 and 101.9 Hz respectively but the actual resonant frequencies were approximately 68 Hz for both. The calculations were based on the values of Young's Modulus obtained from the tensile tests (Chapter 2) and assumed that the material was isotropic. Part 2 of Appendix D shows a representative transfer function (both in log magnitude and linear scales) for 32 time averages of one torsion sample. It also shows the 180° phase shift and coherence function associated with this one torsion test. The collected data from the random input and swept sine tests are listed in Appendix E, part 2.

B. INPUT ACCELERATION -VS- SHEAR STRAIN

Figure 5.1 shows the Input Acceleration -vs- RMS Shear Strain for a random input. This RMS shear strain value is determined exactly in the same manner as it was for the cantilever beam in Chapter 2. The input acceleration also is obtained in this manner. Each sample was tested at 9 different amplification levels with each value of strain and acceleration representing the average value of ten time samples. In this test the shear strain increases with increasing input acceleration in a linear fashion except at the highest levels of input. Figure 5.2 also is a graph of Input Acceleration -vs- Shear Strain but with a swept sine input instead of a random input signal. In this case the shear strain is obtained at the resonant frequency as is the value for the input acceleration (discussed in Chapter 2). The same trend exists between the shear strain and input acceleration using the swept sine input as it did for the random input. In both figures the shear strain increases with aging time, however, the 1 and 2 hour aged samples have very similar results indicating that when tested in the torsion mode the differences in aging times may not be as important as it is in the bending mode.

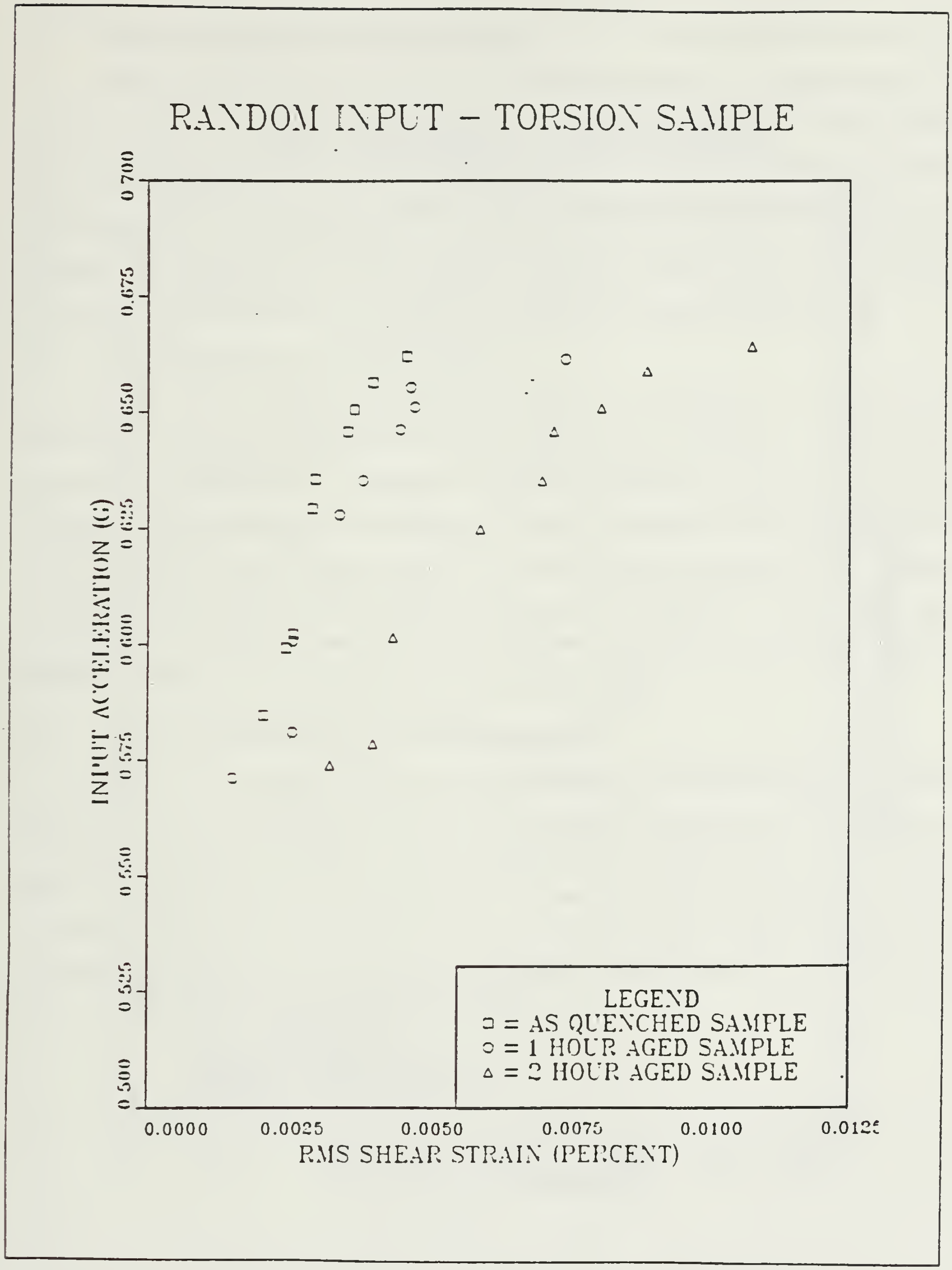

Figure 5.1 Torsion - Input Acceleration -vs Shear Strain (Random Input)

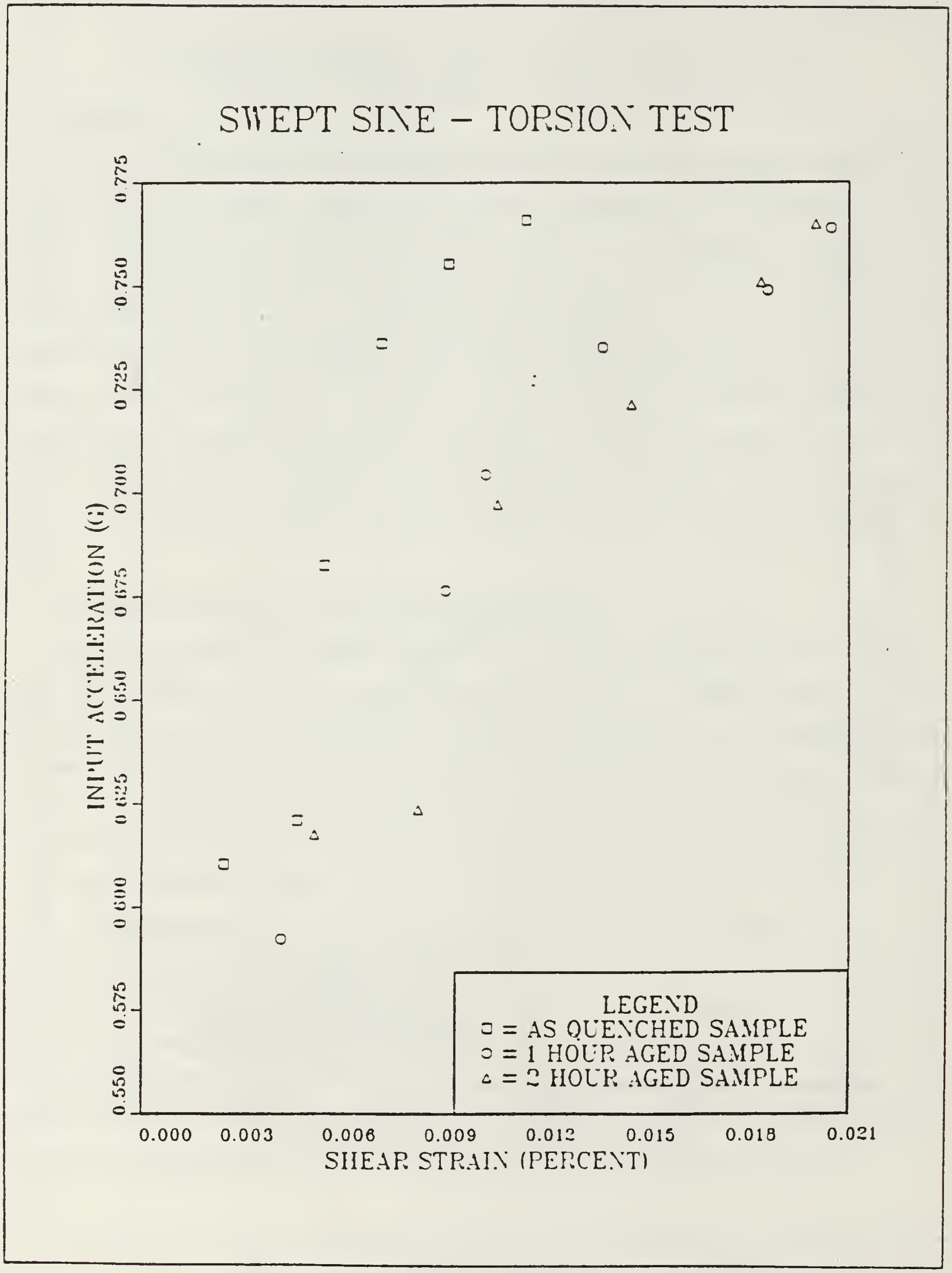

Figure 5.2 Torsion - Input Acceleration -vs- Shear Strain (Swept Sine)

C. LOSS FACTOR -VS- SHEAR STRAIN

Figure 5.3 shows the Loss Factor -vs- RMS Shear Strain for random input. The results are similar to those found for the cantilever beam in that higher levels of strain produce higher loss factors and the loss factor increases with aging time. The results also show that the loss factor depends on shear strain and is very nonlinear for the aged samples. In the torsion case the 1 and 2 hour aged samples give fairly identical results. The torsion test was run a second time using a swept sine input (Figure 5.4). The results from this test are very similar to those of the random input test.

D. SHEAR STRAIN -VS- FREQUENCY

Figure 5.5 is a graph of RMS Shear Strain -vs- Frequency for random input. The resonant frequency shifts downward as the shear strain increases. An increase in shear strain corresponds to a decrease in the Shear Modulus just as an increase in bending strain corresponds to a decrease in Young's Modulus for the cantilever beam. This decrease in Shear Modulus results in a lower resonant frequency which is similar to the results obtained in the cantilever beam tests. Again the 1 and 2 hour aged samples give very similar results. When compared to Figure 5.5, the swept sine test results for Figure 5.6 gives approximately the same results.

E. INPUT ACCELERATION -VS- FREQUENCY

Figure 5.7 is a graph of the Input Acceleration -vs- Frequency for the random input test. As in the cantilever beam case the resonant frequency shifts downward as the input acceleration increases. In the torsion test this is due to the decrease in the Shear Modulus since the input acceleration is directly related to the shear strain. The frequency shift appears to be the same for all three samples. Figure 5.8 graphs the results of the swept sine tests. Again, the frequency shift downward appears although it is not quite as pronounced as with the random test.

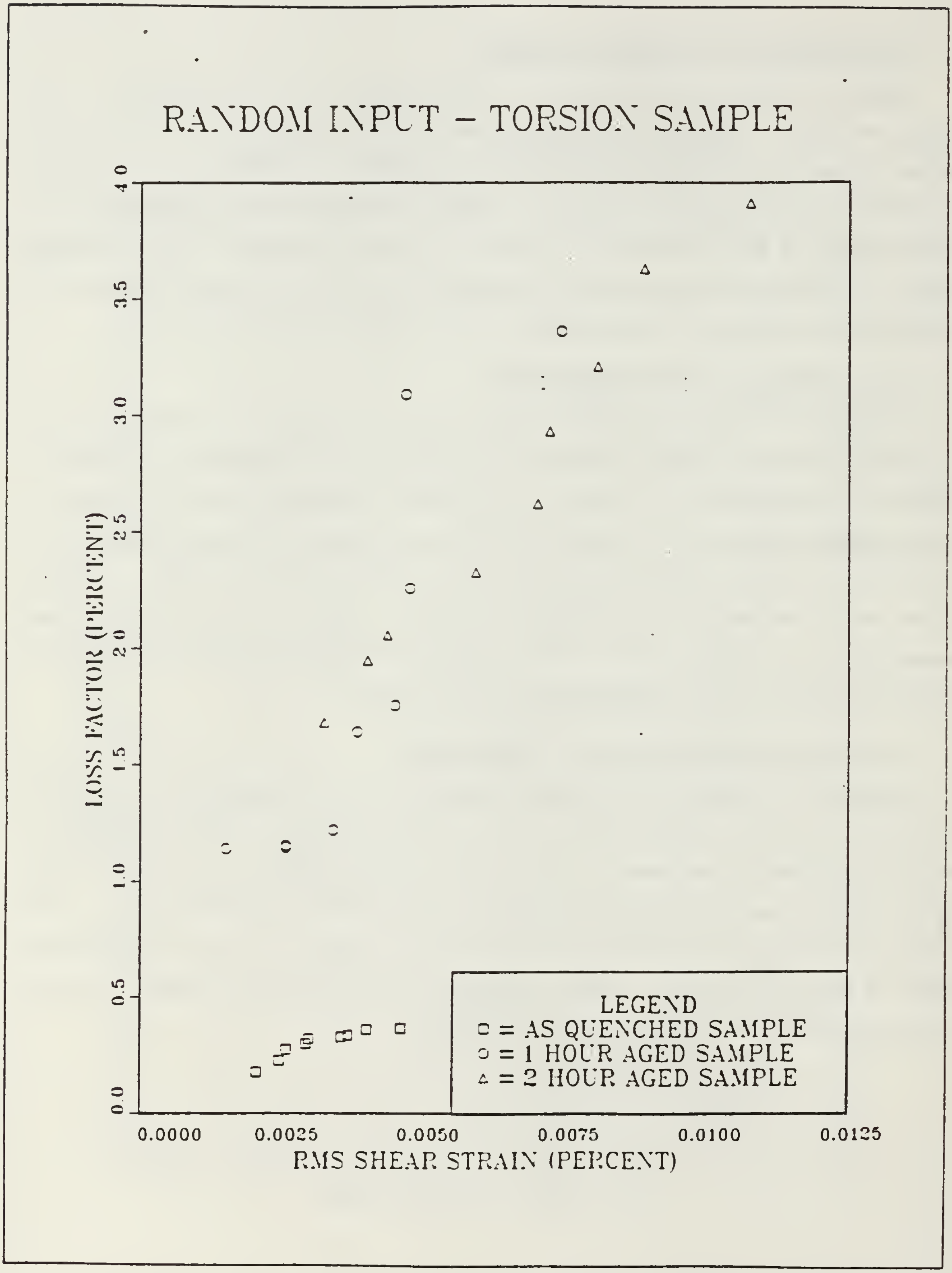

Figure 5.3 Torsion - Loss Factor -vs- Shear Strain (Random Input)

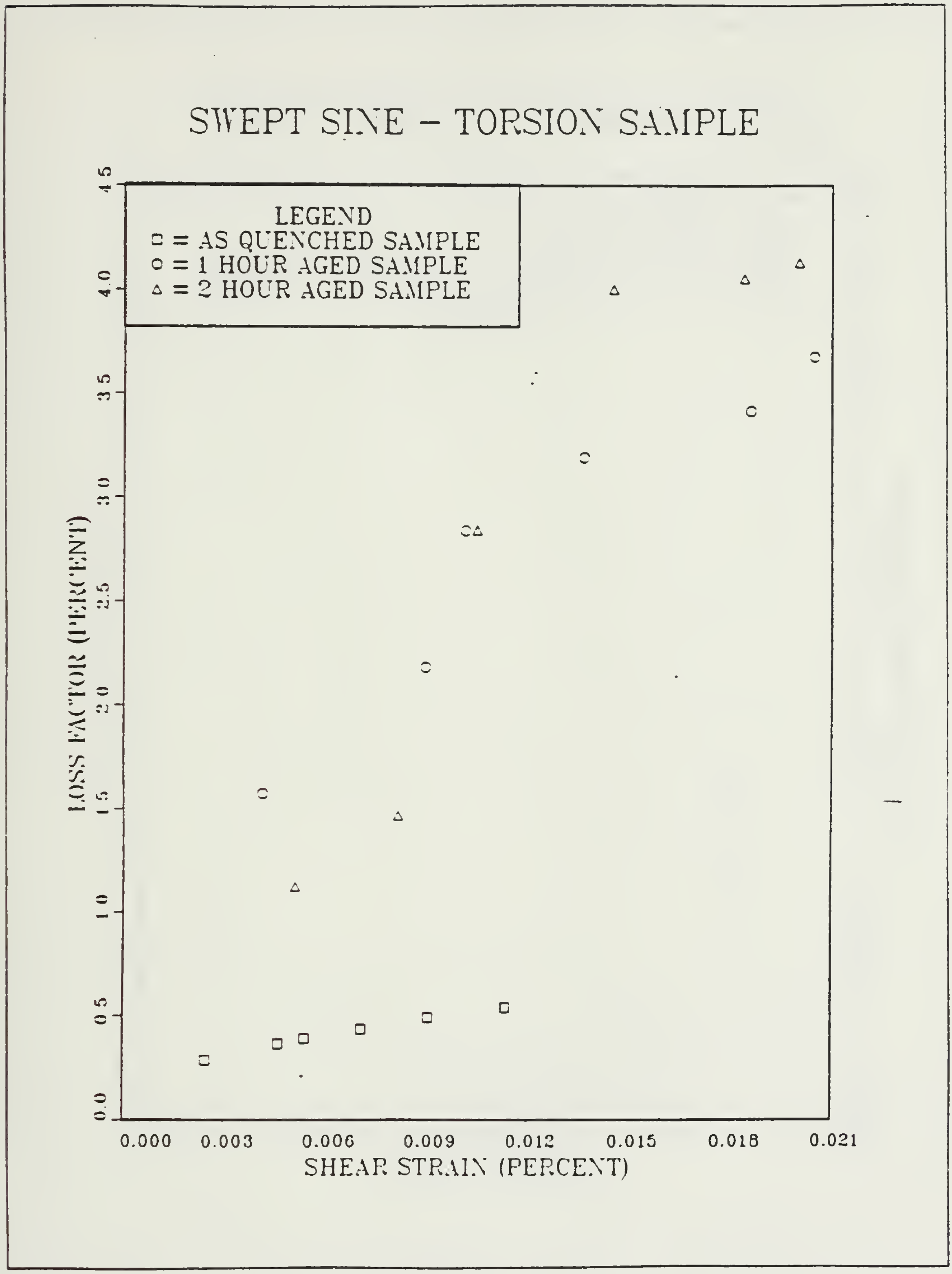

Figure 5.4 Torsion - Loss Factor -vs- Shear Strain
(Swept Sine)

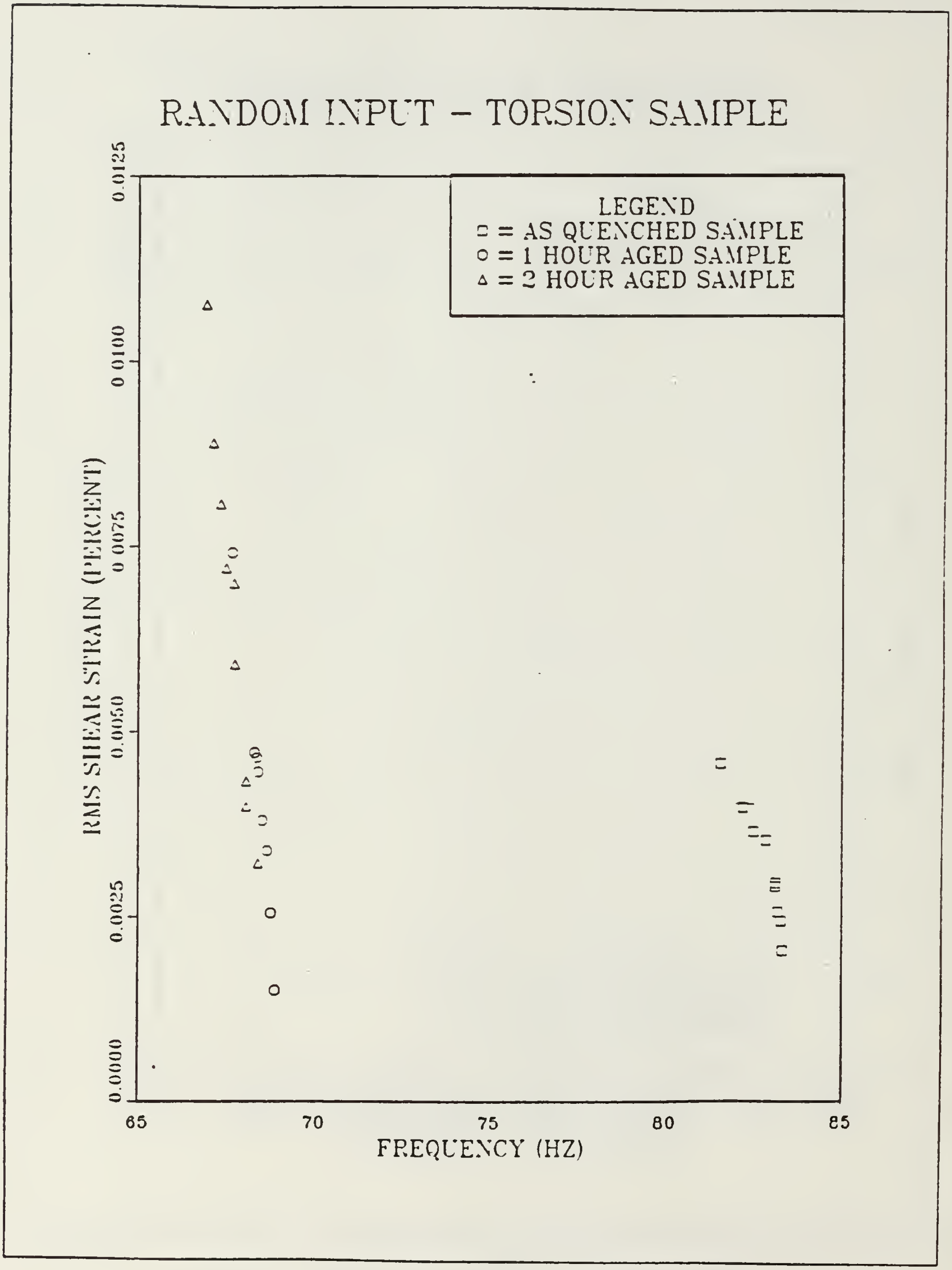

Figure 5.5 Torsion - Shear Strain -vs- Frequency
(Random Input)

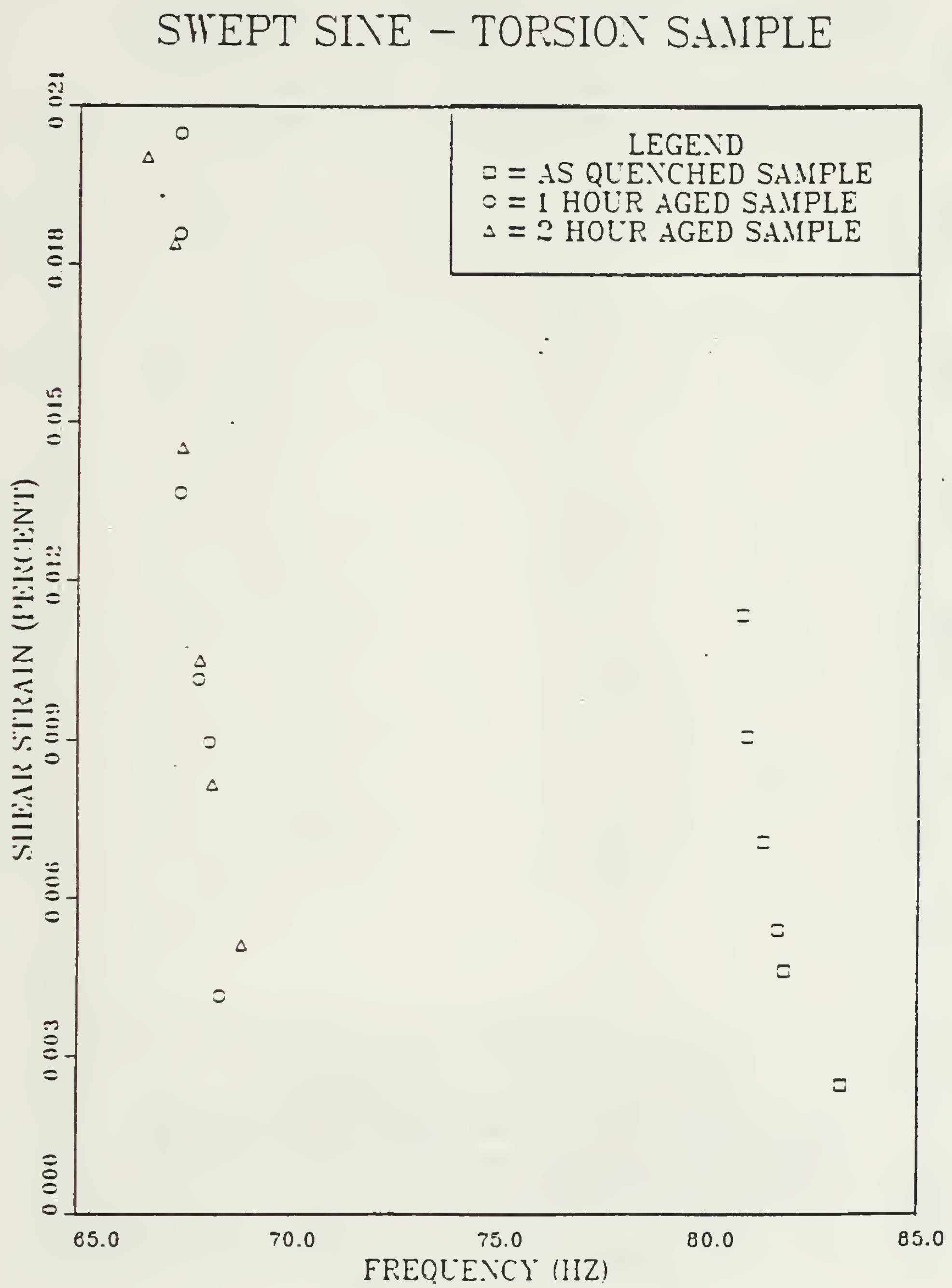

Figure 5.6 Torsion - Shear Strain -vs- Frequency
(Swept Sine)

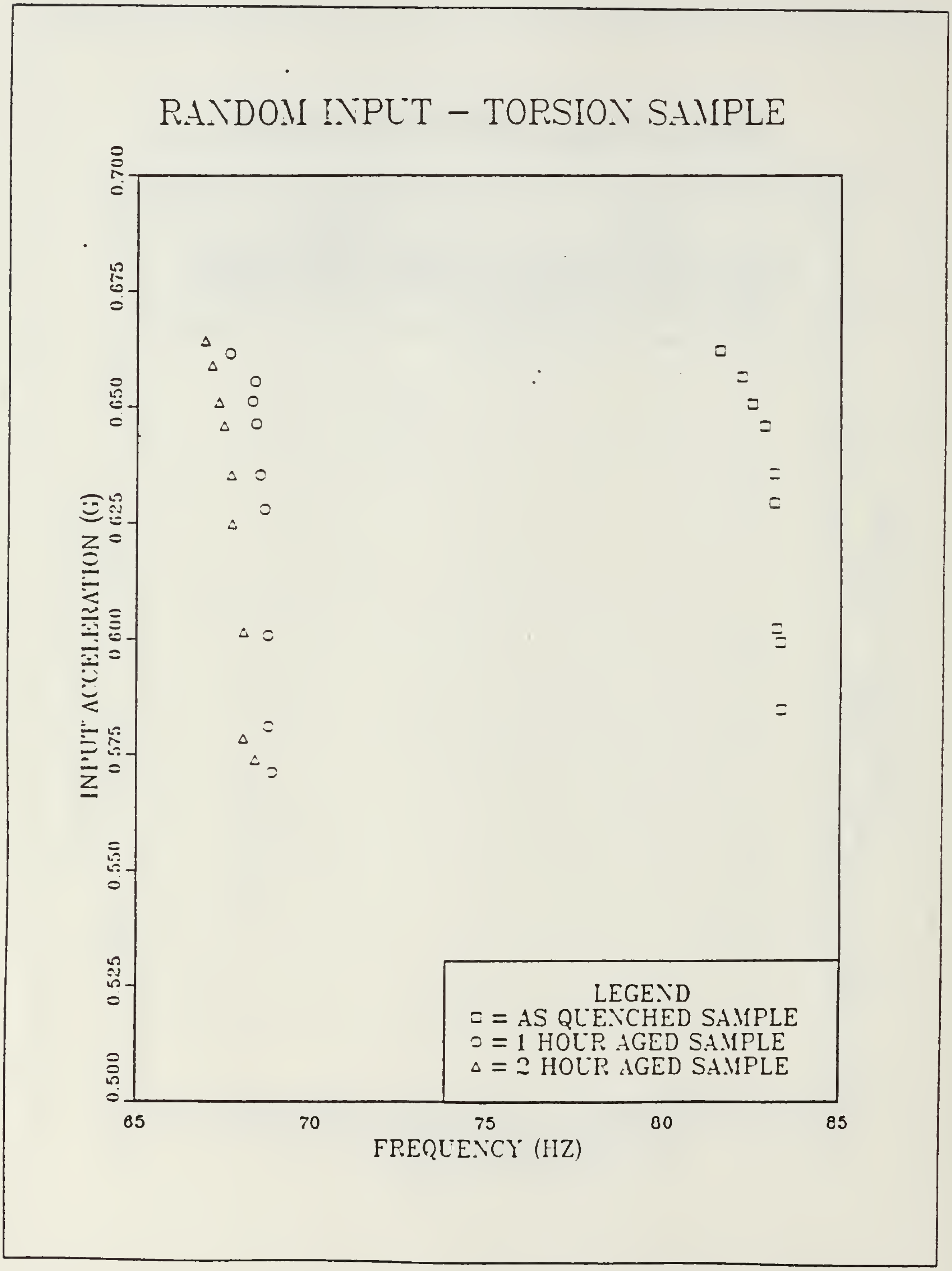

Figure 5.7 Torsion - Input Acceleration -vs- Frequency (Random Input)

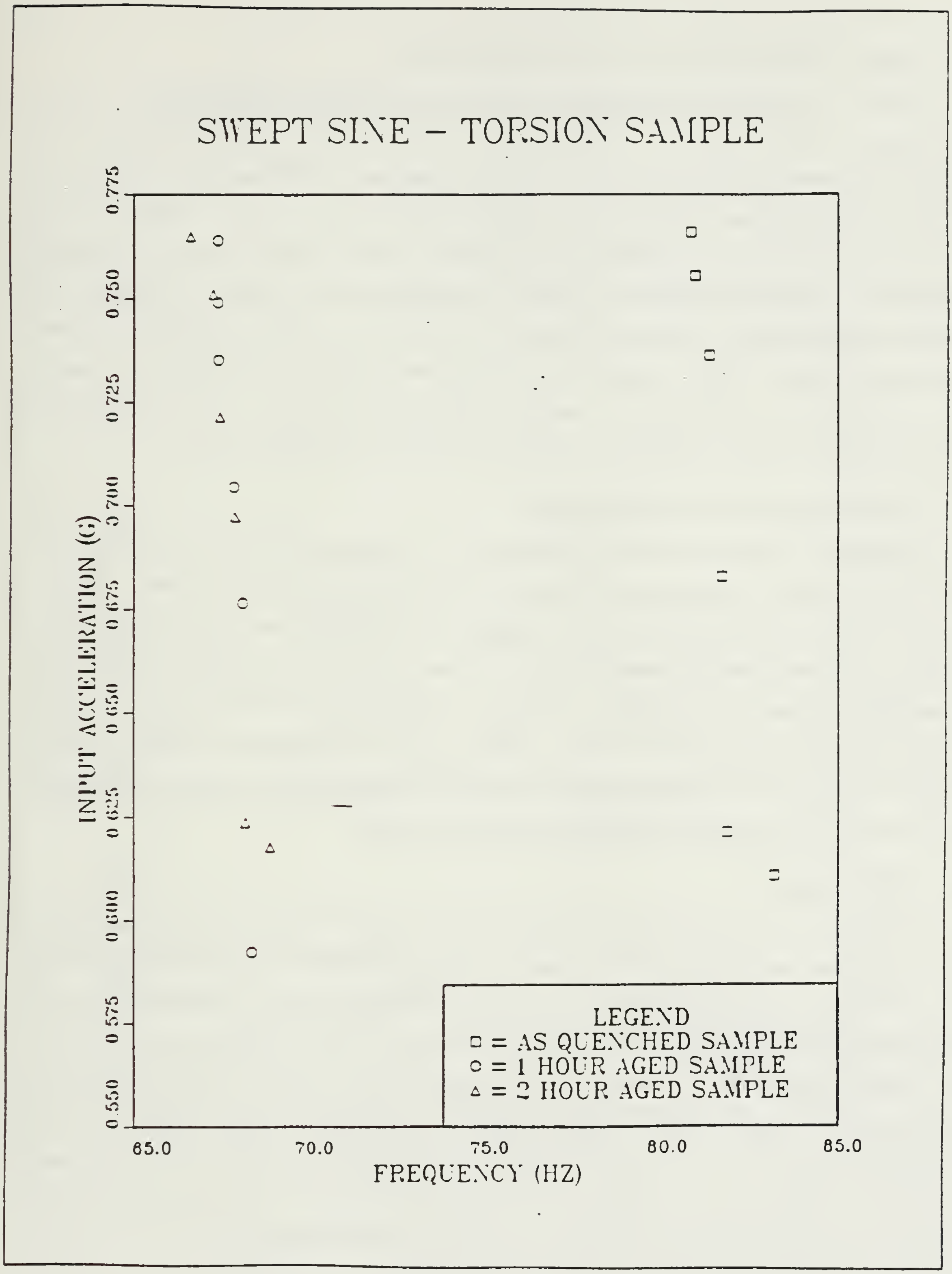

Figure 5.8 Torsion - Input Acceleration -vs- Frequency (Swept Sine)

F. INPUT ACCELERATION -VS- LOSS FACTOR

Figure 5.9 shows the loss factor as a function of the input acceleration. As with the results of Loss Factor -vs- Shear Strain the loss factor increases with both an increase in the input acceleration and with the aging time. The increase in the input acceleration corresponds to an increase in the shear strain and thus an increase in the loss factor. These results are similar to those for the Loss Factor -vs- Shear Strain and are expected. Aging time does play a part in increasing the loss factor but there does not seem to be much of a difference between the 1 hour and 2 hour aged samples when tested in the torsion mode. Figure 5.10 depicts the results of the swept sine tests. These results show a difference in the loss factor between the 1 and 2 hour aged samples although they do follow the same trend as the random input results.

G. LOSS FACTOR -VS- FREQUENCY

Figure 5.11 shows the resonant frequency as a function of the loss factor. As the loss factor increases, the resonant frequency shifts downward for all three samples. This shift is more pronounced for the unaged sample than for the 1 and 2 hour aged samples. The downward frequency shift is a result of an increase in shear strain and the resulting decrease in the Shear Modulus. This increase in the shear strain also causes the increase in the loss factor. Figure 5.12 is the swept sine results. These results are similar to the random input results, again indicating that testing of materials can be conducted using either random or swept sine input.

H. DISCUSSION

The swept sine test results compare favorably with those of the random input tests. Therefore, both tests could be used to compare different materials provided the same geometry was involved since the values obtained are shape dependent and not dependent on the material properties. For lower levels of shear strain the random tests give better results since the swept sine signal-to-noise ratio is very small making measurements of damping and shear strain difficult. Higher levels of shear strain can be obtained using the swept sine input method. Since both random and swept sine inputs give similar results, using swept sine input for higher measurement levels and random input for lower measurement levels gives satisfactory results.

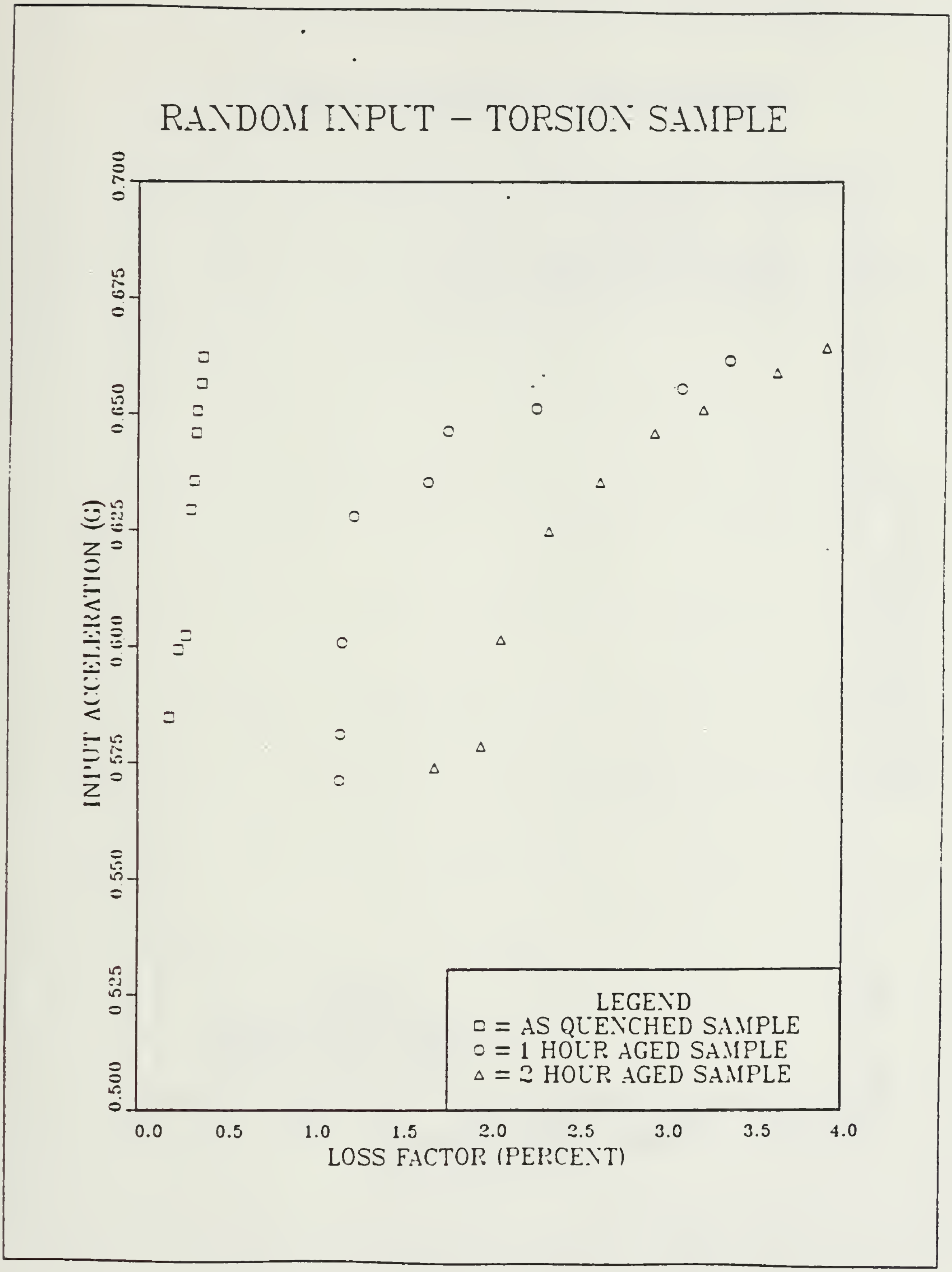

Figure 5.9 Torsion - Input Acceleration -vs- Loss Factor (Random Input)

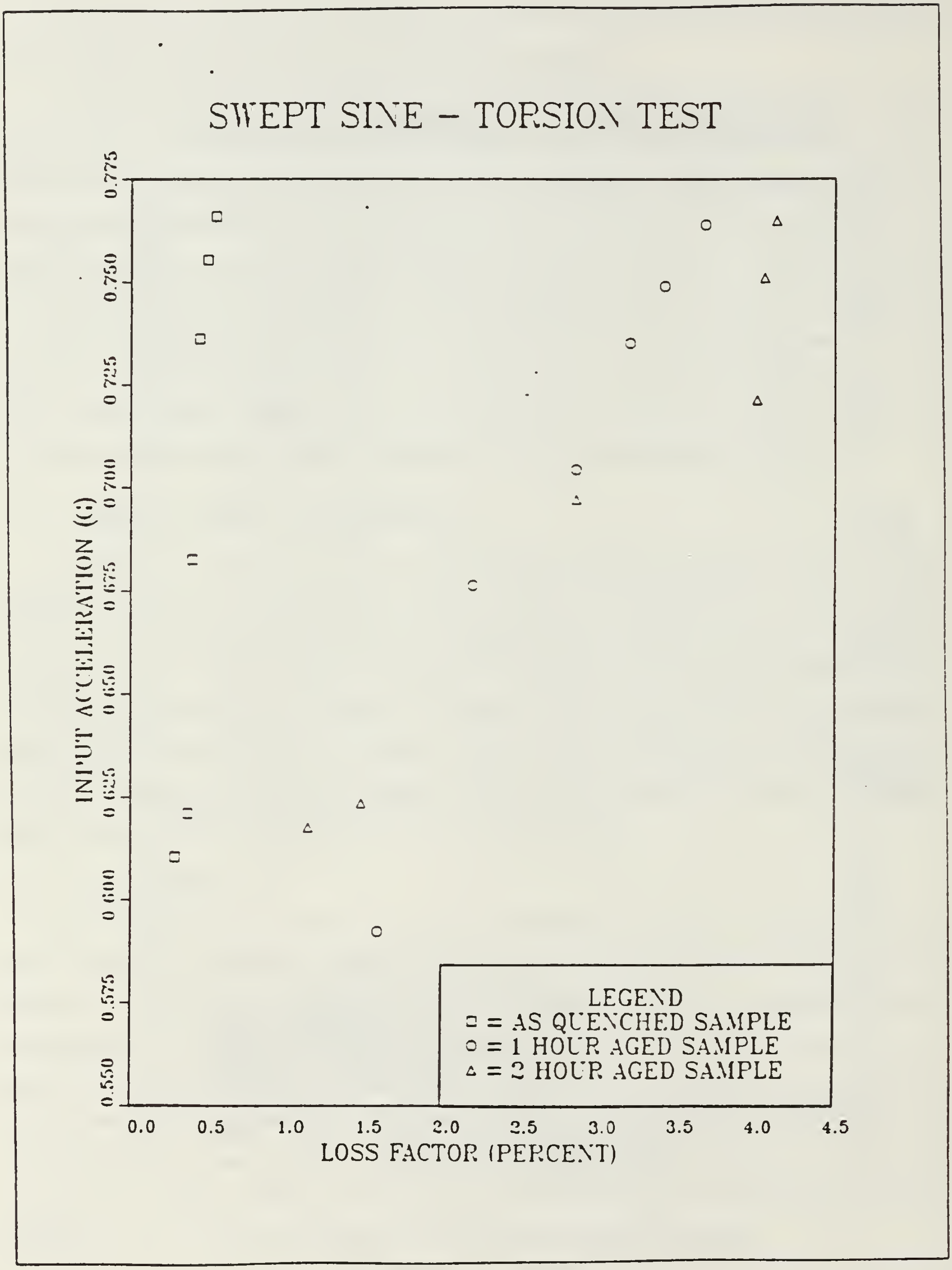

Figure 5.10 Torsion - Input Acceleration -vs- Loss Factor (Swept Sine)

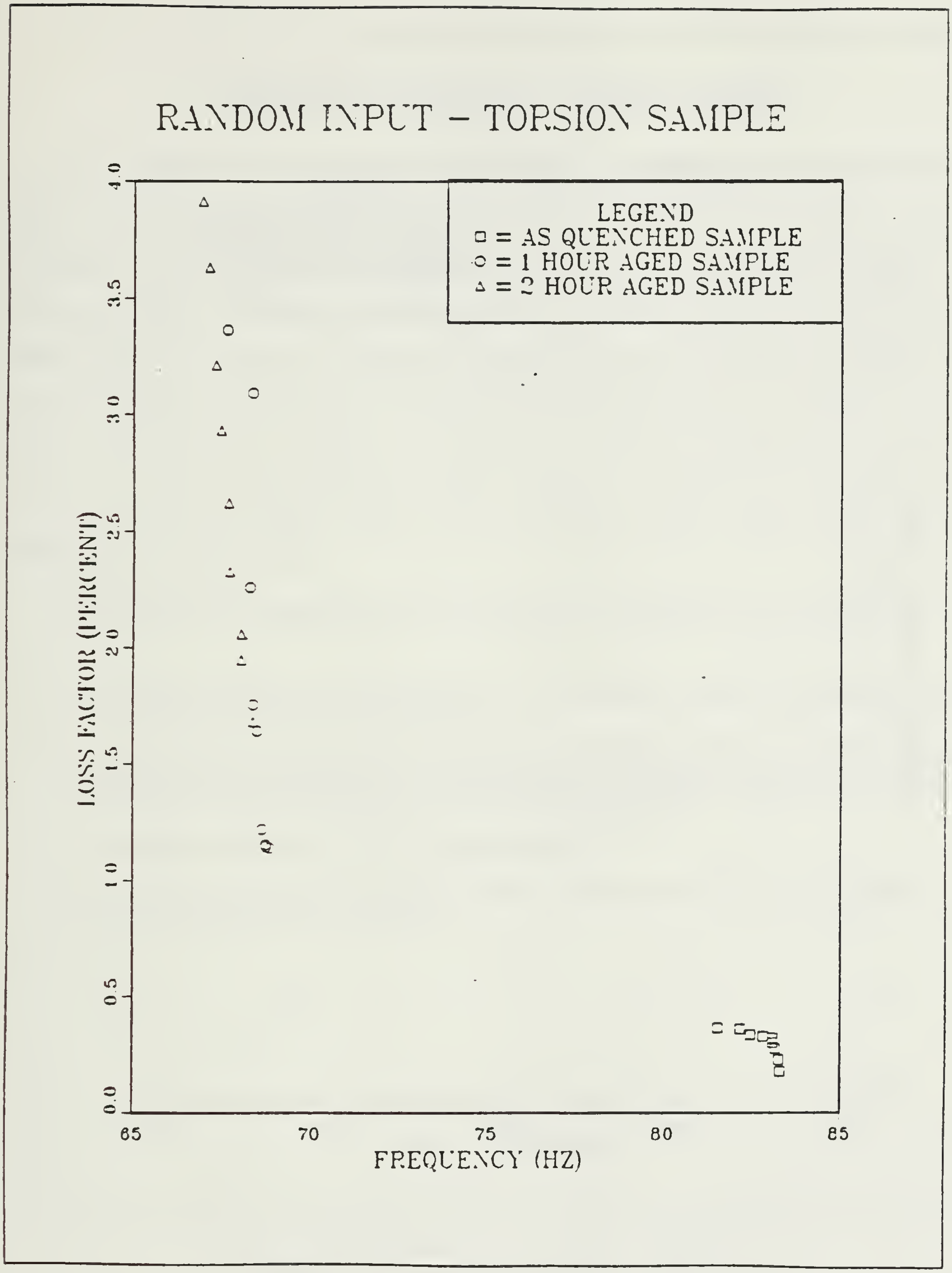

Figure 5.11 Torsion - Loss Factor -vs- Frequency
(Random Input)

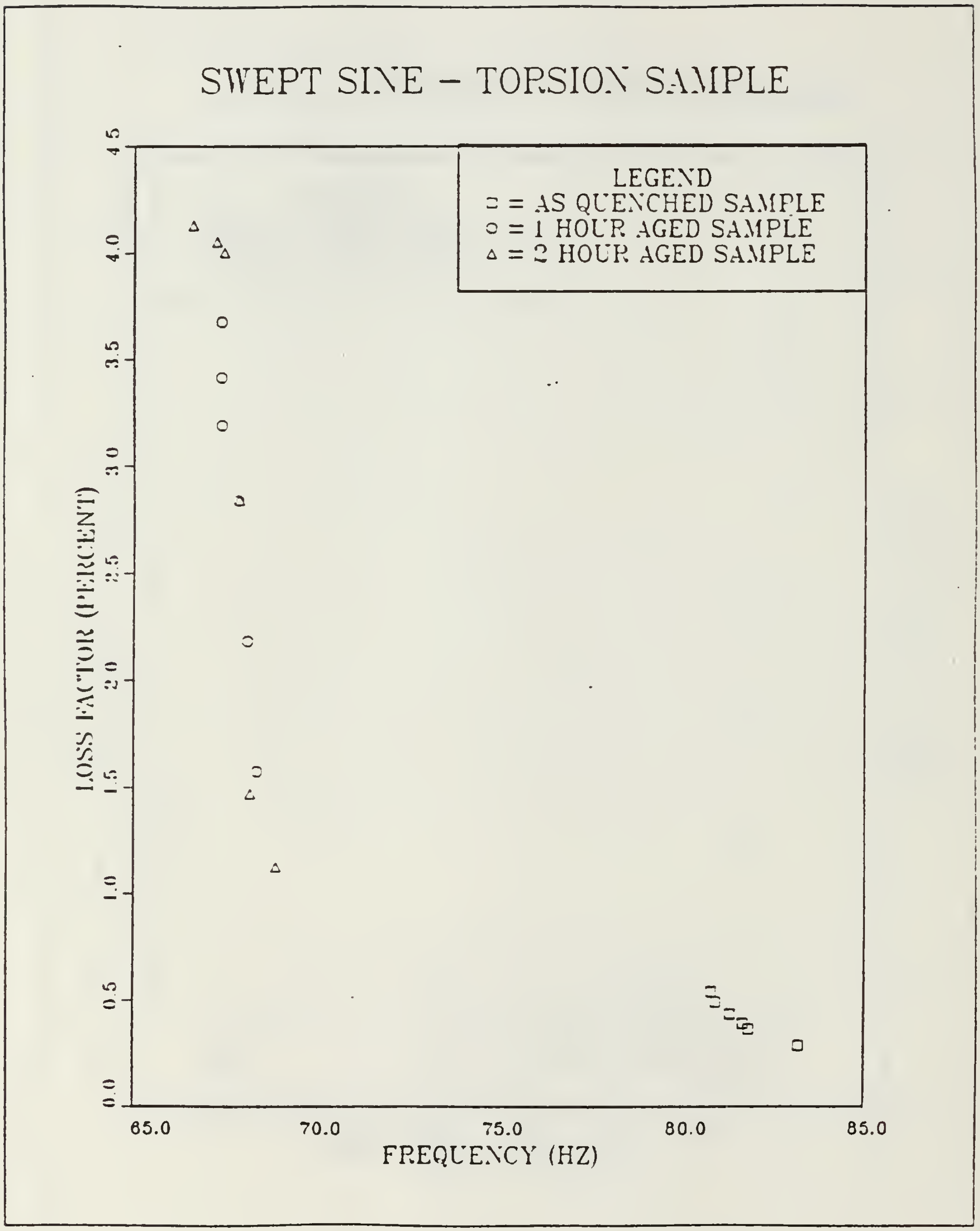

Figure 5.12 Torsion - Loss Factor -vs- Frequency (Swept Sine)

VI. DISCUSSION AND RECOMMENDATIONS

The results of the testing conducted on both the cantilever beam and torsion samples are repeatable whether random input is used for the excitation source or swept sine is used. In all of the cases the geometry of the samples to be compared must be the same in order for analysis of the different mechanical properties of the materials to be accomplished. As mentioned previously using a random input for lower levels of strain (bending or shear) gives better results since the swept sine signal-to-noise ratio is very small making measurements of the strain and damping difficult. The swept sine input should be used for higher levels of strain. Another consideration in deciding which test to run involves the amount of time available for analyzing the samples. The swept sine tests are much faster than the random tests, in this case it was approximately 5 times faster.

The following recommendations are provided to assist follow-on investigations:

1. Investigate higher strain levels. For the cantilever beam arrangement this would involve shorter length samples.
2. Investigate the use of multiple input excitation for the torsion setup. Using two identical vibration generators attached to the turning disc on opposite sides would prevent any possibility of inadvertently exciting a bending mode. This would allow higher levels of shear strain to be obtained.
3. Investigate specimens with longer aging times.
4. Use of a non-contacting excitation scheme would get rid of any damping due to the shaker contacting the sample.

APPENDIX A
HALF-POWER POINT METHOD

Physical systems usually have small values of damping. It is common to find systems with gain factors having sharp peaks and phase factors showing rapid 180° phase shifts. The system, therefore, looks like a narrow bandpass filter, with bandwidth measured in terms of the half-power point bandwidth of the frequency response. These half-power points (Figure A.1) are located at a point .707 of the amplitude of the resonant frequency (ω_n). The bandwidth is then defined as $(\omega_2-\omega_1)/(\omega_n) = (f_2-f_1)/f_n = 2\xi$. The quality factor, Q, which is a measurement of the sharpness of resonance, is also easily obtained by:

$$Q = f_n/(f_2-f_1) = 1/2\xi \qquad \text{(A.1)}$$

If the amplitude is measured in decibels then the half-power points correspond to a 3 db loss from the peak.

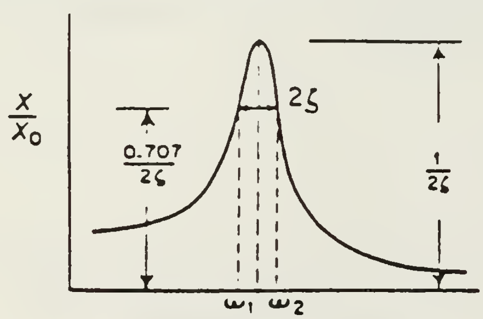

Figure A.1 Half-Power Point Method {Ref. 8}

APPENDIX B

DETERMINATION OF NATURAL FREQUENCIES

1. CANTILEVER BEAM

The differential equation for the lateral vibrations of a cantilever beam comes from Euler's equation for beams. Reference 8 gives a good explanation of how to obtain the resonant frequency of a beam which is determined from:

$$\omega_n = A\sqrt{(EI)/(\mu l^4)} \qquad (B.1)$$

Table B.1 lists values of A for different beam configurations and modes of vibration. In this study the first three modes of the cantilever beam have values for A of 3.52,22.4,and 61.7. The moment of inertia (I) of the beam is found by the equation $(1/12)bh^3$ For the beams in this experiment: (Figure B.1)

$$\text{length}(l) = 7.5 \text{ inches}$$
$$\mu = 41.408 \times 10^{-6}(\text{lb-sec}^2)/(\text{in.}^2)$$
$$\text{width}(b) = 0.5 \text{ inches}$$
$$\text{thickness}(h) = 1/16 \text{ inch}$$
$$I = 10.1725 \times 10^{-6} (\text{in.}^4)$$

The calculated resonant frequencies for the samples tested in this experiment are listed in Table B.2.

TABLE 1

VALUES OF A FOR DIFFERENT BEAM CONFIGURATIONS

{Ref. 8}

BEAMS OF UNIFORM SECTION AND UNIFORMLY DISTRIBUTED LOAD

ANGULAR NATURAL FREQUENCY $\omega_n = A\sqrt{\frac{EI}{\mu l^4}}$ RAD/SEC

WHERE E = YOUNG'S MODULUS, LB/IN^2

I = AREA MOMENT OF INERTIA OF BEAM CROSS SECTION, IN.^{4}

l = LENGTH OF BEAM, IN

μ = MASS PER UNIT LENGTH OF BEAM, LB-SEC^2/IN^2

A = COEFFICIENT FROM TABLE BELOW

NODES ARE INDICATED IN TABLE BELOW AS A PROPORTION OF LENGTH l MEASURED FROM LEFT END

FIXED-FREE (CANTILEVER)	A = 3.52	0.774 A = 22.4	0.500 0.868 A = 61.7	0.356 0.644 0.906 A = 121.0	0.279 0.500 0.723 0.926 A = 200.0
HINGED-HINGED (SIMPLE)	A = 9.87	0.500 A = 39.5	0.333 0.667 A = 88.9	0.25 0.50 0.75 A = 158	0.20 0.40 0.60 0.80 A = 247
FIXED-FIXED (BUILT-IN)	A = 22.4	0.500 A = 61.7	0.359 0.641 A = 121	0.278 0.500 0.722 A = 200	0.227 0.409 0.591 0.773 A = 298
FREE-FREE	0.224 0.776 A = 22.4	0.132 0.500 0.868 A = 61.7	0.094 0.356 0.644 0.906 A = 121	0.073 [illegible] 0.500 0.723 0.927 A = 200	0.060 0.227 0.409 0.591 0.773 0.940 A = 298
FIXED-HINGED	A = 15.4	0.560 A = 50.0	0.384 0.692 A = 104	0.235 [illegible] 0.765 A = 178	[illegible] A = 272
HINGED-FREE	0.736 A = 15.4	0.446 0.853 A = 50.0	0.308 0.616 0.898 A = 104	0.235 0.471 [illegible] 0.922 A = 178	0.190 0.381 0.581 0.763 0.937 A = 272

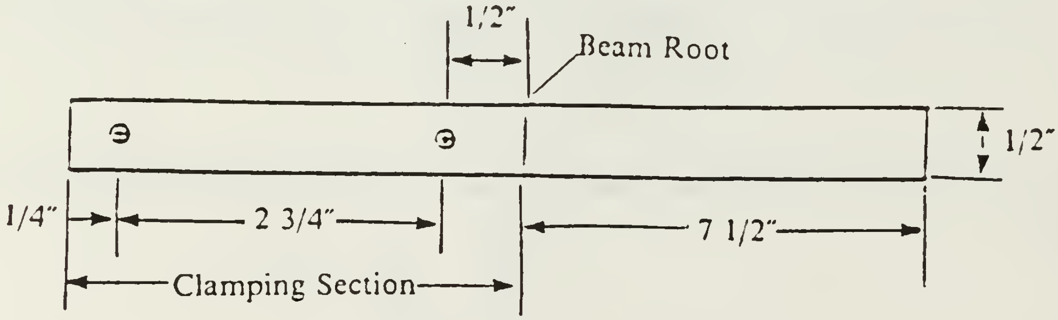

Figure B.1 Sonoston Beam Configuration

TABLE 2

CALCULATED RESONANT FREQUENCIES
OF CANTILEVER BEAMS

	Resonant Frequency (Hz)		
	Mode 1	Mode 2	Mode 3
For the solution annealed beam:	20.6	131.4	361.9
For the 1 hour aged beam:	21.9	139.4	384.0
For the 2 hour aged beam:	24.9	158.6	436.9

2. TORSION

Reference 8 also derives the natural frequency for torsional vibration. The equation for the natural frequency is:

$$\omega_n = \sqrt{K_r/(J_o + 1/3J_1)} \tag{B.2}$$

where: $K_r = G\pi d^4/32l$ $J_1 = 2I_p\rho l_1$ $J_o = \rho b/12(wl^3 + lw^3)$

For the samples tested:

length of the spherical section(l_1) = 12cm
diameter of the spherical section(d) = 0.8cm
length of the bottom section(l_2) = 12.0cm
width of the bottom section(w) = 2.0cm
height of the bottom section(b) = 2.5cm
$I_p = \pi d^4/96$
$J_1 =$ 2(0.0201 cm^4)(7.46 gm/cm^3)12 cm = 3.5998($gm\text{-}cm^2$)
$J_o =$ 5520.4($gm\text{-}cm^2$)
$G = E/(2(1+\nu))$ where $\nu =$ 0.3

The calculated natural frequencies for the torsion samples tested are listed in Table B.3.

TABLE 3

CALCULATED RESONANT FREQUENCIES OF TORSION SAMPLES

	G (Kg/cm^2)	K_r ($Kg\text{-}cm^2$)	Resonant Frequency (Hz)
solution annealed sample:	0.473 x 10^6	1585.0	84.5
1 hour aged sample:	0.5325 x 10^6	1784.0	89.6
2 hour aged sample:	0.6893 x 10^6	2309.0	101.9

APPENDIX C

TORSION DAMPING APPARATUS DESIGN

In designing the torsion damping apparatus several requirements had to be met:

1. Minimizing extraneous energy loss (friction losses at the clamp interface, inherent loss in the clamp material, etc.).
2. Ensuring uniform stress distributions in the specimen.
3. Limiting the shaker to 25 pounds of force (before requiring forced air cooling).
4. The natural frequency of the specimen had to be less than 1000 hz.

The sample fits through the turning disc where it is held in place by 4 set screws (Figures C.1, C.2, and C.3) A bolt rests against the top of the specimen preventing it from moving vertically. The turning disc is supported by tapered roller bearings to prevent both radial and axial motion. The stand was designed to hold the turning disc and provide weight for stability (Figures C.4 and C.5). The shaker excites the apparatus by a "stinger" attached to the turning disc in the horizontal direction. Figure C.6 shows the assembled apparatus. The shaker also had a stand manufactured, elevating it to provide the horizontal input force (Figure C.7). Again, a heavy stand was made to ensure stability (eliminate any created moments). To meet the force requirements for the shaker the following equations were used to determine sample size:

$$\text{Disc Mass} = \pi r^2 h \rho \qquad I(\text{DISC}) = Mr^2/2$$

$$a(\text{disc acceleration}) = r\theta(2\pi f)^2$$

$$F = Ia/r^2$$

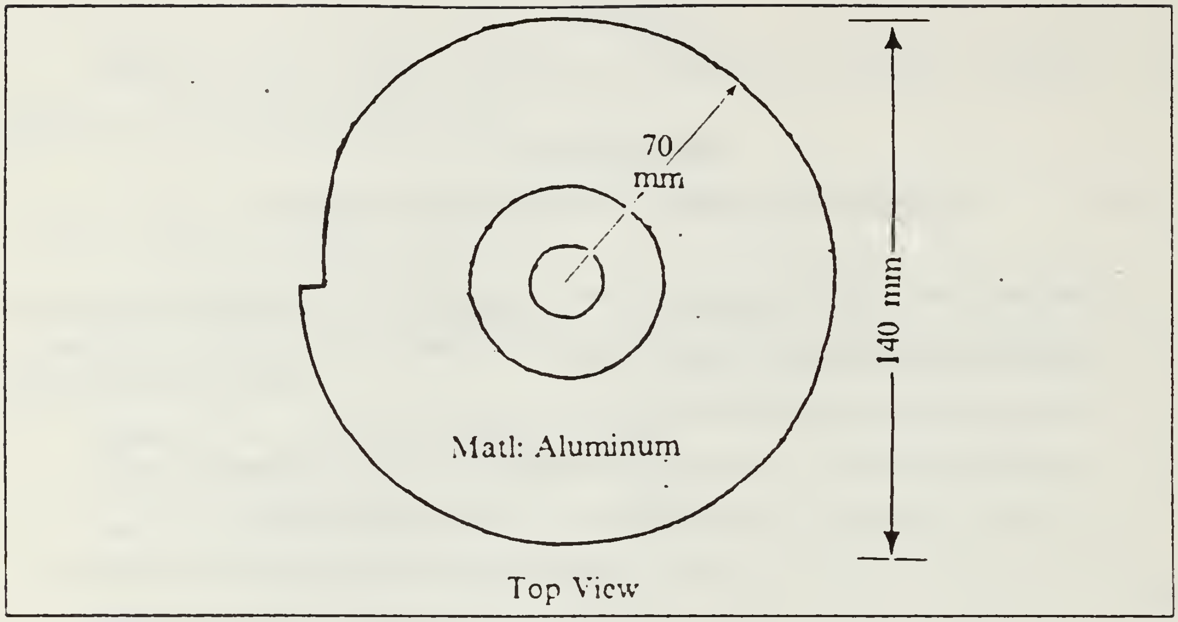

Figure C.2 Turning Disc - Top View

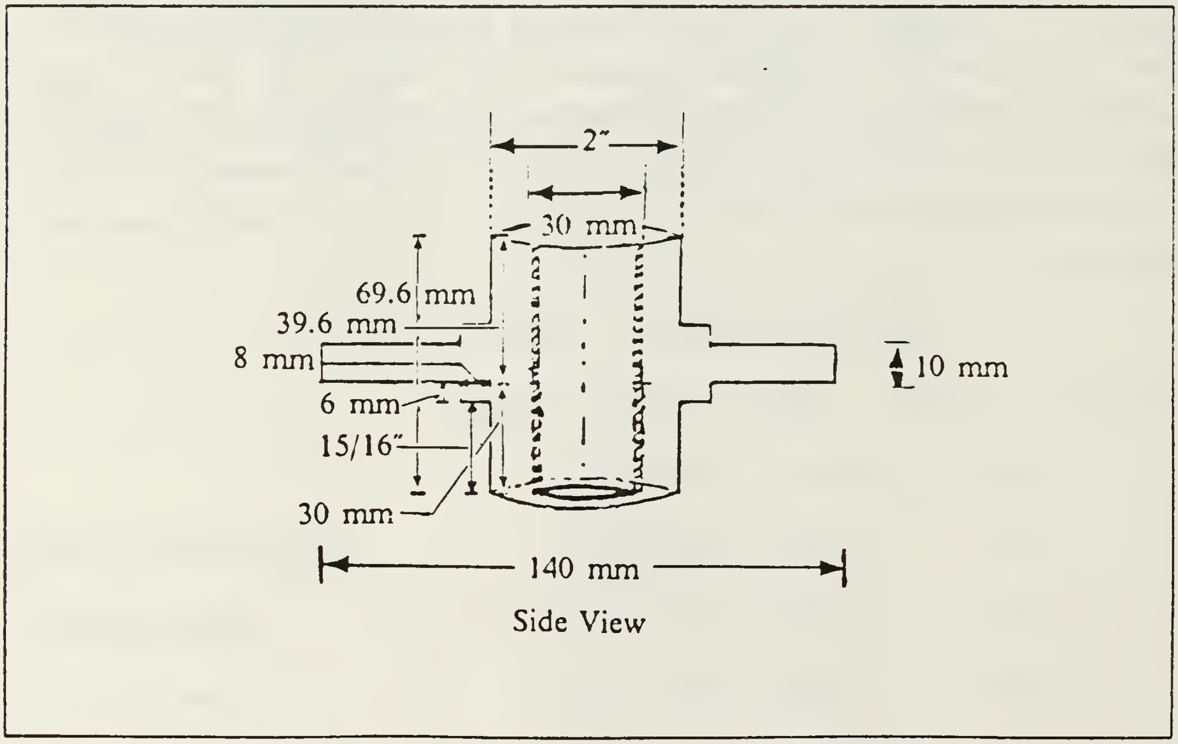

Figure C.3 Turning Disc - Side View

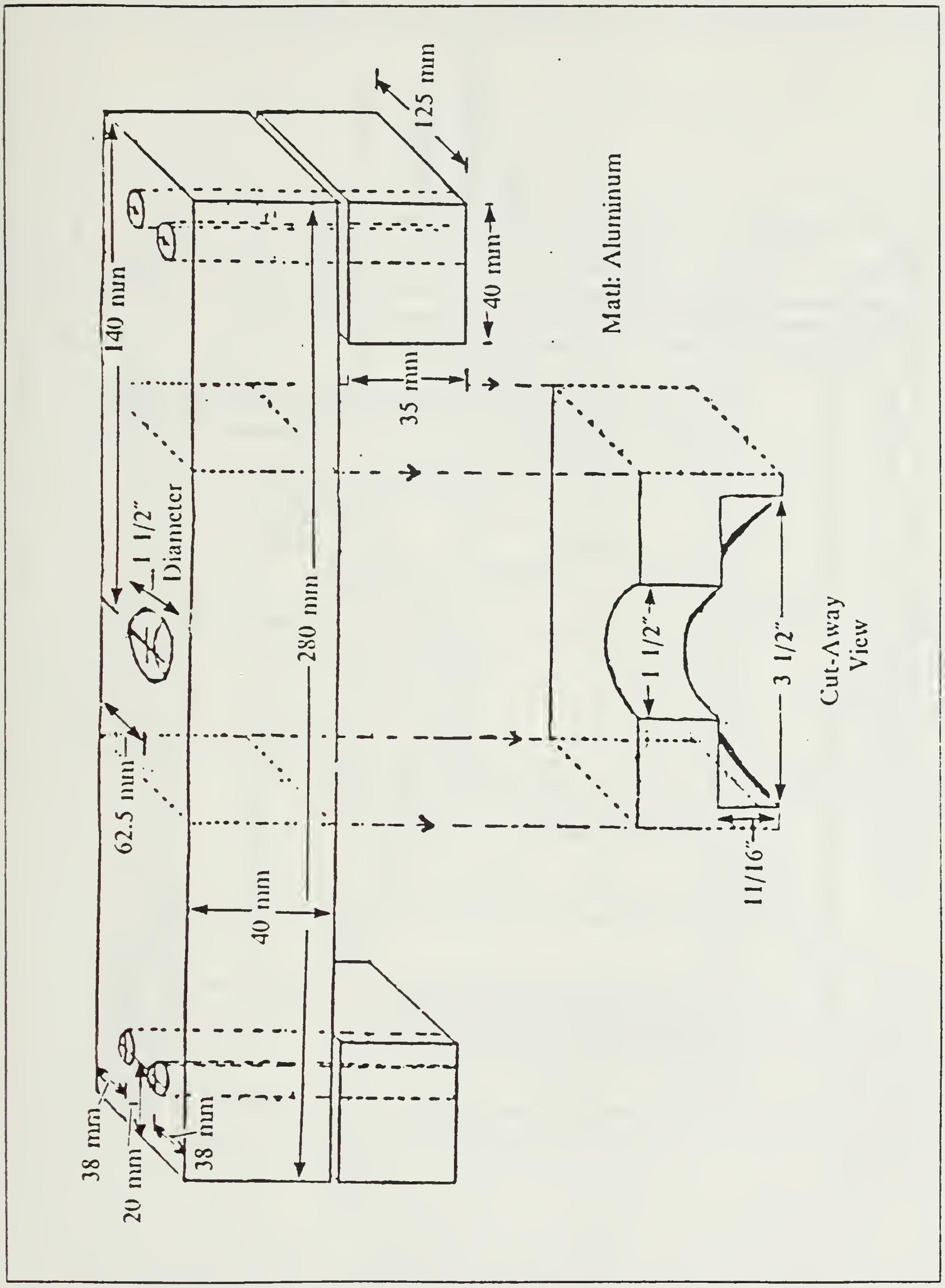

Figure C.4 Torsion Sample Upper Test Stand

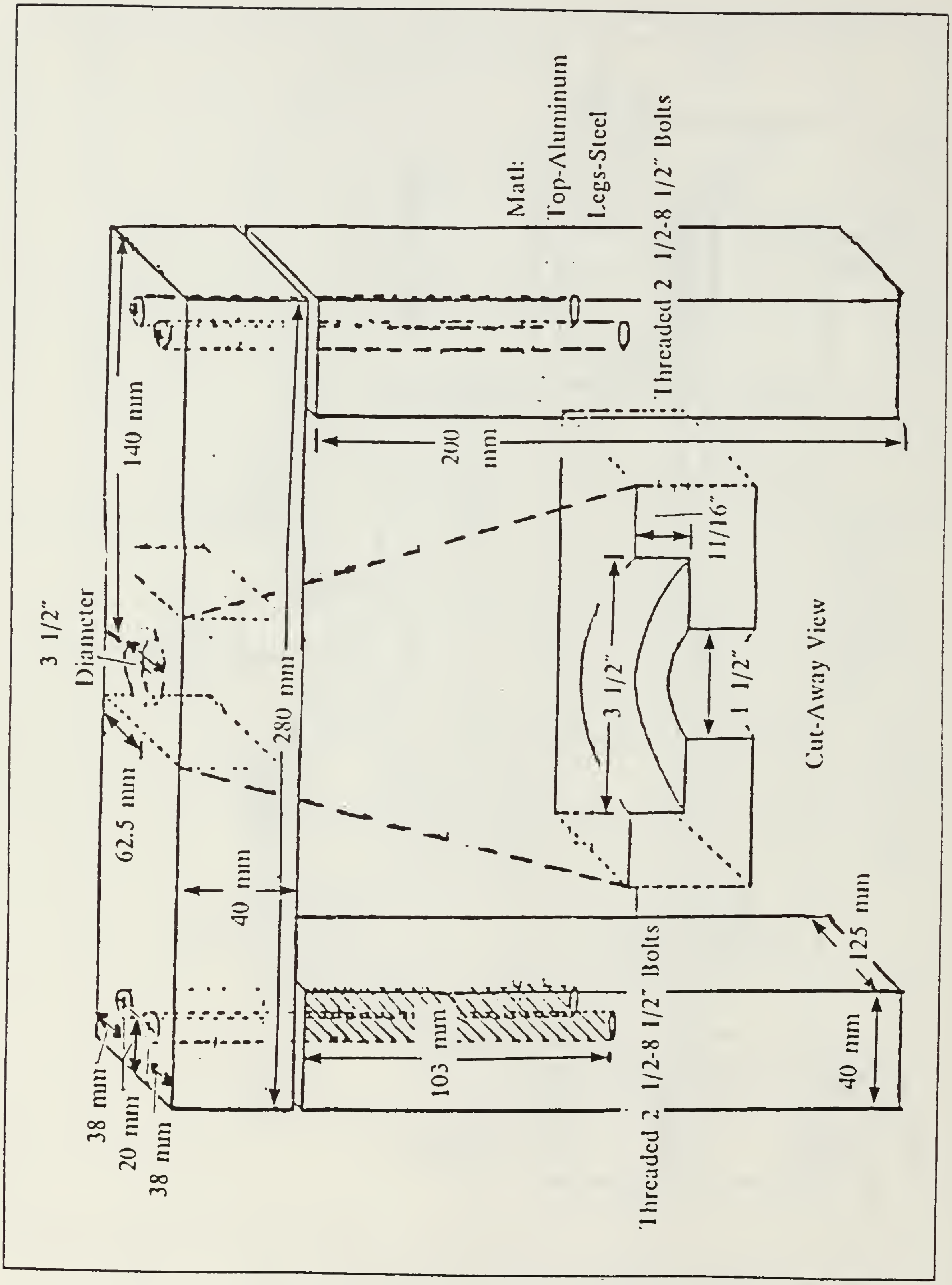

Figure C.5 Torsion Sample Lower Test Stand

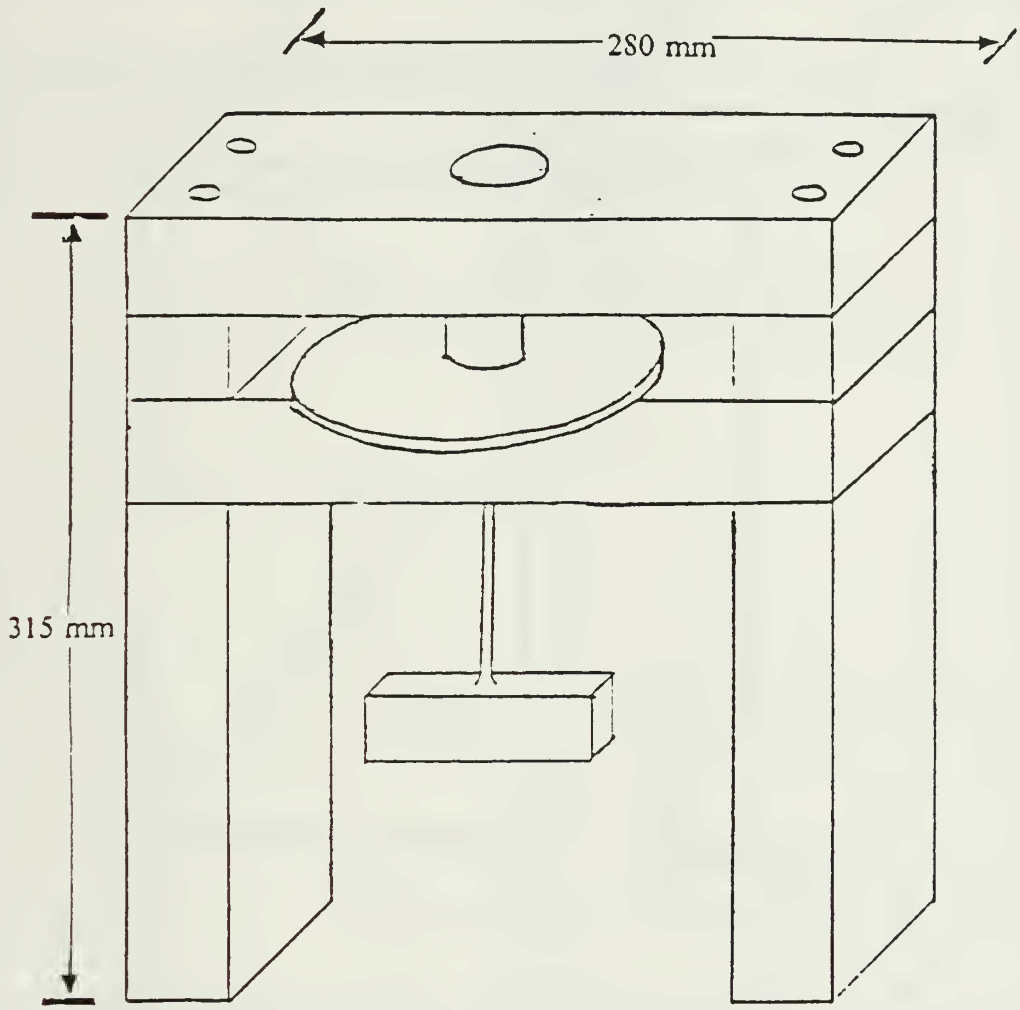

Figure C.6 Assembled Torsion Test Apparatus

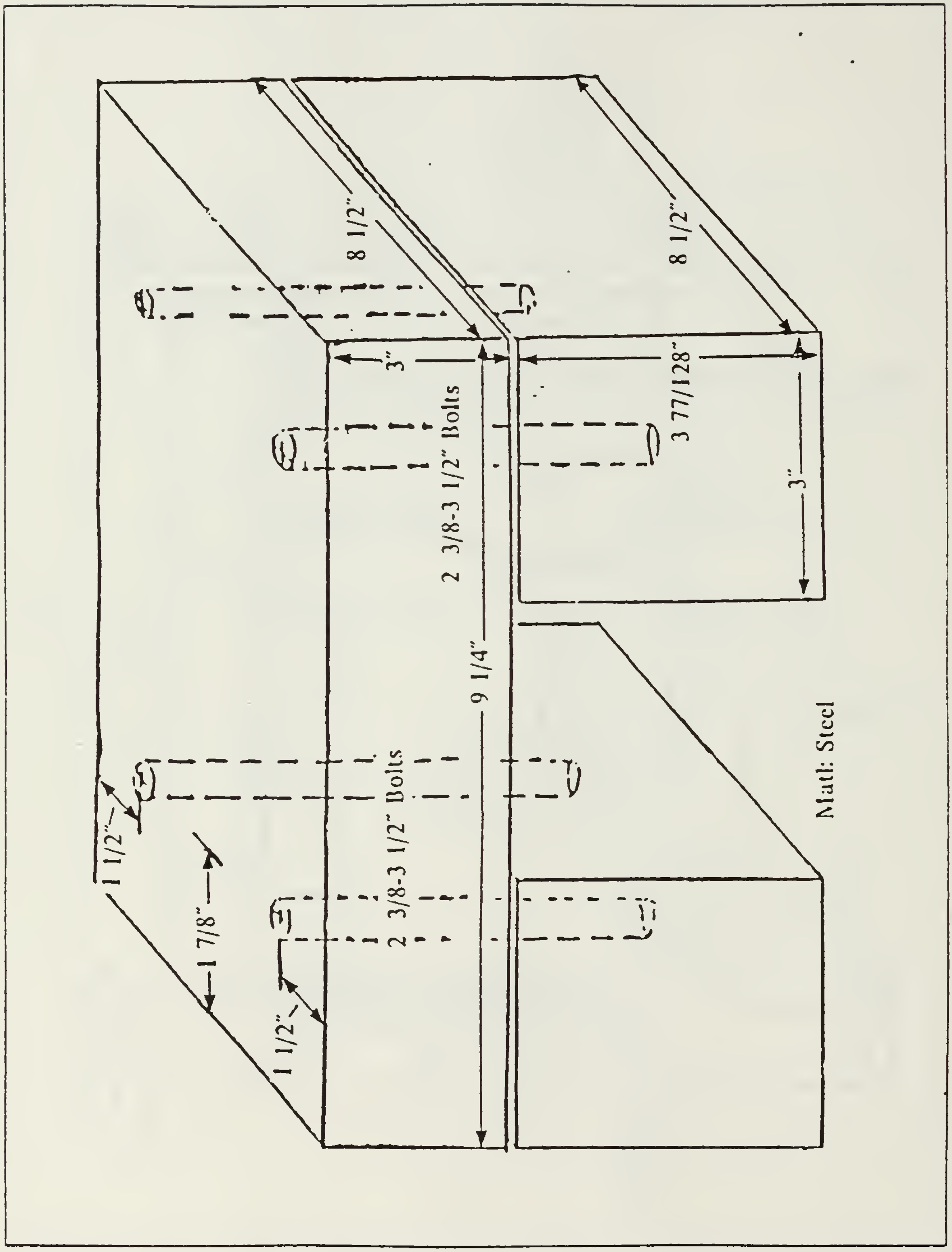

Figure C.7 Electromagnetic Shaker Stand for Torsion Test

APPENDIX D

CANTILEVER BEAM AND TORSION SAMPLE TRANSFER FUNCTION GRAPHS

1. CANTILEVER BEAM REPRESENTATIVE GRAPHS

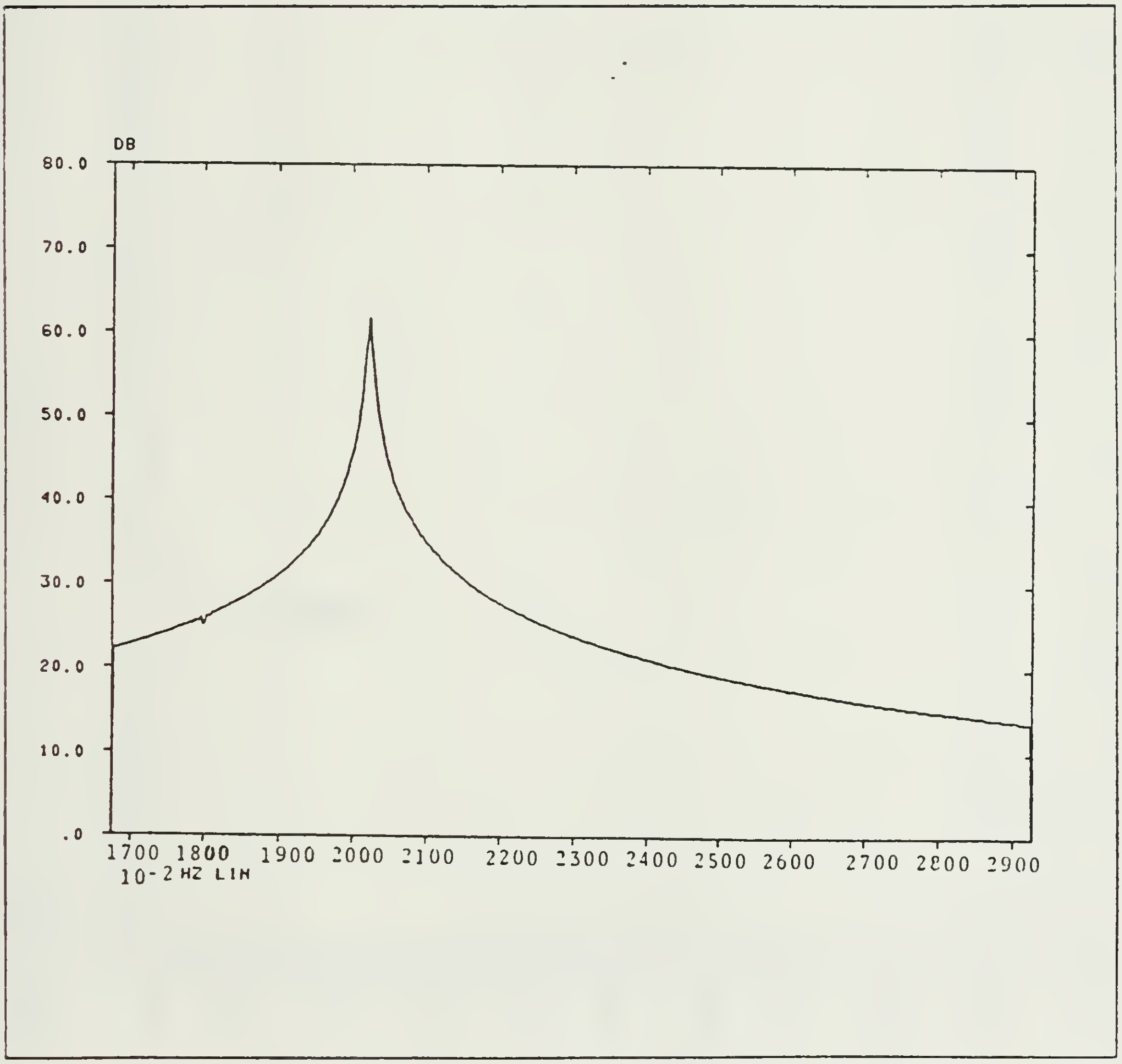

Figure.D.1 Mode 1 - Solution Annealed Sample Transfer Function (Cantilever Beam - Random Input)

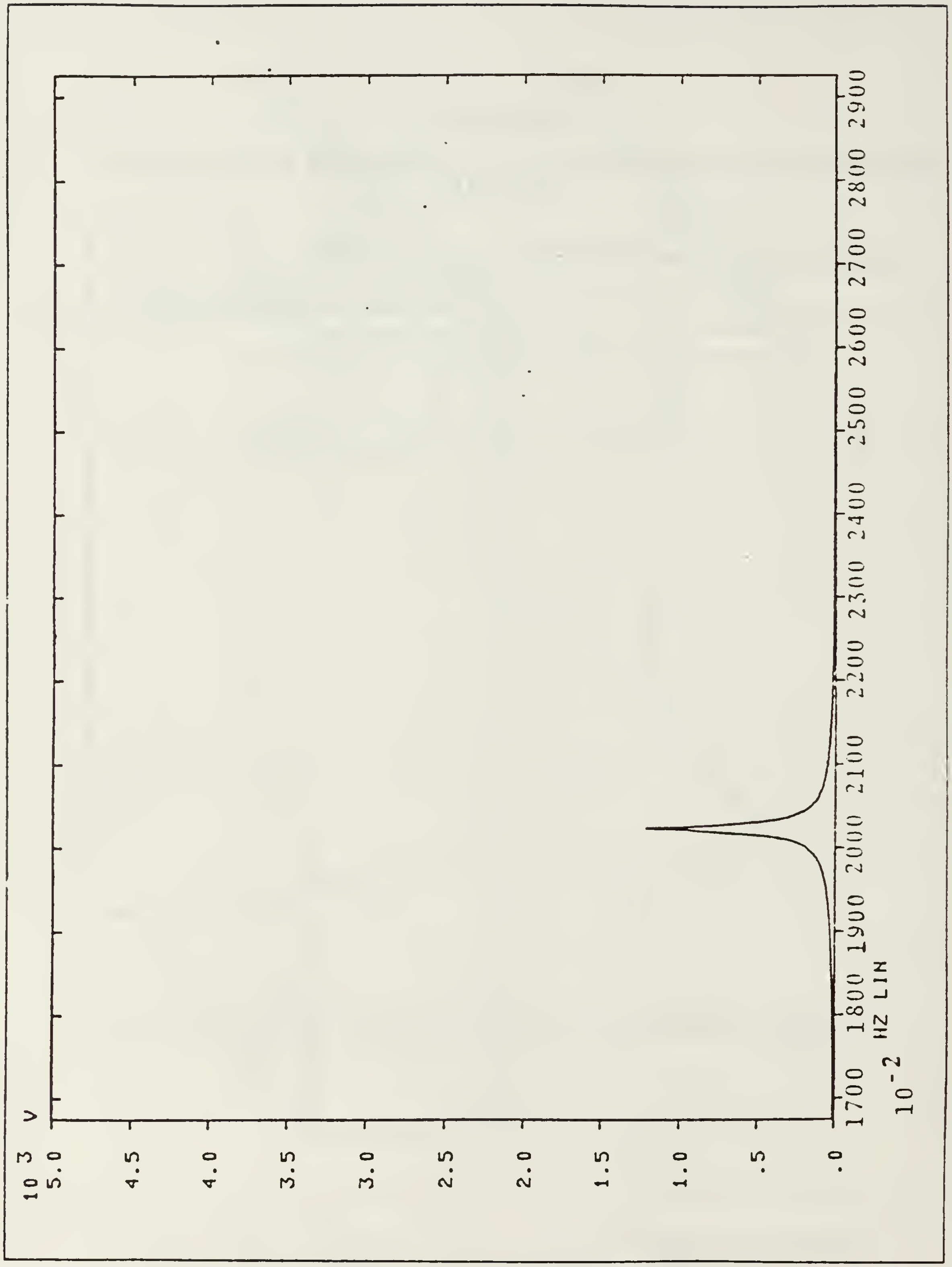

Figure D.2 Solution Annealed Transfer Function - Linear Scale (Cantilever Beam - Random Input)

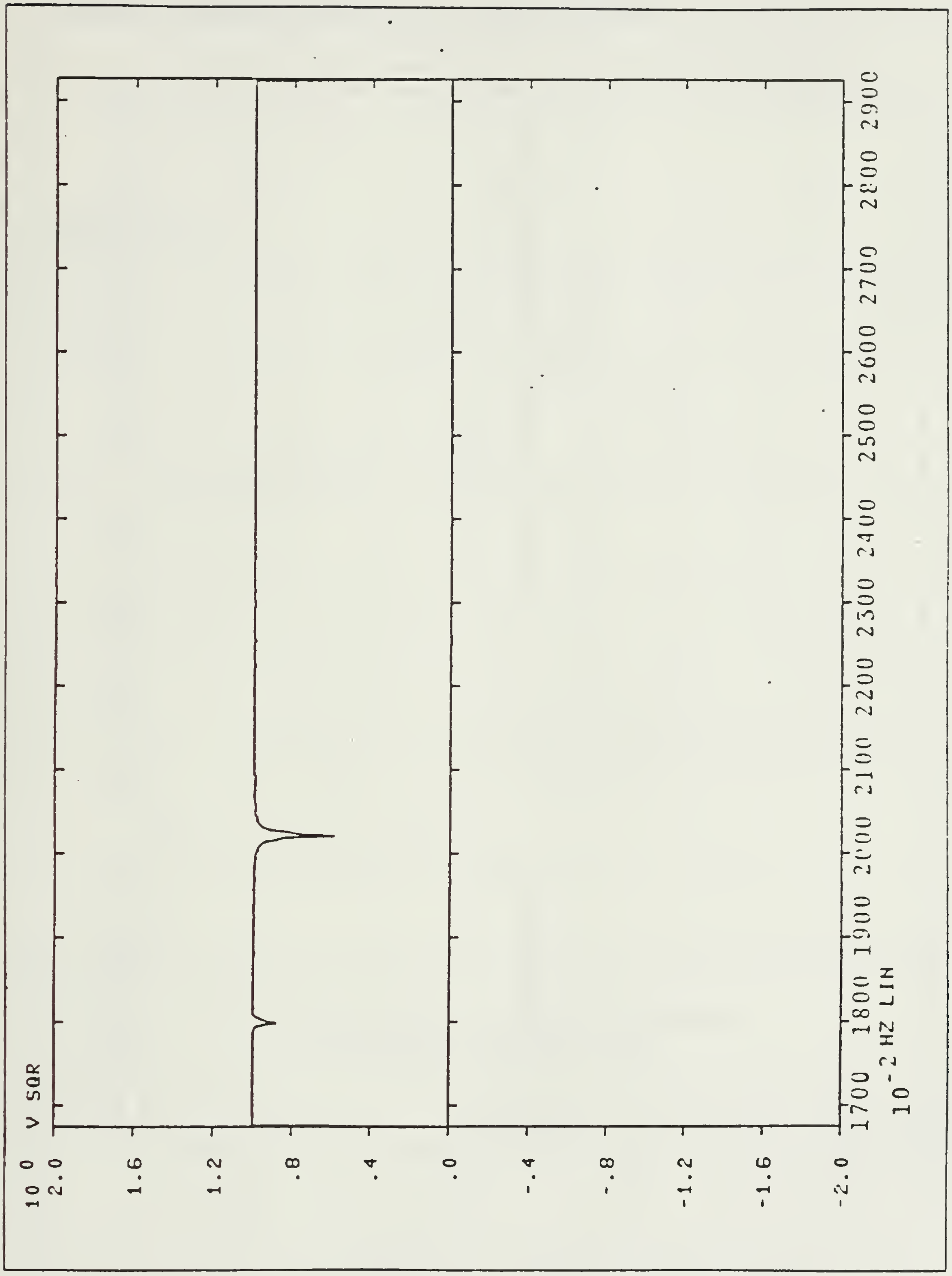

Figure D.3 Mode 1 - Solution Annealed Sample Coherence Function
(Cantilever Beam - Random Input)

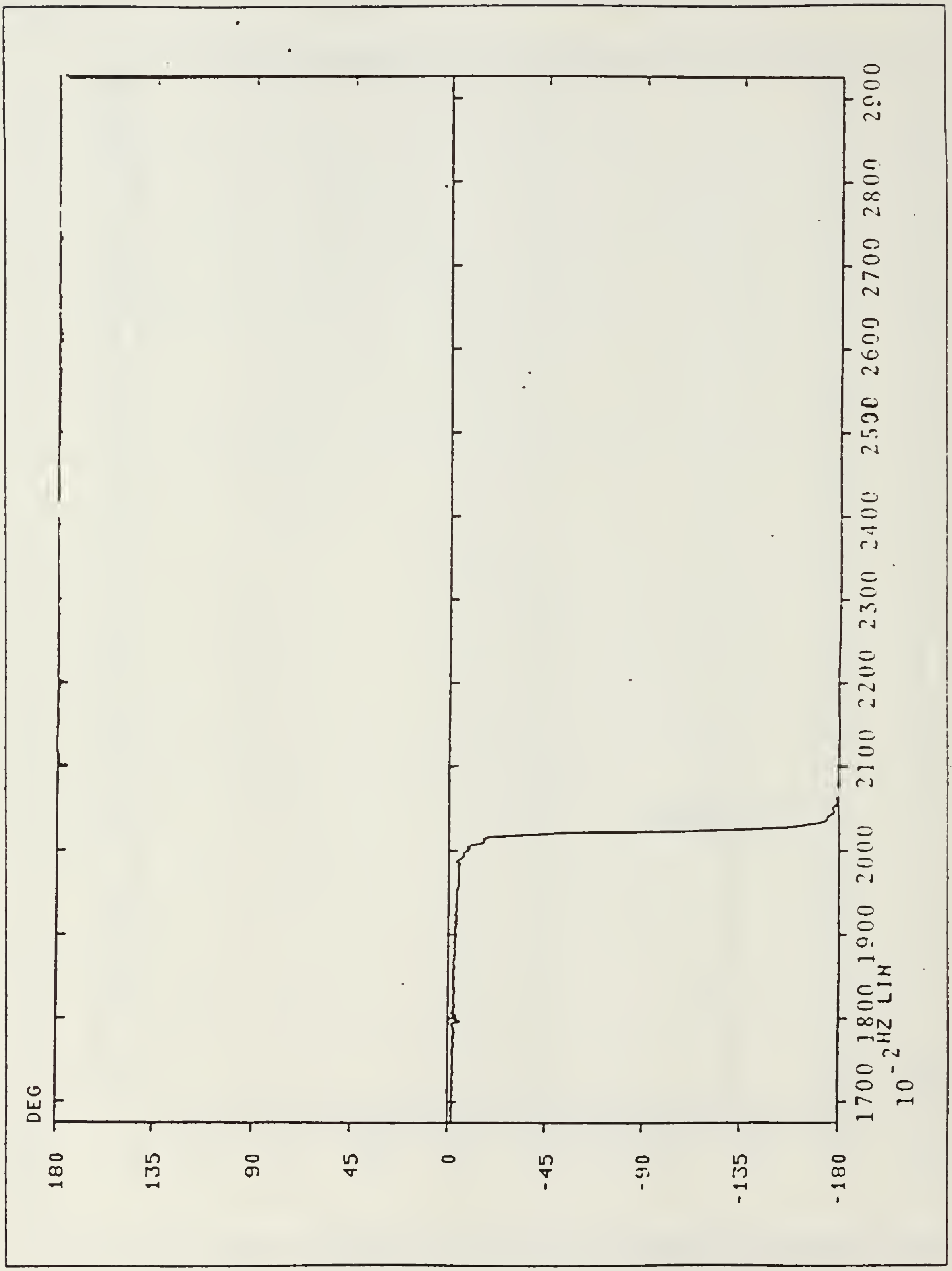

Figure D.4 Mode 1 - Phase Shift for the Solution Annealed Sample
(Cantilever Beam - Random Input)

2. TORSION SAMPLE REPRESENTATIVE GRAPHS

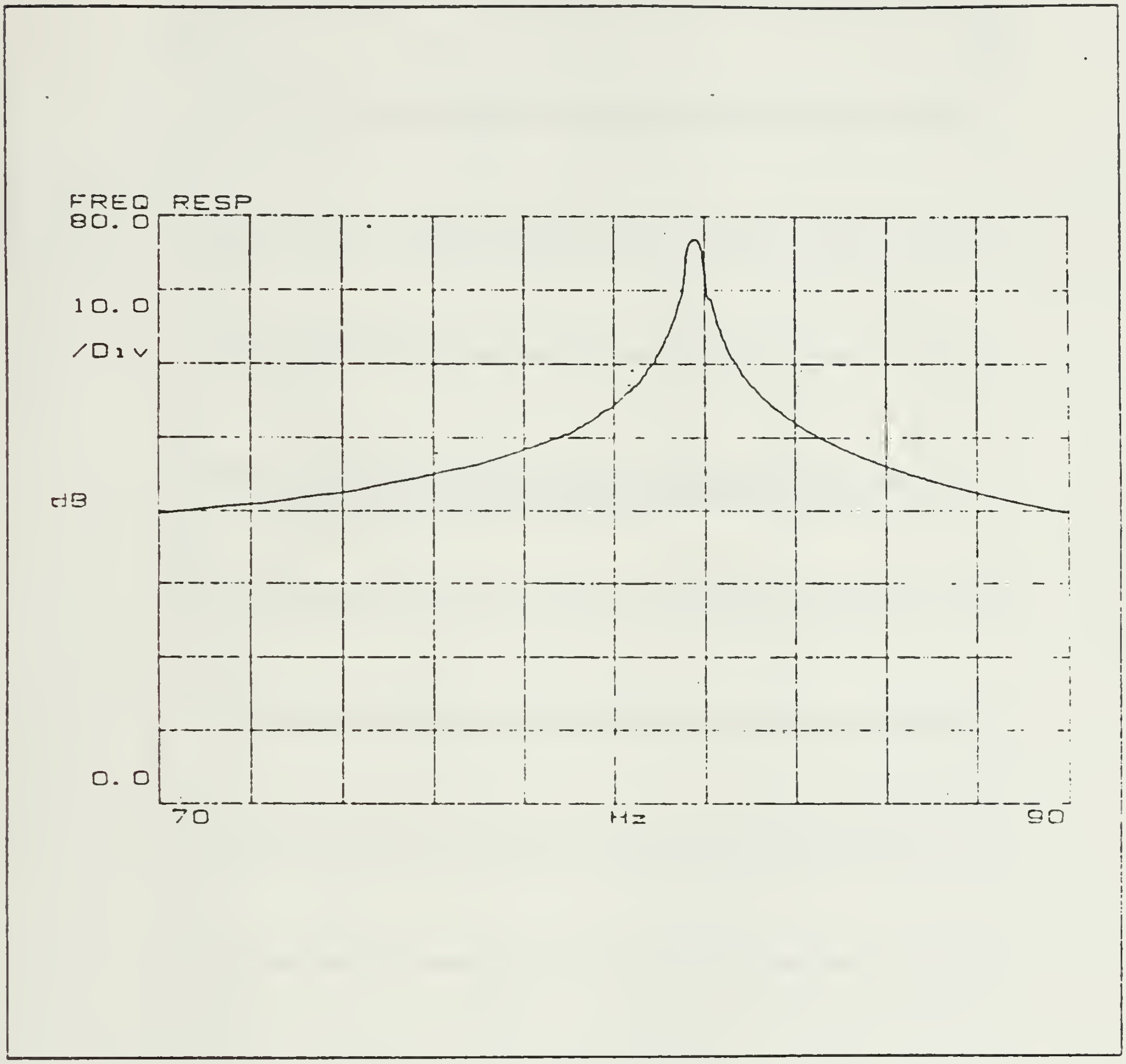

Figure D.5 Solution Annealed Transfer Function
(Torsion Sample - Random Input)

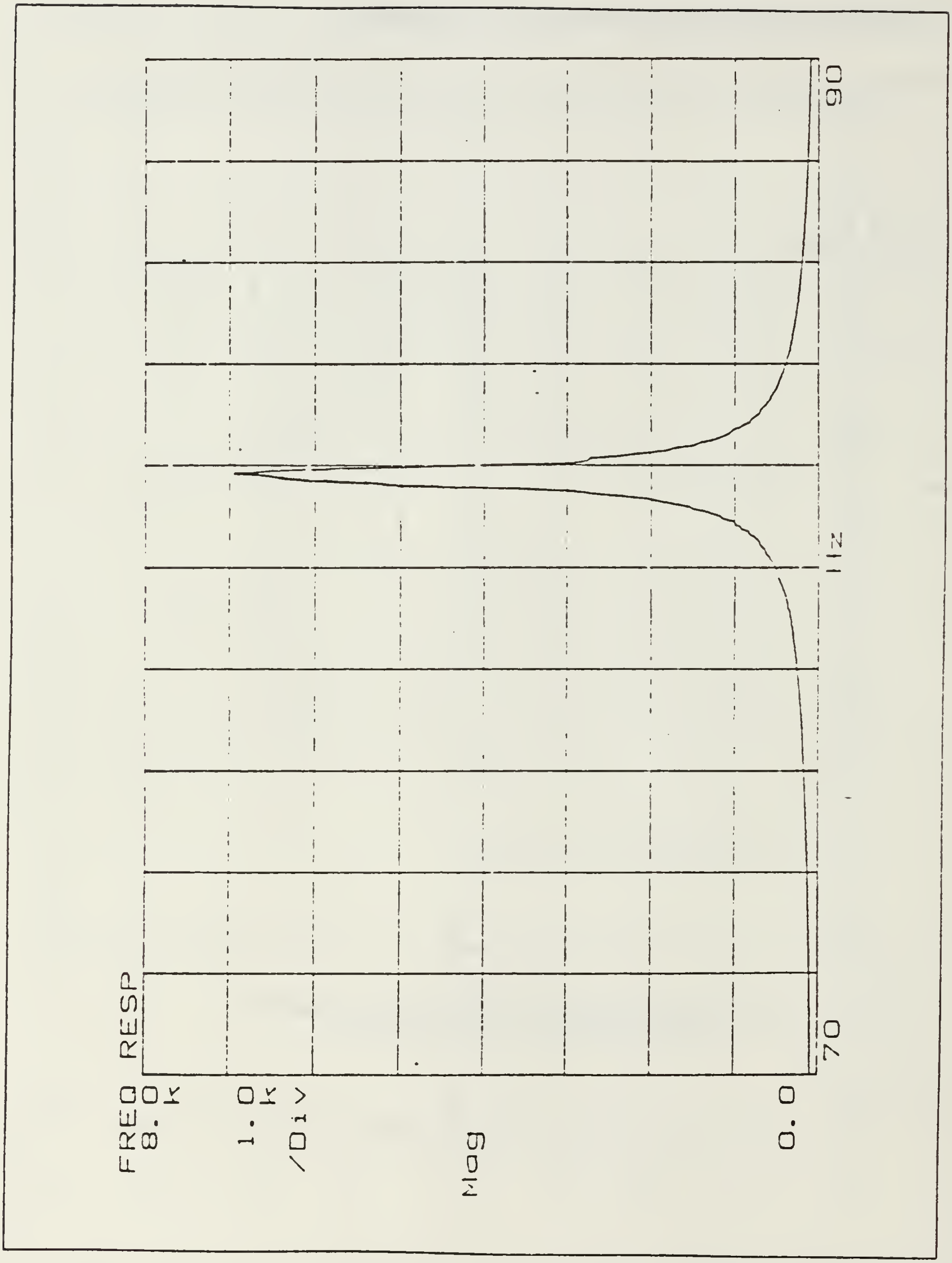

Figure D.6 Solution Annealed Transfer Function - Linear Scale
(TorsionSample - Random Input)

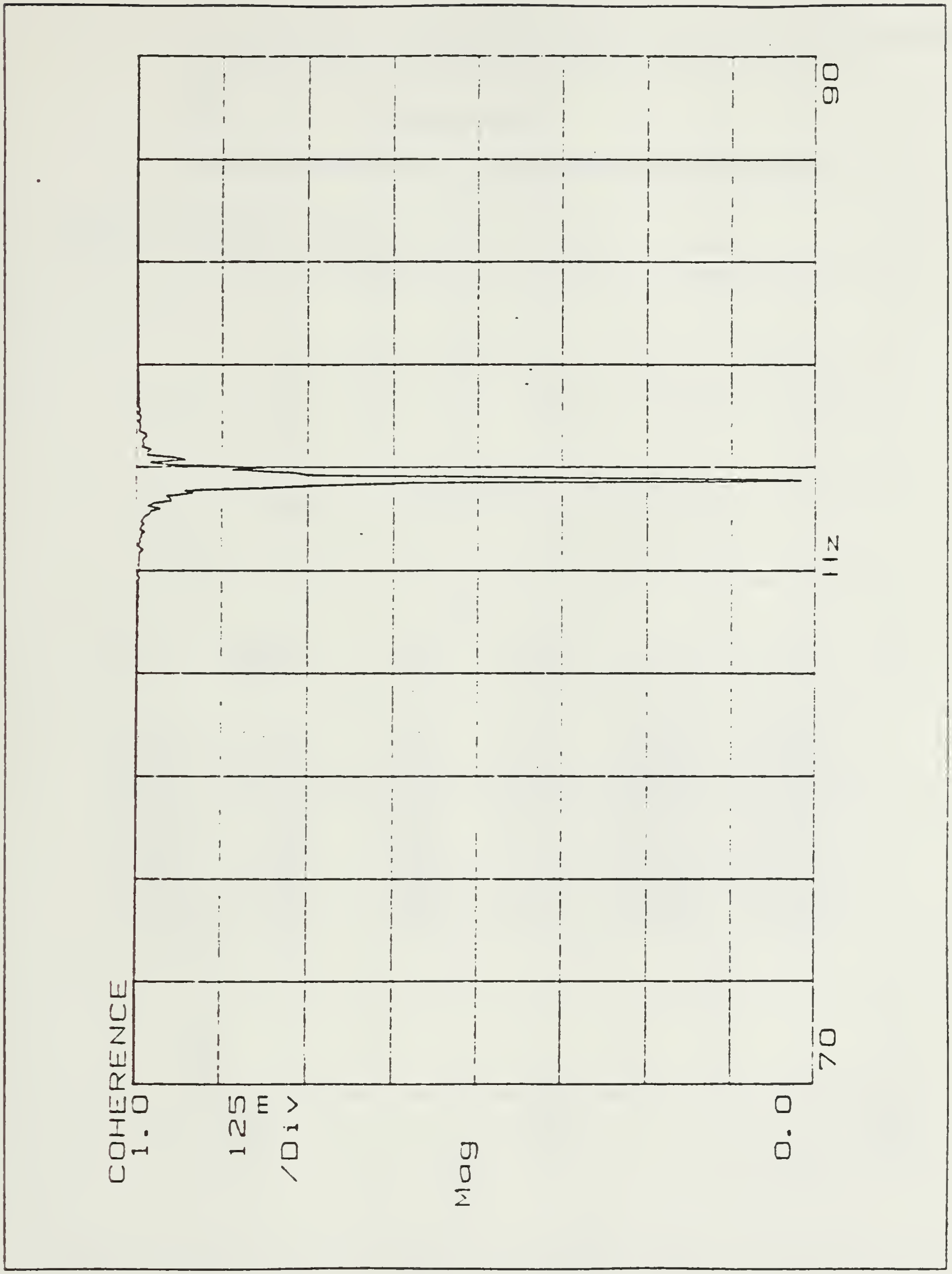

Figure D.7 Solution Annealed Sample Coherence Function
(Torsion Sample - Random Input)

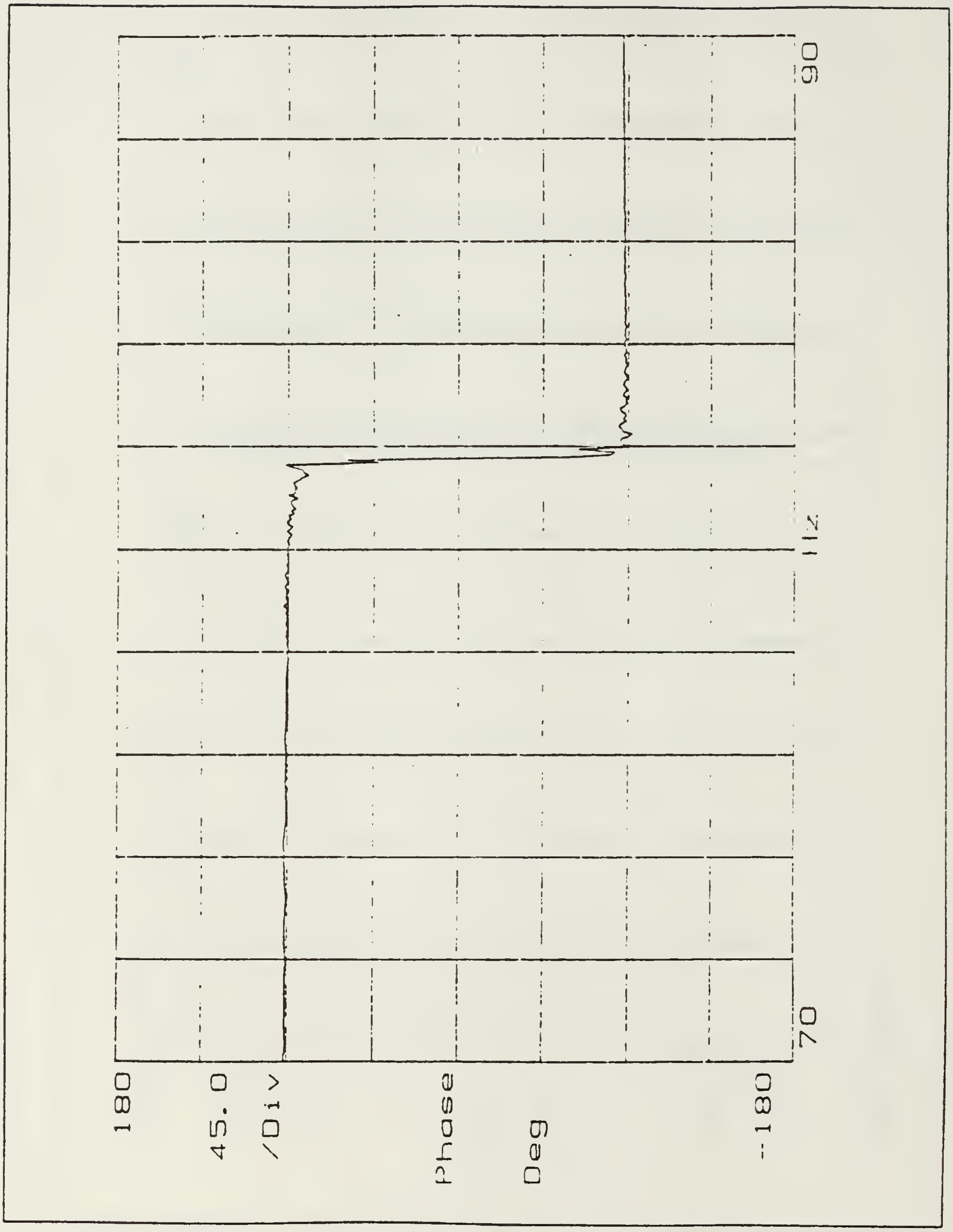

Figure D.8 Torsion - Phase Shift for Solution Annealed Sample
(Torsion Sample - Random Input)

APPENDIX E

CANTILEVER BEAM AND TORSION SAMPLE DATA

1. CANTILEVER BEAM DATA

TABLE 4

MODE 1 - AS QUENCHED SAMPLE

MODE 1

FN (HZ)	LOSS FACTOR (%)	STRAIN (%)	INPUT ACCEL (G)	F1 (HZ)	F2 (HZ)
20.275	.336	.0123	.4978	20.2409	20.3091
20.2909	.3288	.0123	.4978	20.2575	20.3245
20.2476	.329	.0146	.5809	20.2143	20.2809
20.242	.337	.0146	.5809	20.2079	20.2761
20.242	.429	.0167	.6046	20.1986	20.2854
20.237	.4631	.0167	.6040	20.1901	20.2839
20.2176	.4397	.0202	.743	20.1732	20.2620
20.237	.4722	.0202	.743	20.1892	20.2848
20.162	.5308	.02152	.8179	20.1085	20.2155
20.168	.5078	.02152	.8179	20.1168	20.2192
20.1443	.5514	.0225	.8853	20.0888	20.1998
20.15	.5102	.0225	.8853	20.0986	20.2014

TABLE 5

MODE 1 - 1 HOUR AGED SAMPLES

MODE 1

FN (HZ)	LOSS FACTOR (%)	STRAIN (%)	INPUT ACCEL (G)	F1 (HZ)	F2 (HZ)
		SAMPLE #1			
21.8800	1.54	.01436	0.5160	21.7115	22.0485
21.8846	1.38	.01436	0.5160	21.7339	22.0353
21.8635	1.60	.01436	0.5160	21.6881	22.0389
21.8656	1.58	.01564	0.5790	21.6932	22.0320
21.8474	1.69	.01564	0.5790	21.6628	21.9207
21.7456	1.61	.01801	0.6334	21.5705	21.8904
21.7436	1.35	.01801	0.6334	21.5968	21.9384
21.7527	1.71	.01801	0.6334	21.5670	21.9197
21.7274	1.77	.01987	0.7439	21.5351	21.9509
21.7315	2.02	.01987	0.7439	21.5121	21.9568
21.7656	1.76	.01987	0.7439	21.5744	21.8215
21.6512	1.57	.02099	0.8041	21.4809	21.8215
21.7045	2.09	.02099	0.8041	21.4777	21.9313
21.6511	1.62	.02099	0.8041	21.4762	21.8260
21.5445	1.68	.02367	1.0524	21.3635	21.7255
21.5445	1.99	.02367	1.0524	21.3303	21.7587
		SAMPLE #2			
21.8629	1.56	.0145	.5	21.6924	22.0334
21.8740	1.56	.0145	.5	21.7034	22.0446
21.8482	1.59	.01573	.5819	21.6743	22.0221
21.8469	1.59	.01573—	.5819	21.6721	22.0217
21.7527	1.71	.018	.637	21.5670	21.9384
21.7537	1.71	.018	.637	21.5655	21.9419
21.7191	1.76	.01986	.7429	21.5283	21.9099
21.7315	1.80	.01986	.7429	21.5359	21.9271
21.6638	1.82	.02099	.806	21.4671	21.8605
21.6537	1.79	.02099	.806	21.4599	21.8475
21.5489	1.99	.02367	1.04	21.3347	21.7631
21.5545	1.89	.02366	1.04	21.3508	21.7582

TABLE 6

MODE 1 - 2 HOUR AGED SAMPLES

MODE 1

INPUT ACCEL (G)	FN (HZ)	LOSS FACTOR (%)	STRAIN (%)	F1 (HZ)	F2 (HZ)
		SAMPLE #3			
.5637	24.9000	2.6605	.00407	24.5687	25.2312
.5637	24.8700	2.7895	.00407	24.5231	25.2169
.5888	24.7400	3.0397	.00732	24.3640	25.1160
.5888	24.7330	3.0974	.00732	24.3499	25.1160
.5998	24.5600	3.0618	.008296	24.1840	24.9360
.5998	24.5951	3.0496	.008296	24.2201	24.9701
.6535	24.6800	2.9581	.01104	24.3150	25.0450
.6535	24.6750	3.1223	.01104	24.2898	25.0602
.7503	24.4011	3.277	.01317	24.0013	24.8009
.7503	24.5200	3.32411	.01317	24.1125	24.9275
.8025	24.0350	4.6176	.0149	23.4801	24.5899
.8025	24.1000	4.5783	.0149	23.5483	24.6517
		SAMPLE #4			
.4554	25.1600	2.4698	.004099	24.8493	25.4707
.4554	25.1396	2.2733	.004099	24.8538	25.4253
.5611	25.0252	2.8773	.007375	24.6651	25.3852
.5611	25.0000	2.8084	.007375	24.6489	25.3510
.5895	24.6818	2.9718	.00838	24.3150	25.0485
.5895	24.6800	3.0733	.00838	24.3007	25.0592
.6732	24.5674	2.8898	.01085	24.2125	24.9224
.6732	24.5200	3.1648	.01085	24.1320	24.9080
.7502	24.4148	3.3048	.01306	24.0113	24.8182
.7502	24.4400	3.2381	.01306	24.0443	24.8357
.8086	24.0714	4.3338	.0149	23.5498	24.5930
.8086	24.0400	4.59059	.0149	23.4882	24.5918

TABLE 7

MODE 2 - AS QUENCHED SAMPLE

AS QUENCHED SAMPLE

MODE 2

FN (HZ)	LOSS FACTOR (%)	STRAIN (%)	INPUT ACCEL (G)	F1 (HZ)	F2 (HZ)
130.65	.2778	.00587	.5749	130.4370	130.8000
130.5396	.3039	.00587	.5749	130.3869	130.7837
130.587	.3476	.00831	.6438	130.3600	130.8139
130.5396	.3312	.00831	.6438	130.3234	130.7557
130.48	.4982	.01579	.8068	130.1300	130.7800
130.4785	.4001	.01579	.8068	130.1869	130.7090
130.44	.3833	.02143	.9419	130.2500	130.7500
130.338	.3646	.02143	.9419	130.2250	130.7006
130.413	.3297	.02843	1.336	130.1980	130.6280
130.3869	.3411	.02843	1.336	130.1449	130.6396
130.347	.3168	.03412	1.775	130.2000	130.6130
130.348	.3237	.03412	1.775	130.2344	130.6564

TABLE 8
MODE 2 - 1 HOUR AGED SAMPLES

MODE 2

FN (HZ)	LOSS FACTOR (%)	STRAIN (%)	INPUT ACCEL (G)	F1 (HZ)	F2 (HZ)
SAMPLE #1					
138.6977	2.7278	0.02614	1.2949	136.8060	140.5894
138.2788	2.7500	0.02614	1.2949	136.3775	140.1801
139.6987	2.1672	0.02000	0.8612	138.1849	141.2125
139.8792	1.9806	0.02000	0.8612	138.4939	141.2644
142.6800	1.7833	0.01625	0.8059	141.4078	143.9522
142.5700	1.8637	0.01625	0.8059	141.2415	143.8985
143.0200	1.1086	0.01410	0.7252	142.2272	143.8128
143.0400	0.8816	0.01410	0.7252	142.4095	143.6705
142.6000	0.8811	0.00995	0.6008	141.4718	143.2282
144.0000	0.8430	0.00995	0.6008	143.3930	144.6064
144.0700	0.2710	0.00635	0.5181	143.8748	144.2652
144.1300	0.2853	0.00635	0.5181	143.9244	144.3356
SAMPLE #2					
144.1100	0.2730	0.0064	0.5184	143.9133	144.3067
144.0800	0.2750	0.0064	0.5184	143.8819	144.2781
144.1000	0.8560	0.00989	0.6021	143.4833	144.7167
143.8000	0.8732	0.00989	0.6021	143.1722	144.4278
143.0100	0.8875	0.01450	0.7227	142.3754	143.6446
143.0140	0.8984	0.01450	0.7227	142.3716	143.6564
142.6400	1.7943	0.01632	0.8066	141.3603	143.9197
142.5900	1.8217	0.01632	0.8066	141.2912	143.8888
139.6982	1.9432	0.02250	0.8620	138.3409	141.0555
139.7006	2.0321	0.02250	0.8620	138.2812	141.1200
138.4352	2.7184	0.02598	1.2391	136.5536	140.3168
138.5217	2.7337	0.02598	1.2391	136.6283	140.4151

TABLE 9
MODE 2 - 2 HOUR AGED SAMPLES

MODE 2

FN. (HZ)	LOSS FACTOR (%)	STRAIN (%)	INPUT ACCEL (%)	F1 (HZ)	F2 (HZ)
		SAMPLE #3			
159.4200	1.0780	.0044	.5221	158.5608	160.2793
159.4600	1.0600	.0044	.5221	158.6148	160.3051
159.1600	1.1815	.0067	.6008	158.2197	160.1002
159.1800	1.1865	.0067	.6008	158.2356	160.1243
158.6800	1.2690	.0085	.6510	157.6732	159.6868
158.7200	1.2740	.0085	.6510	157.7089	159.7310
158.6100	1.3311	.0088	.7192	157.5543	159.6656
158.6000	1.3657	.0088	.7192	157.5169	159.6830
158.2600	1.4239	.0116	.8094	157.1332	159.3867
158.2000	1.3607	.0116	.8094	157.1237	159.2763
157.8300	1.8664	.0177	1.1575	156.3572	159.3029
157.6800	1.8273	.0177	1.1575	156.2393	159.1206
		SAMPLE #4			
159.4837	1.0346	.0042	.4606	158.6587	160.3087
159.4794	1.0500	.0042	.4606	158.6422	160.3167
159.1600	1.1889	.0067	.6005	158.2137	160.1060
159.1437	1.1894	.0067	.6005	158.1972	160.0901
158.7600	0.9700	.0084	.6473	157.9899	159.5299
158.7265	1.2114	.0084	.6473	157.7651	159.6879
158.5200	1.1134	.0097	.7190	157.6375	159.4025
158.5048	1.0978	.0097	.7190	157.6347	159.3748
158.2000	1.4587	.0115	.8067	157.0461	159.3538
158.1750	1.3427	.0115	.8067	157.1131	159.2369
157.8000	2.0025	.0176	1.1538	156.2199	159.3799
157.8200	1.8745	.0176	1.1538	156.3409	159.2992

TABLE 10

MODE 3 - AS QUENCHED SAMPLE

MODE 3

FN (HZ)	LOSS FACTOR (%)	STRAIN (%)	INPUT ACCEL (G)	F1 (HZ)	F2 (HZ)
361.8380	.2109	.0025	.4997	361.3750	362.1380
361.8370	.1858	.0025	.4997	361.4500	362.1223
361.2750	.2192	.0027	.6034	360.8380	361.6380
361.2371	.3041	.0027	.6034	360.8099	361.9086
361.1750	.263	.0031	.6846	360.6500	361.6000
361.1235	.2955	.0031	.6846	360.5667	361.6339
361.0130	.3357	.0039	.7322	360.4750	361.6870
361.0540	.3381	.0039	.7322	360.4131	361.6339
361.0130	.426	.0045	.8793	360.2220	361.7500
361.0235	.4227	.0045	.8793	360.2605	361.7865
360.912	.4200	.0054	1.1274	360.1540	361.6700
360.9014	.4229	.0054	1.1274	360.1383	361.6645

TABLE 11
MODE 3 - 1 HOUR AGED SAMPLES

MODE 3

FN (HZ)	LOSS FACTOR (%)	STRAIN (%)	INPUT ACCEL (G)	F1 (HZ)	F2 (HZ)
		SAMPLE #1			
384.6400	1.0294	.0016	.5815	382.6603	386.6197
384.6286	1.1075	.0016	.5815	382.4987	386.7585
383.4921	1.2459	.0019	.6373	381.1031	385.8811
383.4800	1.3038	.0019	.6373	380.9801	385.9799
382.5002	1.2092	.0026	.6934	380.1876	384.8128
382.6000	1.2337	.0026	.6934	380.2399	384.9601
382.0427	1.2632	.0034	.7436	379.6297	384.4557
381.9200	1.3091	.0034	.7436	379.4201	384.4199
381.5849	1.1797	.0035	.8975	379.3341	383.8357
381.4400	1.1745	.0035	.8975	379.1999	383.6800
381.4704	1.3993	.0038	1.1833	378.8014	384.1394
381.2800	1.4464	.0038	1.1833	378.5226	384.0374
		SAMPLE #2			
384.6052	1.0524	.0016	.5892	382.5814	386.6289
384.6327	1.1005	.0016	.5892	382.5163	386.7491
383.4917	1.2743	.0020	.6451	381.0483	385.9351
383.4852	1.3009	.0020	.6451	380.9908	385.9796
382.5132	1.2143	.0027	.7029	380.1908	384.8356
382.5894	1.2247	.0027	.7029	380.2466	384.9322
382.6427	1.2821	.0034	.7444	380.1898	385.0956
382.0952	1.3020	.0034	.7444	379.6078	384.5826
381.5721	1.1800	.0036	.9001	379.3208	383.8234
381.4982	1.1762	.0036	.9001	379.2546	383.7418
381.3527	1.4020	.0038	1.1578	378.6794	384.0259
381.4407	1.4243	.0038	1.1578	378.7243	384.1571

TABLE 12

MODE 3 - 2 HOUR AGED SAMPLES

MODE 3

FN (HZ) (G)	LOSS FACTOR (%)	STRAIN (%)	INPUT ACCEL (G)	F1 (HZ)	F2 (HZ)
SAMPLE #3					
444.9035	1.5876	.00248	.4343	441.3719	448.4351
444.9600	1.6000	.00248	.4343	441.4003	448.5197
444.7191	1.7136	.00266	.4754	440.9087	448.5295
444.7200	1.7612	.00266	.4754	440.8038	448.6362
444.6498	1.7080	.00304	.6830	440.8525	448.4471
444.6800	1.8463	.00304	.6830	440.5749	448.7851
444.2365	1.8789	.00306	.7312	440.0631	448.4099
444.2600	1.8484	.00306	.7312	440.1541	448.3659
443.7800	1.9779	.00451	.8867	439.3912	448.1688
443.6787	2.0117	.00451	.8867	439.2159	448.1414
443.2249	2.1801	.00588	1.1966	438.3935	448.0563
443.1200	2.1709	.00588	1.1966	438.3102	447.9298
SAMPLE #4					
444.2800	1.6362	.00261	.4676	440.6453	447.9147
444.2600	1.6132	.00261	.4676	440.6766	447.8434
444.2000	1.7929	.00278	.4797	440.2179	448.1820
444.2467	1.7868	.00278	.4797	440.2778	448.2156
443.9553	1.8376	.00310	.7027	439.8762	448.0344
444.0400	1.8154	.00310	.7027	440.0094	448.0706
443.9600	1.8780	.00313	.7379	439.7912	448.1288
443.9169	1.8488	.00313	.7379	439.8133	448.0205
443.8400	2.0128	.00400	.8686	439.3732	448.3068
443.8784	2.0191	.00400	.8686	439.3972	448.3596
443.1600	2.1866	.00613	1.2920	438.3149	448.0051
443.1500	2.2051	.00613	1.2920	438.2640	448.0359

TABLE 13

MODE 1 - UNAGED SAMPLE (SWEPT SINE)

MODE 1
SWEPT SINE TEST

FN (HZ)	LOSS FACTOR (%)	STRAIN (%)	INPUT ACCEL (G)	F1 (HZ)	F2 (HZ)
20.2750	.3951	.0123	.5529	20.2349	20.3150
20.2750	.3951	.0146	.5558	20.2349	20.3150
20.2590	.4136	.0167	.5599	20.2171	20.3009
20.2570	.6447	.0215	.5675	20.1917	20.3223
20.2450	.5947	.0225	.5757	20.1848	20.3052
20.1750	.7891	.0235	.5870	20.0954	20.2546

TABLE 14

MODE 1 - 1 HOUR AGED SAMPLES (SWEPT SINE)

MODE 1
SWEPT SINE

FN (HZ)	LOSS FACTOR (%)	STRAIN (%)	INPUT ACCEL (G)	F1 (HZ)	F2 (HZ)
		SAMPLE #1			
21.8600	1.4904	.01530	0.5204	21.6971	22.0229
21.8200	1.5399	.01484	0.5316	21.6520	21.9880
21.7200	1.6400	.01583	0.5822	21.5419	21.8981
21.7000	1.7005	.01792	0.6287	21.5155	21.8845
21.6800	1.6799	.01964	0.7269	21.4979	21.8621
21.6500	1.8199	.02101	0.7943	21.4530	21.8470
21.5400	1.9898	.02287	1.0109	21.3257	21.7543
		SAMPLE #2			
21.8600	1.5297	.01463	0.5204	21.6928	22.0272
21.8400	1.5897	.01602	0.5795	21.6664	22.0136
21.7500	1.7205	.01834	0.6298	21.5629	21.9371
21.7100	1.7402	.01977	0.7431	21.5211	21.8989
21.6600	1.7996	.02084	0.8019	21.4651	21.8549
21.5400	1.9601	.02321	1.1000	21.3289	21.7511
21.4900	1.8799	.02481	1.0880	21.2880	21.6920

TABLE 15

MODE 1 - 2 HOUR AGED SAMPLES (SWEPT SINE)

2 HOUR AGED SAMPLES

MODE 1
SWEPT SINE

FN (HZ)	LOSS FACTOR (%)	STRAIN (%)	INPUT ACCEL (G)	F1 (HZ)	F2 (HZ)
SAMPLE #3					
25.010	1.8760	.0023	.4851	24.7754	25.2446
24.98	1.9055	.0033	.5333	24.7420	25.2180
24.96	2.9223	.0071	.5819	24.5953	25.3247
24.58	3.0016	.0097	.6305	24.2111	24.9489
24.54	3.0391	.0120	.6789	24.1621	24.9079
24.51	3.2060	.0123	.7270	24.1171	24.9029
24.27	3.8475	.0138	.7759	23.8031	24.7369
SAMPLE #4					
25.013	1.8806	.0023	.4912	24.7778	25.2482
24.992	1.9094	.0031	.5298	24.7534	25.2306
24.927	2.8989	.0048	.5752	24.5657	25.2883
24.571	3.0125	.0099	.6317	24.2009	24.9411
24.543	3.0289	.0128	.6804	24.1713	24.9147
24.498	3.2141	.0126	.7275	24.1043	24.8917
24.301	3.8624	.0137	.7801	23.8317	24.7703

TABLE 16

MODE 2 - UNAGED SAMPLE (SWEPT SINE)

AS QUENCHED SAMPLE

MODE 2
SWEPT SINE TEST

FN (HZ)	LOSS FACTOR (%)	STRAIN (%)	INPUT ACCEL (G)	F1 (HZ)	F2 (HZ)
130.6500	.3253	.0053	.5503	130.4375	130.8625
130.4250	.3734	.0057	.5615	130.1815	130.6685
130.3750	.3835	.0060	.5835	130.1250	130.6250
130.3500	.4218	.0105	.6132	130.0751	130.6249
130.3750	.4349	.0115	.6201	130.0915	130.6585
130.4500	.4638	.0124	.6521	130.1475	130.7525

TABLE 17

MODE 2 - 1 HOUR SAMPLES (SWEPT SINE)

1 HOUR HEAT TREATED SAMPLES

MODE 2
SWEPT SINE

FN (HZ)	LOSS FACTOR (%)	STRAIN (%)	INPUT ACCEL (G)	F1 (HZ)	F2 (HZ)
SAMPLE #1					
138.1487	2.8100	.03104	1.3109	136.2077	140.0897
140.8892	2.1006	.02064	0.9012	139.4095	142.3689
142.4606	1.8427	.01584	0.8259	141.1480	143.7732
142.9968	1.1820	.01488	0.7189	142.1517	143.8419
144.0149	0.8430	.01095	0.6143	143.4079	144.6219
144.1266	0.3253	.00742	0.5421	143.8922	144.3610
SAMPLE #2					
144.0080	0.2854	.0039	0.5873	143.8025	144.2135
144.1250	0.8723	.01205	0.6117	143.4964	144.7536
143.1980	0.8984	.01534	0.7341	142.5548	143.8412
142.6100	1.7793	.01721	0.7998	141.3413	143.8787
140.0841	2.0145	.02540	0.8451	138.6731	141.4951
138.5522	2.7069	.02848	1.2895	136.6769	140.4274

TABLE 18

MODE 2 - 2 HOUR SAMPLES (SWEPT SINE)

2 HOUR AGED SAMPLES

MODE 2
SWEPT SINE

FN (HZ)	LOSS FACTOR (%)	STRAIN (%)	INPUT ACCEL (G)	F1 (HZ)	F2 (HZ)
SAMPLE #3					
159.730	0.9103	.0031	.4851	159.0030	160.4570
159.380	1.1068	.0048	.5333	158.4980	160.2620
159.210	1.1406	.0059	.5819	158.3020	160.1180
158.960	1.2217	.0071	.6305	157.9890	159.9310
158.670	1.3008	.0086	.6789	157.6380	159.7020
158.590	1.3652	.0089	.7274	157.5075	159.6725
158.340	1.4092	.01037	.7759	157.2243	159.4557
SAMPLE #4					
159.690	0.9115	.0033	.4902	158.9628	160.4178
159.350	1.1099	.0050	.5365	158.4657	160.2343
159.240	1.1601	.0060	.5824	158.3163	160.1637
158.930	1.2207	.0072	.6334	157.9600	159.9000
158.580	1.3026	.0086	.6821	157.5472	159.6128
158.520	1.3984	.0090	.7301	157.4116	159.6284
158.360	1.4118	.0103	.7780	157.2421	159.4779

TABLE 19

MODE 3 - UNAGED SAMPLE (SWEPT SINE)

MODE 3
SWEPT SINE TEST

FN (HZ)	LOSS FACTOR (%)	STRAIN (%)	INPUT ACCEL (G)	F1 (HZ)	F2 (HZ)
361.8000	.1899	.00113	.4560	361.4563	362.1437
361.3750	.2119	.00141	.4899	360.9921	361.7579
361.1000	.2875	.00209	.6099	360.5809	361.6191
360.8000	.3983	.00273	.6799	360.0815	361.5185
360.7500	.3900	.00348	.7820	360.0465	361.4535

TABLE 20

MODE 3 - 1 HOUR AGED SAMPLES (SWEPT SINE)

MODE 3
SWEPT SINE

FN (HZ)	LOSS FACTOR (%)	STRAIN (%)	INPUT ACCEL (G)	F1 (HZ)	F2 (HZ)
		SAMPLE #1			
384.620	1.2155	.0020	.6015	382.2825	386.9575
383.420	1.2868	.0024	.6279	380.9531	385.8869
382.640	1.2569	.0029	.7015	380.2353	385.0447
381.880	1.3121	.0033	.7581	379.3747	384.3853
381.360	1.3214	.0037	.9032	378.8404	383.8796
381.200	1.4541	.0038	1.1698	378.4285	383.9715
		SAMPLE #2			
384.640	1.1876	.0018	.5882	382.3560	386.9240
383.540	1.2074	.0024	.6190	381.2246	385.8554
382.860	1.2208	.0028	.7002	380.5230	385.1970
382.360	1.2786	.0036	.7641	379.9156	384.8044
381.860	1.3284	.0037	.9011	379.3237	384.3963
381.240	1.4021	.0040	1.1769	378.5673	383.9127

TABLE 21

MODE 3 - 2 HOUR SAMPLES (SWEPT SINE)

MODE 3
SWEPT SINE

FN (HZ)	LOSS FACTOR (%)	STRAIN (%)	INPUT ACCEL (G)	F1 (HZ)	F2 (HZ)
SAMPLE #3					
444.7091	1.7542	.00266	.4851	440.8086	448.6096
444.7137	1.7831	.00261	.5333	440.7489	448.6785
444.6998	1.7812	.00269	.5819	440.7393	448.6603
444.6947	1.7907	.00286	.6305	440.7131	448.6763
444.6902	1.8395	.00299	.6789	440.6002	448.7802
444.3011	1.8575	.00300	.7274	440.1747	448.4275
444.3007	1.8963	.00395	.7759	440.0881	448.5133
SAMPLE #4					
444.7184	1.7802	.00271	.4902	440.7599	448.6768
444.7102	1.8131	.00284	.5284	440.6787	448.7417
444.6681	1.8324	.00285	.5823	440.5941	448.7421
444.6754	1.8136	.00292	.6312	440.6431	448.7077
444.6732	1.8582	.00325	.6777	440.5417	448.8047
444.3241	1.8664	.00318	.7301	440.1777	448.4705
444.3[illegible]00	1.9192	.00385	.7782	440.0365	448.5635

2. TORSION SAMPLE DATA

TABLE 22

TORSION - SOLUTION ANNEALED SAMPLE (RANDOM INPUT)

SOLUTION ANNEALED SAMPLE

FN (HZ)	LOSS FACTOR (%)	INPUT ACCEL (G)	STRAIN (%)
83.32	.1776	.5846	.002045
83.28	.2282	.5992	.002439
83.18	.2741	.6022	.002564
83.12	.3008	.6292	.002911
83.12	.3200	.6355	.002958
82.84	.3283	.6458	.003539
82.5	.3345	.6505	.003655
82.19	.3601	.6564	.003986
81.56	.3654	.6621	.004577

TABLE 23

TORSION - SOLUTION ANNEALED SAMPLE (SWEPT SINE)

SOLUTION ANNEALED SAMPLE

SWEPT SINE

FN (HZ)	LOSS FACTOR (%)	INPUT ACCEL (G)	STRAIN (%)
83.20	.2860	.6104	.002445
81.85	.3665	.6210	.004611
81.70	.3917	.6826	.005393
81.35	.4376	.7362	.007064
80.95	.4917	.7553	.009055
80.823	.5419	.7659	.011366

TABLE 24

TORSION - 1 HOUR AGED SAMPLE (RANDOM INPUT)

1 HOUR AGED SAMPLE

FN (HZ)	LOSS FACTOR (%)	INPUT ACCEL (G)	STRAIN (%)
68.875	1.1397	.5711	.001505
68.775	1.1458	.5810	.002552
68.750	1.1549	.6007	.002553
68.650	1.2207	.6279	.003393
68.525	1.6417	.6353	.003805
68.400	1.7544	.6463	.004459
68.300	2.2577	.6512	.004723
68.375	3.0903	.6554	.004653
67.650	3.3629	.6615	.007416

TABLE 25

TORSION - 1 HOUR AGED SAMPLE (SWEPT SINE)

1 HOUR AGED SAMPLE

SWEPT SINE

FN (HZ)	LOSS FACTOR (%)	INPUT ACCEL (G)	STRAIN (%)
68.400	1.6812	.5739	.003224
68.075	1.9464	.5785	.003988
68.075	2.0566	.6015	.004333
67.725	2.3256	.6247	.005900
67.700	2.6209	.6353	.007004
67.475	2.9306	.6459	.007213
67.325	3.2107	.6509	.008068
67.125	3.6305	.6589	.008889
66.925	3.9137	.6642	.010762

TABLE 26

TORSION - 2 HOUR AGED SAMPLE (RANDOM INPUT)

2 HOUR AGED SAMPLE

FN (HZ)	LOSS FACTOR (%)	INPUT ACCEL (G)	STRAIN (%)
68.346	1.5714	.5923	.004135
68.100	2.1806	.6764	.008949
67.844	2.8389	.7044	.010144
67.400	3.1899	.7351	.013658
67.375	3.4137	.7489	.018575
67.375	3.6735	.7639	.020472

TABLE 27

TORSION - 2 HOUR AGED SAMPLE (SWEPT SINE)

2 HOUR AGED SAMPLE

SWEPT SINE

FN (HZ)	LOSS FACTOR (%)	INPUT ACCEL (%)	STRAIN (%)
68.875	1.1252	.6176	.005121
68.175	1.4668	.6236	.008149
67.875	2.8405	.6973	.010497
67.450	4.0030	.7214	.014514
67.250	4.0537	.7509	.018386
66.600	4.1290	.7649	.020028

LIST OF REFERENCES

1. Hills, A.H., *A Study of the Influence of Stress and Temperature on the Damping Capacity of Mn-Cu Alloys for Ship SilencingApplications*, M.E. Thesis, Naval Postgraduate School, Monterey, California, June 1979.

2. Heidgerken, R.A., *The Design of a Test Procedure for the Measurement of Acoustic Damping of Materials at Low Stress*, M.S. Thesis, Naval Postgraduate School, Monterey, California, September 1983.

3. Knouse, S.T., *Effect of Boundary Conditions on the Damping Characteristics of a Randomly Excited Cast Nickel-Aluminum Bronze Specimen at Low Stress Levels*, M.S. Thesis, Naval Postgraduate School, Monterey, California, September 1984.

4. Milster, F.P. *Effects of Temperature and Environmental Changes on the Damping Prop Properties of Randomly Excited Metal Plate Specimens*, M.E. Thesis, Naval Postgraduate School, Monterey, California, December 1984.

5. Henderson, J.P., Jones, D.I.G., and Nashif, A.D., *Vibration Damping*, John Wiley & Sons, 1985.

6. Naval Postgraduate School Report NPS-59Ps74061, *Materials Approaches to Ship Silencing*, by A.J. Perkins, G.R. Edwards, and N.A. Hills, June 1974.

7. Czyryca, E.J. and Vassilaros, M.G., *Development of Improved Alloys for Navy Ship's Propellers*, Department of the Navy, Naval Ship Research and Development Center, 1971.

8. Thomson, W.T., *Theory of Vibration with Applications*, Sec. Ed., Prentice-Hall, Inc., New Jersey, 1981.

BIBLIOGRAPHY

Beards, C.F., "Damping in Structural Joints," *The Shock and Vibration Digest*, vol. 17, pp. 17-20, November 1985.

Bert, C.W., "Material Damping: An Introductory Review of Mathematical Models, Measures and Experimental Techniques," *Journal of Sound and Vibration*, vol. 29, pp. 129-153, 1973.

Coltell ,G.A., Euturistle, K.M., and Thompson, F.C., "The Measurement of the Damping Capacity of Metals in Torsional Vibration," *Journal Inst. Metals*, pp. 373-424, 1974.

Harris, C.M. and Crede, C.E., *Shock and Vibration Handbook*, McGraw-Hill, New York, Sec. Ed., Chapter 36.

Hedley, J.A., "The Mechanism of Damping in Manganese-Copper Alloys," *Metal Science Journal*, pp. 129-137, July 1968.

Defense Technical Information Center Report AMMRC 76-30, *Noise Abatement and Internal Vibration Absorption in Potential Structural Materials*, by L. Kaufman, S.A. Kulin, and P.P. Neshe, September 1976.

To, C.W.S., "The Response of Nonlinear Structures to Random Excitation," *The Shock and Vibration Digest*, vol. 16, pp. 13-33, April 1984.

INITIAL DISTRIBUTION LIST

		No. Copies
1.	Defense Technical Information Center Cameron Station Alexandria, Virginia 22304-6145	2
2.	Library, Code 0142 Naval Postgraduate School Monterey, California 93943-5002	2
3.	Dean of Science and Engineering, Code 06 Naval Postgraduate School Monterey, California 93943-5000	2
4.	Research Administrations Office, Code 012 Naval Postgraduate School Monterey, California 93943-5000	1
5.	Department Chairman, Code 69 Department of Mechanical Engineering Naval Postgraduate School Monterey, California 93943-5000	1
6.	Professor Y.S. Shin, Code 69Sg Department of Mechanical Engineering Naval Postgraduate School Monterey, California 93943-5000	5
7.	Mrs. Kathy Wong, Code 2812 David W. Taylor Naval Ship R&D Center Annapolis, Maryland 21402	5
8.	Mr. Robert Hardy, Code 2803 David W. Taylor Naval Ship R&D Center Annapolis, Maryland 21402	2
9.	Dr. D.J. Vendittis, Code 196 David W. Taylor Naval Ship R&D Center Ship Acoustics Department (196) Bethesda, Maryland 20084	1
10.	Mr. V.J.Castelli, Code 2844 David W. Taylor Naval Ship R&D Center Annapolis, Maryland 21402	1
11.	Professor Perkins, Code 69Ps Department of Mechanical Engineering Naval Postgraduate School Monterey, California 93943-5000	1
12.	Dr. Kil Soo Kim, Code 69Sg Department of Mechanical Engineering Naval Postgraduate School Monterey, California 93943-5000	1
13.	LCDR.D.D.Dew, USN 117 Southwold Circle Goosecreek, South Carolina 29445	2